Thesis submitted in fulfillment of the requirements for the degree of
Doctor of Engineering Sciences (Doctor in de Ingenieurswetenschappen) by

ir. Gustavo Quintana Carapia

# Statistical analysis and experimental validation of data-driven dynamic measurement methods

**PROMOTERS**                      prof. dr. ir. Ivan Markovsky
                                   ELEC Department, Vrije Universiteit Brussel, Belgium

                                   prof. dr. ir. Rik Pintelon
                                   ELEC Department, Vrije Universiteit Brussel, Belgium


**MEMBERS OF THE JURY**            prof. dr. ir. Patrick Guillaume (President)
                                   MECH Department, Vrije Universiteit Brussel, Belgium

                                   prof. dr. ir. Roger Vounckx (Vice-President)
                                   ETRO Department, Vrije Universiteit Brussel, Belgium

                                   dr. ir. Philippe Dreesen (Secretary)
                                   ELEC Department, Vrije Universiteit Brussel, Belgium

                                   prof. dr. ir. Nikolaos Deligiannis
                                   ETRO Department, Vrije Universiteit Brussel, Belgium

                                   prof. dr. ir. Lyudmila Mihaylova
                                   ACSE Department, University of Sheffield, United Kingdom

                                   prof. dr. ir. Stephane Chretien
                                   ERIC Laboratory, University Lyon 2, France

                                   prof. dr. ir. Guillaume Mercère
                                   LIAS Laboratory, Université de Poitiers, France

# Contents

# List of Abbreviations

**CRLB**    Cramér-Rao Lower Bound

**EIV**    Errors in Variables

**FRF**    Frequency Response Function

**LS**    Least Squares
**LTI**    Linear Time Invariant
**LTV**    Linear Time Varying

**MC**    Monte Carlo
**ML**    Maximum Likelihood
**MSE**    Mean Squared Error

**RLS**    Recursive Least Squares
**RMS**    Root Mean Square

**SISO**    Single-Input Single-Output
**SNR**    Signal-to-Noise Ratio

**TV**    Time-Varying

# Nomenclature

A list of the symbols used in this thesis is found in the following list.

| | |
|---|---|
| $a, b$ | true parameters an affine input model |
| $\widehat{a}, \widehat{b}$ | estimated parameters an affine input model |
| $\mathbf{A}, \mathbf{B}, \mathbf{C}, D$ | matrices of an LTI dynamic system state space representation |
| $\widehat{\mathbf{A}}, \widehat{\mathbf{B}}, \widehat{\mathbf{C}}, \widehat{D}$ | estimated matrices of an LTI dynamic system state space representation |
| $\widehat{\mathbf{A}}_{\mathrm{a}}, \widehat{\mathbf{C}}_{\mathrm{a}}$ | estimated matrices of an autonomous LTI dynamic system state space representation |
| $\mathbf{A}_{\mathrm{a}}, \mathbf{C}_{\mathrm{a}}$ | matrices of an autonomous LTI dynamic system state space representation |
| $\mathbf{b}\left(\widehat{\boldsymbol{\theta}}\right)$ | bias of the estimate $\boldsymbol{\theta}$ |
| $\mathbf{b}_{\mathrm{p}}\left(\widehat{\boldsymbol{\theta}}\right)$ | predicted bias of the estimate $\boldsymbol{\theta}$ obtained from exact data |
| $\widetilde{\mathbf{b}}_{\mathrm{p}}\left(\widehat{\boldsymbol{\theta}}\right)$ | predicted bias of the estimate $\boldsymbol{\theta}$ obtained from measured data |
| $\mathbf{b}_{\widetilde{\mathrm{p}}[1]}$ | first element of the estimation predicted bias obtained from measured data |
| $b_{\mathrm{e}}$ | empirical bias of the step input estimate |
| $b_{\mathrm{p}}$ | bias prediction computed using exact data |
| $b_{\widetilde{\mathrm{p}}}$ | sample mean of the step input estimation bias, computed from observed data predictions |
| $\mathbf{B}_1, \mathbf{B}_2, \mathbf{B}_3, \mathbf{B}_4$ | matrices of the bias prediction formulas computed from exact data |
| $\widetilde{\mathbf{B}}_1, \widetilde{\mathbf{B}}_2, \widetilde{\mathbf{B}}_3, \widetilde{\mathbf{B}}_4$ | matrices of the bias prediction formulas computed from measured data |

$\mathbf{C}\left(\widehat{\boldsymbol{\theta}}\right)$ covariance matrix of the estimate $\boldsymbol{\theta}$

$\mathbf{C}_{\mathrm{p}}\left(\widehat{\boldsymbol{\theta}}\right)$ predicted covariance of the estimate $\boldsymbol{\theta}$ obtained from exact data

$\widetilde{\mathbf{C}}_{\mathrm{p}}\left(\widehat{\boldsymbol{\theta}}\right)$ predicted covariance of the estimate $\boldsymbol{\theta}$ obtained from measured data

$\mathbf{C}_{\widetilde{\mathrm{p}}[1,1]}$ first element of the estimation predicted covariance obtained from measured data

$\mathbf{C}_1, \mathbf{C}_2$ matrices of the covariance prediction formulas computed from exact data

$\widetilde{\mathbf{C}}_1, \widetilde{\mathbf{C}}_2$ matrices of the covariance prediction formulas computed from measured data

$\mathbf{C}_{\mathbf{z}}$ covariance matrix of a linear in the measurements problem $e(\widehat{\boldsymbol{\theta}}, \widetilde{\mathbf{z}}) = \mathbf{M}_1(\widehat{\boldsymbol{\theta}})\, \widetilde{\mathbf{z}}$

$\mathrm{CRLB}(\boldsymbol{\theta})$ Cramér-Rao lower bound of the estimate $\boldsymbol{\theta}$

$\mathbf{D}_{r \times c}^{1,d}$ and $\mathbf{D}_{r \times c}^{2,d}$ first and second-order finite differences matricial operators of dimensions $r \times c$ starting from the subdiagonal $d$

$\Delta$ signals first difference operator, defined as $\Delta y(k) = y(k+1) - y(k)$

$\Delta \mathbf{x}(k)$ autonomous system state vector at time $k$

$\Delta y(k)$ sample of an autonomous system response at time $k$

$\mathbf{E}$ measurement noise that is added to the regression matrix in a system of linear equations

$\epsilon$ measurement noise that is added to the system response

$\epsilon(k)$ samples of the measurement noise at time $k$

$\epsilon_{\mathbf{z}}$ perturbation noise of a linear in the measurements problem $e(\widehat{\boldsymbol{\theta}}, \widetilde{\mathbf{z}}) = \mathbf{M}_1(\widehat{\boldsymbol{\theta}})\, \widetilde{\mathbf{z}}$

$\mathbb{E}\{\cdot\}$ mathematical expectancy operator

$\mathbf{Fi}(\boldsymbol{\theta})$ Fisher information matrix

$\mathbf{G}$ static gain matrix of an LTI dynamic system

$\mathbf{H}(s), \mathbf{H}(z)$ continuous and discrete time transfer functions of a dynamic system, respectively

$\mathcal{H}(y)$ and $\mathscr{H}(\epsilon)$ $n \times n$ Hankel matrices constructed from the system response $y$ and the measurement noise $\epsilon$, respectively

$\mathcal{H}_{L+1}(\Delta y)$ Hankel matrix of $L+1$ block rows constructed from $\Delta y$

$\mathbf{I}_n$ $n \times n$ identity matrix

$\mathbf{J} = \partial \mathbf{r} / \partial \boldsymbol{\theta}$ Jacobian matrix of the residual $\mathbf{r}$

$k$ $k-$th instant of time

$\mathbf{K}$ regression matrix in a system of linear equations constructed from exact data

$\widetilde{\mathbf{K}}$ regression matrix in a system of linear equations constructed from measured data

$\widetilde{\mathbf{k}}_k$ row of matrix $\widetilde{\mathbf{K}}$ that corresponds to the $k-$th sample of the measured response

$\mathbf{K}^{\dagger}$ pseudo-inverse of the matrix $\mathbf{K}$

$k_{\mathrm{T}}$ temperature coefficienct of a first-order thermometer model

$\kappa$ scalar gain in the recursive least-squares algorithm

$l$ likelihood function of an estimation problem

$\ell$ linear transformation of the initial conditions in the data-driven step input estimation method

$\lambda$ eigenvalues of a dynamic system

$m, k_{\mathrm{s}}, k_{\mathrm{d}}$ mass, stiffness and damping coefficients of a second-order weighing system model

$\boldsymbol{\mu}\left(\widehat{\boldsymbol{\theta}}\right)$ expected value of the estimate $\boldsymbol{\theta}$

$\mathrm{MSE}_{\mathrm{e}}$ mean-squared error computed using the empirical results in the Monte Carlo simulation

$\mathrm{MSE}_{\mathrm{p}}$ mean-squared error computed using the predictions from exact data

$\mathrm{MSE}_{\widetilde{\mathrm{p}}}$ mean-squared error computed using the predictions from observed data

$n$ order of a dynamic system

$N$ maximum number of available system response samples

$N_{\mathrm{MC}}$ number of Monte Carlo runs

$\mathcal{O}$ observability matrix of an LTI dynamic system

$\mathcal{O}_{\mathrm{a}}$ observability matrix of an autonomous LTI dynamic system

$\omega$ weighing factor of the recursive least-squares algorithm

$\boldsymbol{\Omega}$ diagonal matrix of descending powers of the weight factor $\omega$

$\mathbf{P}_{\perp} = \mathbf{I} - \mathbf{K}\mathbf{K}^{\dagger}$ orthogonal matrix computed from exact data

$\widetilde{\mathbf{P}}_{\perp} = \mathbf{I} - \widetilde{\mathbf{K}}\widetilde{\mathbf{K}}^{\dagger}$ orthogonal matrix computed from measured data

$\boldsymbol{\Psi}$ covariance matrix of the recursive least-squares algorithm algorithm

$\mathbf{r}(\boldsymbol{\theta}) = \widetilde{\mathbf{y}} - \widehat{\mathbf{y}}(\boldsymbol{\theta})$ residual difference between the measured response $\widetilde{\mathbf{y}}$ and the simulated response $\widehat{\mathbf{y}}(\boldsymbol{\theta})$

$\mathbf{R}_n$ $n \times n$ reversal matrix

| | |
|---|---|
| $s(t)$ | unit step input |
| $\sigma_e^2$ | empirical variance of the step input estimate |
| $\sigma_{e,err}$ | standard error associated to the the estimation empirical bias in the Monte Carlo simulation |
| $\sigma_E^2$ | variance of the measurement noise matrix $\mathbf{E}$, assuming its columns are stacked in a vector |
| $\sigma_{\widetilde{p},err}$ | standard error of the of the empirical estimate Monte Carlo simulation |
| $\sigma_\epsilon^2$ | variance of the measurement noise $\epsilon$ |
| $\mathcal{T}$ | Markov parameters matrix of an LTI dynamic system |
| $\boldsymbol{\theta}$ | true value of the to-be-estimated parameters in a linear regression problem |
| $\widehat{\boldsymbol{\theta}}$ | estimated parameters in a linear regression problem |
| $u(t)$ | input signal applied to a dynamic systems |
| $\widehat{u}$ | estimated input signal |
| $u(k)$ | sample of the input signal at time $k$ |
| $\mathbf{u}$ | vector constructed from samples of the input signal |
| $\mathbf{U}, \boldsymbol{\Sigma}, \mathbf{V}$ | singular value decomposition matrices |
| $v_p$ | variance prediction computed using exact data |
| $v_{\widetilde{p}}$ | sample mean of the step input estimation variance, computed from observed data predictions |
| $\mathbf{x}(k)$ | system state vector at time $k$ |
| $\mathbf{x}_{ini}$ | initial conditions of a dynamic system |
| $\mathbf{x}_{ini,c}$ | initial conditions of a compensator dynamic system |
| $\mathbf{X}_{ini}$ | matrix of the initial conditions of a dynamic system at different instant of time |
| $\mathbf{x}_a(0)$ | initial conditions of an autonomous dynamic system |
| $\mathbf{x}_a(k)$ | autonomous system state vector at time $k$ |
| $y(t)$ | exact response of a dynamic system |
| $\widehat{y}$ | simulated exact response signal |
| $\widetilde{\mathbf{y}} = \mathbf{y} + \boldsymbol{\epsilon}$ | observed system response afected by measurement noise |
| $y(k)$ | sample of the exact response signal at time $k$ |
| $\mathbf{y}$ | vector constructed from samples of the system response signal |
| $\widetilde{\mathbf{z}} = \mathbf{z} + \boldsymbol{\varepsilon_z}$ | vector constructed by stacking the perturbation noise of the regressor and the regression matrix of the EIV problem |
| $\widetilde{\mathbf{Z}}$ | instrumental variable constructed from measured data |

# 1. Summary

Measurements are dynamical processes where the input is estimated using the sensor response. The users cannot wait for the sensor to reach a steady regime when the sensor response closely approximates the sensor static gain times the input. To obtain a fast input estimation, one approach is filtering the sensor transient response with another dynamical system, aiming to compensate the estimation time. The compensator is commonly built after a sensor model to perform deconvolution. Another approach is estimating the input with data-driven methods that are independent from the sensor model. Current digital signal processors (DSP) allow the implementation of both model-based and data-driven estimation methods.

There exists a data-driven method that directly estimates the step input level from the sensor step response. The formulation of this method is a Hankel-structure errors-in-variables (EIV) problem, where the regression matrix and the regressor are correlated. The structured EIV problem is solved with recursive least-squares for real-time implementation. The independence from the sensor model of the estimation method broadens its range of application.

The uncertainty of the step input estimation method is unknown and is not straightforwardly evident. To validate the method for metrology applications, we studied the stochastic properties of the step input estimation. A statistical analysis yields the estimation bias and variance, and thus, the estimation uncertainty.

Both with simulations and experiments, the sample mean squared error (MSE) of the step input estimation method is compared to its analytical Cramér-Rao bound. The Cramér-Rao bound determines the minimum theoretical variance of the estimation. It was found that the data-driven step input estimation is biased but has small variance, and the estimation MSE is less than one order of magnitude larger than the Cramér-Rao bound. Moreover, in practical experiments, the step input estimation method is robust when the measurement noise is not Gaussian and white.

# 2. Introduction

A measurement is a dynamic process, and a sensor is a dynamic system. The physical quantities of interest are the inputs of the system, and the outputs are the electrical signals collected from the sensor. The inputs interact with the sensor, and there are energy transfers between them that modify the sensor state. The sensor output response depends on the applied inputs and on the sensor's initial conditions.

Take for example the case of a thermometer. To measure temperature, the thermometer is put in contact with the substance or object of interest. According to the Newton's law of cooling, the temperature $y$ of the thermometer changes proportionally to its difference with the temperature $u$ of the matter under study:

$$\frac{dy}{dt} = k_T (u - y) \tag{2.1}$$

where the proportionality constant $k_T$ is a parameter of the thermometer's first order model. The input $u$ is unknown and its estimation is the objective of the measurement. It is customary to take the reading from the thermometer once the temperature stops changing.

Another popular example of a measurement is found in weighing. In most of modern scales, the object of interest is placed on top of a weighing sensor. A simple model of the weighing sensor is a second order mass-spring-damper model shown in Figure 2.1. In this model, the unknown mass $u(t)$, that can be time-dependent, causes a displacement $y$ of the scale and the dynamics of the sensor are described by the differential equation:

$$\frac{d}{dt} \left( (u(t) + m) \ \frac{dy}{dt} \right) + k_d \frac{dy}{dt} + k_s y = (u(t) + m) g \tag{2.2}$$

where $m$ is the own mass of the scale, $k_d$ is the damping constant, $k_s$ is the elasticity constant, and $g = 9.81 \text{ m/s}^2$ is the gravitational acceleration.

For illustration purposes, Figures 2.2 and 2.3 show the responses of the thermo-
meter and the weighing sensors, respectively, after the application of a constant
input $u$, which can be represented by a step input.
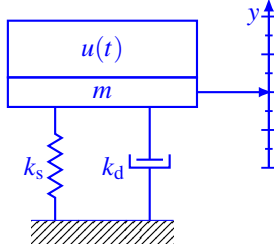


Figure 2.1.: A second order mass-spring-damper model represents the weighing
sensor. The application of the mass $u$ causes a change in the position $y$
of the scale.
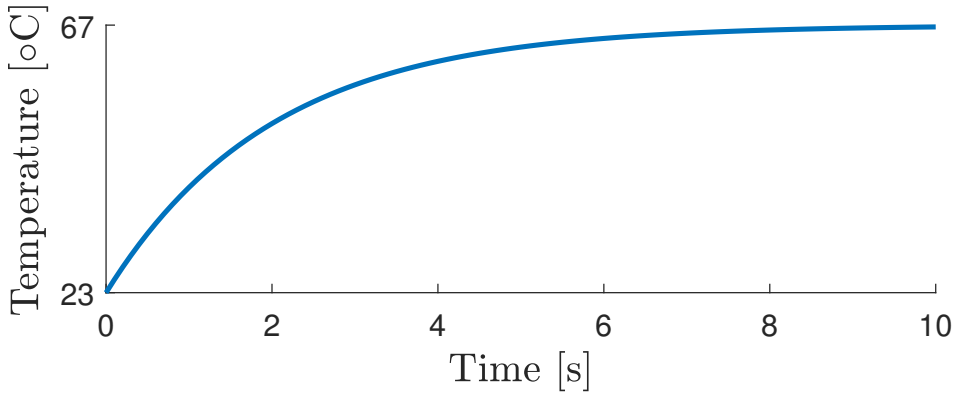


Figure 2.2.: This simulation shows an example of the temperature change experi-
mented by a thermometer, with $k_T = 0.5s^{-1}$, caused by a step input of
$67\,°C$ when the thermometer was initially at $23\,°C$. In this example,
we should wait $10\,s$ to have an estimation of the input with a relative
error lower than $0.5\,\%$.

In Eichstädt et al. [2012] is illustrated a force measurement sensor modeled after
a cascade of two damped mass-spring systems. The transfer function of the sensor
is $H(s) = H_1(s)/H_2(s)$, where each of the two parts are described by

$$H_i(s) = \frac{(2\pi f_{0,i})^2}{s^2 + 2\delta_i (2\pi f_{0,i}) s + (2\pi f_{0,i})^2} \tag{2.3}$$
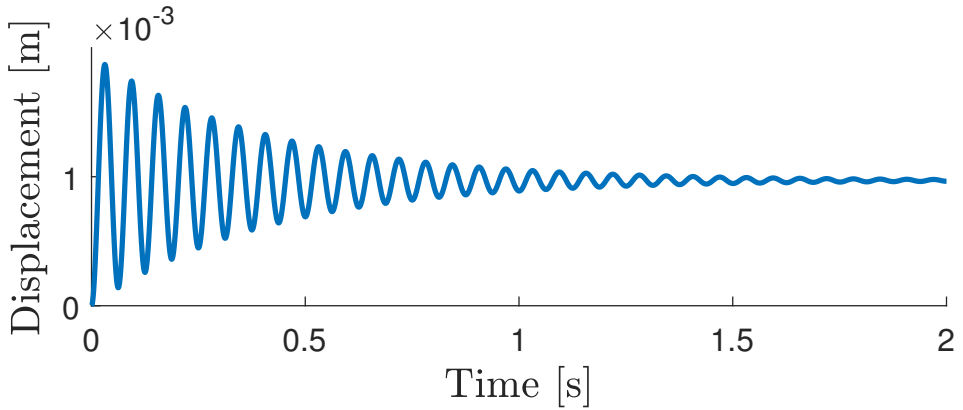
Figure 2.3.: This simulation illustrate the displacement observed when a constant input $u = 1$kg is applied to a weighing sensor in equilibrium. The sensor parameters are $k_d = 5$ N s/m, $m = 5$ g, and $k_s = 10250$ N/m. In this conditions, the user has to wait more that 2 s to observe a stabilization on the scale and to estimate the mass from reading the final value of the displacement with a relative error smaller than 0.72 %.

where $\delta_1 = 0.1$, $\delta_2 = 0.2$, $f_{0,1} = 1.9$ Hz, and $f_{0,2} = 7$ Hz are the system parameters. The response of this sensor to a unit step input, shown in Figure 2.4, takes at least 5 s to in which the transient response is predominant.

The handbook of sensors written by Fraden [2016] describes a pressure sensor that detects sudden changes in the pressure inside a room. These changes can be caused by the opening of a door or by the movement of a person. The principle of operation of detecting minute pressure gradients is the flowmeter that compares the pressure at both outlets of a tube. An experimental identification of such a flowmeter is described in Wiklund and Peluso [2002], where a secod order model is proposed to explain the dynamics with the transfer function

$$H(s) = \frac{e^{-\tau_{delay}s}}{(1 + \tau_1 s)(1 + \tau_2 s)} \tag{2.4}$$

where $\tau_{delay} = 0.07$ s is the dead time, and $\tau_1 = 0.01$ s and $\tau_2 = 1.6$ s are two time constants. The step response simulation of this dynamic model results in the sensor step response shown in Figure 2.5. We have a response to a unit step function that is m and increasing exponential that requires 7 s approximately to reach its maximum value.
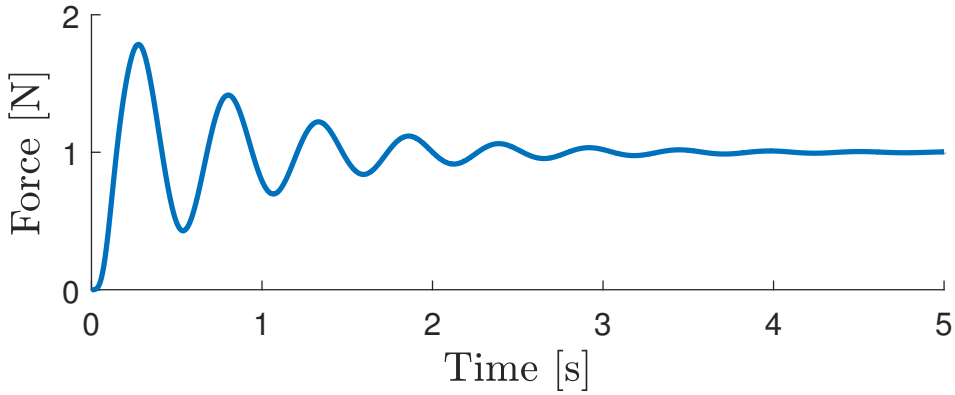
Figure 2.4.: The simulation of a force sensor based on a double mass-spring system in cascade also shows that the stabilization after a unit step input is not instantaneous. In the plot we infer that the user has to wait 5 s to estimate the force from the sensor in equilibrium.
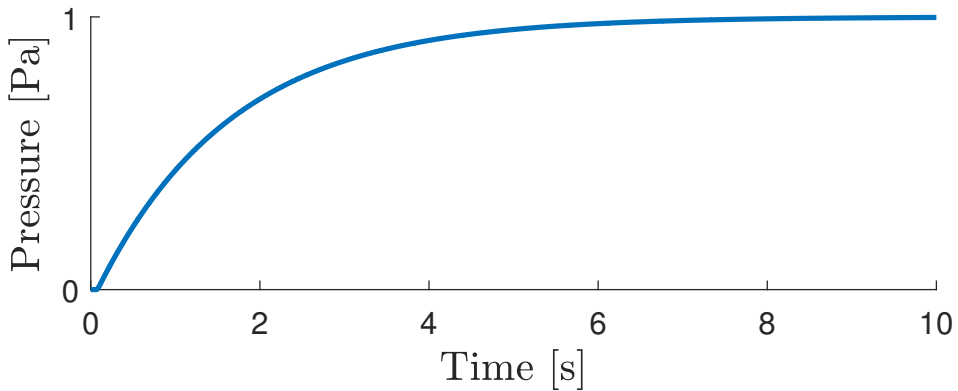


Figure 2.5.: The response of a flowmeter to a sudden change in its pressure gradient acrros the extremes of a tube is an overdamped transient response. Ideally we would expect the the transient response follows closely the shape of the unit step input applied, but instead an exponential response is observed, that last for more than 7 s.

There is a trade-off between speed and accuracy when measuring with a linear time-invariant sensor. The input excitation drives the sensor into a transient regime, and when the transient response is below the noise level, we say that the sensor is in steady state. During the sensor transient regime, the response does not directly represent the input, but in steady state, the sensor response is proportional to the excitation. The input can be estimated accurately from the sensor steady state response using the sensor static gain. However, waiting for the steady state is not always possible for practical applications that need fast measurements. In these practical applications, the input must be estimated during the transient regime.

One approach to get a fast input estimation is filtering the sensor transient response with another dynamical system that inverts the dynamics of the sensor. The filter output is an input estimate that compensates for the time span of the sensor transient regime. The transient duration of the compensation filter should be smaller than that of the sensor. The compensator is designed after a sensor model to deconvolve the sensor response.

Another approach relies on the use of digital signal processors (DSP) to estimate the input value from the sensor transient response. DSPs offer an extra versatility level since they allow to implement methods that do not necessarily simulate the dynamics of linear systems, such as digital filters. A suitable data-driven method in a DSP can provide faster input estimations than with the model-based compensators.

An example of a data-driven method devised for a DSP is the direct step input level estimation from the sensor step response introduced in Markovsky [2015a]. This method formulates a Hankel structured errors-in-variables (EIV) problem with correlation. The regression matrix has a block-Hankel structure. The correlation exists because the transient response, perturbed by measurement noise, constructs both the regression matrix and the regressor. The measurement noise is assumed to have zero mean and finite variance. The method is implemented in real-time using a recursive least-squares (RLS) solution of the structured EIV problem.

The main advantage of the data-driven step input estimation method is that it does not identify the sensor model, but instead, it directly estimates the input. The direct estimation differs from the standard two-stage methodology that first identifies the sensor model and later estimates the input. In this approach, the output-error (OE) problem is converted into an EIV problem that is harder to solve, but the RLS solution is easy to compute. The range of application of the data-driven input estimation method is extensive because it is independent of the sensor model. The main disadvantage of the data-driven input estimation

method is that its stochastic properties are not straightforwardly evident. It is more complex to find the stochastic properties of EIV problems when they have structure and correlation.

The estimation uncertainty assessment is needed to validate the estimation methods for metrology applications. The uncertainty of the data-driven step input estimation method described in Markovsky [2015b] is unknown. The estimation bias and variance define the estimation uncertainty, as it is explained in Pintelon and Schoukens [2012], and they can be obtained by conducting an elementwise statistical analysis. The validation of the step input estimation method requires also to demonstrate its effectiveness on real-life measurements. Temperature and mass sensors are suitable for real-life measurement experiments. One challenge of using real-life sensor outputs is that the noise may not fulfill the whiteness assumed in the estimation problem formulation and in the statistical analysis. The experimental and simulation results permit to evaluate the step input estimation method performance.

The step input estimation method concepts raise the curiosity towards the design of estimation methods for other input models. The affine input model, for example, is found in conveyor dynamic weighing systems. The dynamic weighing estimates the mass of materials or products during their transportation. When the conveyor belt moves at a constant speed, the weighing sensor is excited with an affine profile, described by the slope and the intercept parameters. The affine input parameters can be estimated by adapting the step input estimation method.

## 2.1.  State of the art

The scientific literature contains metrology studies that deal with the dynamic process effects of measurements. This subsection presents a list of relevant works published in relation with the thesis topic. These works study theoretical aspects like the estimation of inherent dynamical errors presented in Hessling [2006], the dynamic correction in time domain proposed in Hessling [2008]; and experimental aspects like the increment of the amount of sensors in production lines for quick decision making in autonomous control described in Esward et al. [2009].

To implement input estimation methods in the practice, the compensation filters based on deconvolution explained by Eichstädt et al. [2010] are the preferred methodology to develop, for example, analog filters in Jafaripanah et al. [2005], adaptive digital filters in Shu [1993], lattice adaptive filters in Hernandez [2006], compensators for simultaneous responses of different sensors in Boschetti et al.

[2013], regularized deconvolution compensators in Dienstfrey and Hale [2014], and a multiple choice set of filters in Huang et al. [2016]. All these methods have in common the use of the measurement system model parameters to build the compensator.

A list of measurement methods based on digital signal processors (DSP) include a data-driven dynamic error correction and its impact on the measured temperature studied in Saggin et al. [2001], a modulation quality measurement of microwave access systems presented in Angrisani and Napolitano [2010], a real-time rotational speed estimation method using correlation introduced in Wang et al. [2014], a biology-inspired electronic nose developed in Jing et al. [2016], and impedance measurements for material damage estimation method using cross-correlation introduced in de Castro et al. [2019]. The data-driven step input estimation method proposed by Markovsky [2015a] is added to this list, highlighting the fact that it can be implemented for the measurement of different physical magnitudes because it is model-independent.

In metrology, a measurement is an estimation, represented as a random variable. The measurement noise always exists, and therefore, the input estimation is commonly expressed with its two first statistical moments as it is described in Ferrero and Salicone [2006]. The guidelines listed in BIPM et al. [2008], and accepted by the metrology community, recommend the standardization of the uncertainty assessment. The typical measurement uncertainty analysis is reviewed in Hack and ten Caten [2012]. The Monte Carlo method is an uncertainty evaluation tool according to Cox and Siebert [2006], that supports the use of simulation techniques for quantifying measurement uncertainties as suggested by Esward [2016]. One example of the Monte Carlo method application is a dynamic measurement uncertainty evaluation of clinical thermometers described in Ogorevc et al. [2016].

Nevertheless, researchers like Esward et al. [2009], and Hessling [2010] still pinpoint the need to study more the uncertainty assessment methods. Diniz et al. [2017] recommends to consider the uncertainties of all the measurement chain components, and to avoid the direct uncertainty propagation from the calibration towards the to-be-measured quantity. Methods for evaluating the uncertainty associated with the output of compensation filters have been investigated for a discrete-time infinite-response filter in Link and Elster [2009], a discrete-time finite-response filter in Elster et al. [2007]; Elster and Link [2008], and the Kalman filter in Eichstädt et al. [2016]. All these works propagate the uncertainty through the filter, but it is also necessary to upward the propagation up to the sensor model to include all systematic error contributions, as it is explained by Hessling [2011].

## 2.2. Original contributions

This thesis describes research work initiated after the data-driven step input estimation method proposed by Markovsky [2015a]. This method aims for metrology applications but it lacked an uncertainty assessment, and, therefore, its appropriateness was questionable. The first research work conducted was a statistical analysis to elucidate the bias and the covariance of the estimate that the data-driven step input estimation method provides. After obtaining these statistical moments, the estimation uncertainty was assessed, and thus, the effectiveness of the method was appraised. The second research work was a series of experiments conducted to validate the data-driven step input estimation method in real-life applications. The experiments were realizations of the step input excitation using temperature and mass sensors. The step input estimation method showed robustness when the measurement noise is not Gaussian and white, as it was assumed in the theoretical analyses. The third research work conducted was the estimation of affine input parameters following the data-driven approach for real-time applications. The data-driven method uses exponential weighing in the recursive least-squares solution of a structured errors-in-variables problem, to give preference to recent samples over the older samples. The methodology and performance of the data-driven affine input estimation method were compared to those of a maximum-likelihood method.

### 2.2.1. Statistical analysis

The data-driven step input estimation method formulates a structured errors-in-variables (EIV) problem. In linear estimation EIV problems, the measurement noise perturbs the regression matrix and the regressor, as it is detailed in Van Huffel and Vandewalle [1991] and Markovsky and Van Huffel [2007]. The regression matrix, in structured EIV problems, has a structure that depends on the problem formulation. Hankel and Toeplitz matrices appear in several application problems such as those described by Markovsky [2015a] in metrology, by Söderström [2007] in system identification, by Feiz and Rezghi [2017] in image restoration, by Cai et al. [2016] in nuclear magnetic resonance spectroscopy, by Pan et al. [2018] in direction-of-arrival estimation, and by Jia et al. [2018] in time-of-arrival estimation.

The data-driven step input estimation method introduced by Markovsky [2015a] directly estimates the input from the sensor transient response. The perturbations in the formulated EIV problem come from the sensor output, since it is the only observed signal, and from this signal both the regression matrix and the regressor

are built. The structure in the regression matrix is block-Hankel. The data-driven direct estimation methodology estimates the input faster than the classical two-stage approach described in Azam et al. [2015] and Niedźwiecki et al. [2016], which first identifies a sensor model and later estimates the input using the sensor model.

Instead of using a total least-squares (TLS) solution of the structured EIV problem, the step input estimation method uses the recursive least-squares solution (RLS). In the review conducted by Markovsky and Van Huffel [2007] it is shown that the TLS solution of unstructured EIV problems is consistent when the perturbations have zero mean with a given positive definite covariance, and the TLS solution is equivalent to the maximum likelihood (ML) solution when the disturbances of the EIV problems are i.i.d. normally distributed . However, the studies of structured EIV problems presented in Van Huffel et al. [2007] demonstrate that the TLS estimator does not give general results since each structure requires a specific treatment. Moreover, Rhode et al. [2014] found that the ML estimator leads to non-convex optimization when applied to structured EIV problems, and the global optimum is not guaranteed. Also, the computational complexity of TLS and ML inhibits their real-time implementation. Thus, the least-squares (LS) estimator is a suboptimal but simple solution to structured EIV problems that admits a recursive form (RLS) suitable for real-time implementation.

The previously published works that propose LS estimators to solve structured EIV problems do not study the required statistical moments to know the uncertainty of the data-driven step input estimation method. In the literature we find the design of a fast algorithm for matrices with small displacement rank in Mastronardi and O'Leary [2007], the study of the LS estimator consistency in Palanthandalam-Madapusi et al. [2010], the determination of the bias, and the mean squared error of the parameter estimates in the identification of AR models in Kiviet and Phillips [2012], Kiviet and Phillips [2014], and a discussion of the causes of bias and inconsistency in homogeneous estimators in Yeredor and De Moor [2004]. The literature does not address the uncertainty of LS estimators for structured EIV problems.

The uncertainty of an estimation method is expressed in Pintelon and Schoukens [2012] using the bias and covariance of the estimate. To know the uncertainty of the data-driven step input estimation method, we quantified the bias and covariance of the LS solution of EIV problems, for unstructured and structured cases. The bias and covariance quantification extend the perturbation analysis that was investigated in Stewart [1990] and in Vaccaro [1994]. The conducted analysis provides insight into the impact that the structure and the correlation have on

the LS estimation uncertainty. The study presented in this thesis illustrates a methodology to conduct statistical analysis for any structured EIV problem.

We derived expressions that quantify the bias and covariance by obtaining the mathematical expectation of the LS estimate approximated by the second-order Taylor series expansion. Using Monte Carlo simulations, we validated the accuracy of the bias and covariance expressions. These expressions estimate the bias and covariance that the data-driven step input estimation method will exhibit for a given sample size and perturbation level. We compared in Quintana-Carapia et al. [2019a] the mean squared error of the LS estimate to the minimum variance specified by the Cramér-Rao lower bound of the structured EIV problem, to determine the conditions under which the data-driven step input estimation method is appropriate for practical applications.

## 2.2.2. Experimental validation

The validation of the data-driven step input estimation method in a practical application was necessary to demonstrate the usefulness of the method. The method performance was studied in Markovsky [2015a] using simulations and temperature experiments on a digital signal processor (DSP) of low cost. The method estimates the unknown level of step inputs by processing the sensor step response, and avoiding the sensor modeling stage. The formulation of the estimation method is a correlated errors-in-variables (EIV) problem with block-Hankel structure.

Other methods for input estimation mainly compensate the sensor transient response, for example, by recursive estimation of the compensator parameters in Shu [1993], finite impulse response (FIR) filtering in Elster et al. [2007], Niedźwiecki and Pietrzak [2016] and infinite impulse response (IIR) filtering in Pintelon et al. [1990], Elster and Link [2008]. The uncertainty propagation for these model-based compensators is based on the transfer function or state-space representations of the LTI sensor and filter systems in Link and Elster [2009] and Hale et al. [2009]. Another way to assess the measurement uncertainty is by observing the results of multiple practical measurements as it is described in Pietrzak et al. [2014] for mass and in Ogorevc et al. [2016] for temperature sensors.

To validate the data-driven step input estimation method we built a weighing system setup based on a load cell sensor. The weighing setup was constructed to ensure repeatability and reproducibility, along with different experimental realizations. Load cell sensors are versatile devices that are applied for heart and breathing physiological signal monitoring in Lee et al. [2016], clinical analysis of

sleep quality in Zahradka et al. [2018], automobile safety studies in Ballo et al. [2016], wind turbine design in Rossander et al. [2015], civil engineering structure studies in Olmi [2016], and sport bicycle design in Casas et al. [2016], to name a few.

The signal from the load cell sensor in the weighing system is conditioned using operational amplifiers. The signal conditioning amplifier has a low-pass filter to prevent aliasing from the noise. The observed measurement noise has non-white noise properties, mainly due to the characteristics of the load cell sensor. One of the assumptions of the step input estimation method formulation is that the measurement noise is Gaussian and white. Nevertheless, the estimation results discussed in Quintana-Carapia et al. [2019b] show that the method is still able to provide useful input estimations.

The empirical bias and covariance obtained after repeating the weighing experiment was compared to the bias and covariance estimations obtained in our previous research work (Quintana-Carapia et al. [2019a]), and to the minimal variance given by the Cramér-Rao lower bound (CRLB) of the structured EIV problem. We found that the mean squared error (MSE) of the step input estimate is near the CRLB, and the distance between the MSE and the CRLB provides a confidence interval for the input estimate with respect to the level of the measurement noise.

## 2.2.3. Affine input estimation

A dynamic measurement is present when the fluctuations of the measurand impact on the input estimation, such as when a low-bandwidth sensor is excited with a fast changing input. The detection of input characteristics is of interest in several scientific and industrial applications, such as those described for measuring temperature in Saggin et al. [2001], pressure in Matthews et al. [2014], acceleration in Link et al. [2007], force in Vlajic and Chijioke [2016], Hessling [2008], and mass in Shu [1993], Boschetti et al. [2013].

We developed a method to estimate the parameters of inputs that vary at a constant rate, influenced by the data-driven signal processing method that estimates the step level value using subspace techniques introduced in Markovsky [2015a], Markovsky [2015b]. An input varies at a constant rate in applications where the magnitude of interest activates the sensor gradually. An example of this affine activation is the measurement of mass while the to-be-weighted object is transported by a conveyor belt, and the profile of the input is a saturated ramp. Current solutions described in Tasaki et al. [2007], Pietrzak et al. [2014] use low pass filters to estimate the mass in motion based on the saturated part of the ramp

input. The signal processing affine input estimation methods are motivated by the need to obtain the mass of the object from the ramp before it reaches saturation.

We propose in Quintana-Carapia and Markovsky [2020] a data-driven method that estimates the affine input, which is parameterized as a straight line model where the slope and the intercept are the parameters of interest. The data-driven affine input estimation method formulates a structured errors-invariables (EIV) problem, similar to the one formulated for the step input estimation. An exponential weight is added to the recursive least-squares. This is a forgetting factor that considers that the newer samples are more relevant for the input parameters estimation. The data-driven affine input estimation method is a recursive algorithm that can be implemented in real-time since it has low computational cost.

The performance of the proposed method is compared to that of a maximum-likelihood (ML) estimation method based on local-optimization and a time-varying compensation filter. The ML method simulates the response of a sensor model to an affine input, and minimizes a cost function that is the sum of the squared differences between the actual and the simulated sensor responses. The ML method resembles the model predictive control approach, explained in Mayne [2014], in the sense that a cost function is minimized iteratively to optimize the parameters of a sensor model using the observed sensor response in a receding time horizon. The difference is that the ML method aims to estimate the unknown value of the affine input parameters instead of identifying a model and controlling the dynamic system.

After observing the simulation results, the data-driven affine input estimation method is suitable for real-time applications since it requires low computational resources. The ML method is more appropriate for off-line processing of the sensor transient response, but it can estimate also the parameters of a sensor model, and the initial conditions of the sensor. The main drawback of the ML method is the need of high computational resources.

# 3. Preliminaries

In metrology, we use the concepts of linear systems theory to estimate the value of an unknown quantity. A sensor is considered to be a causal linear time-invariant (LTI) system. The unknown quantity is the input $u$ of the sensor, and the consequences of this excitation are a change in the sensor state $\mathbf{x}$, from the initial conditions $\mathbf{x}_{\text{ini}}$, and a transient response in the sensor output $y$, see Figure 3.1. A measurement estimates the input value using the sensor response.
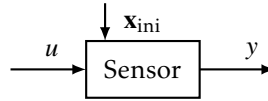


Figure 3.1.: Block diagram of an LTI sensor. The input $u$ excites the sensor and generates the sensor response $y$. To estimate the input value it is necessary to process the response.

The input estimation is a linear system problem, and can be done with or without a sensor model. The discrete-time state-space representation of a single-input single output (SISO) LTI system is

$$\begin{aligned}
\mathbf{x}(k+1) &= \mathbf{A}\mathbf{x}(k) + \mathbf{B}u(k), \quad \text{with} \quad \mathbf{x}_{\text{ini}} = \mathbf{x}(0) \\
y(k) &= \mathbf{C}\mathbf{x}(k) + Du(k) + \varepsilon(k),
\end{aligned} \tag{3.1}$$

where $\mathbf{A} \in \mathbb{R}^{n \times n}$, $\mathbf{B} \in \mathbb{R}^n$, $\mathbf{C} \in \mathbb{R}^{1 \times n}$, and $D \in \mathbb{R}$, are the model matrices, $\varepsilon$ is the measurement noise, and $n$ is the system order.

Under certain condition on the input, a discrete-time representation of the continuous-time dynamics is exact without any approximation. It is demonstrated in Ljung [1987] and in Middleton and Goodwin [1990] that when the input

is piecewise constant, then the step-invariant transformation

$$\mathbf{H}(z) = \left(1 - z^{-1}\right) \mathscr{Z}\left\{\mathscr{L}^{-1}\left\{\frac{\mathbf{H}(s)}{s}\right\}\right\} \tag{3.2}$$

is a zero-order hold sampling of the continuous time step response that leads to an exact representation of the system dynamics in discrete time with the transfer function $\mathbf{H}(z)$. It worths stating this fact here since the method studied in this thesis estimates the true value of a step input by processing samples of a sensor step response.

The methodology presented in this work is explained with SISO LTI systems, but can also be generalized to systems with multiple inputs and outputs. An example of SISO LTI sensor is the temperature sensor, but there are sensors that have single input and multiple outputs, like the gas sensors described in Munther et al. [2019], and sensors that have multiple inputs and multiple outputs, like three-axis accelerometers D'Emilia et al. [2016], radio-frequency intruder-detection sensors Ushiki et al. [2013], and radar sensors Kueppers et al. [2017].

The discrete-time state-space representation suggests that, when the model and the initial conditions are known, and in absence of measurement noise, it is sufficient to solve the system of equations

$$\underbrace{\begin{bmatrix} y(0) \\ y(1) \\ y(2) \\ \vdots \\ y(N) \end{bmatrix}}_{\mathbf{y}} = \underbrace{\begin{bmatrix} \mathbf{C} \\ \mathbf{CA} \\ \mathbf{CA}^2 \\ \vdots \\ \mathbf{CA}^N \end{bmatrix}}_{\mathcal{O}} \mathbf{x}(0) + \underbrace{\begin{bmatrix} D & & & & \\ \mathbf{CB} & D & & & \\ \mathbf{CAB} & \mathbf{CB} & D & & \\ \vdots & & \ddots & & \\ \mathbf{CA}^{N-1}\mathbf{B} & \cdots & \mathbf{CAB} & \mathbf{CB} & D \end{bmatrix}}_{\mathcal{T}} \underbrace{\begin{bmatrix} u(0) \\ u(1) \\ u(2) \\ \vdots \\ u(N) \end{bmatrix}}_{\mathbf{u}}, \tag{3.3}$$

to find the input. This system of equations $\mathbf{y} = \mathcal{O}\mathbf{x}(0) + \mathcal{T}\mathbf{u}$ is constructed from the recursions of (3.1), where $\mathcal{O}$ is the observability matrix of the system, and $\mathcal{T}$ is a Toeplitz matrix of the Markov parameters of the system.

The input estimation problem is more complex when one or more of these assumptions are not fulfilled. If the initial conditions and the measurement noise are unknown, the typical approach is to feed the output $y$ to an additional system. This additional system is built to invert the dynamics of the sensor by doing an operation that is equivalent to deconvolution, see Figure 3.2. The output $\widehat{u}$ of the additional system aims to estimate the input $u$. This system is called compensator because the transient time of the input estimation $\widehat{u}$ is smaller than the transient time of $y$.

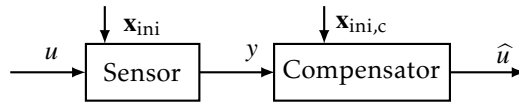Figure 3.2.: Input estimation using a compensator that processes the sensor response $y$. The compensator is an additional system that inverts the dynamics of the sensor.

In the next sections the input is modeled as a multiple of the unit step function, to describe methods for estimating the input step level in two conditions: when the model of the sensor is a-priori given and when the method is not available.

## 3.1. Step input estimation with system model

With a step input $u$, where $u(k) = u$, for $k \geq 0$, and $u(k) = 0$, for $k < 0$, the discrete-time state-space representation of the LTI sensor is equivalent to an augmented autonomous system

$$
\mathbf{x}_a(k+1) = \underbrace{\begin{bmatrix} \mathbf{A} & \mathbf{B} \\ 0 & 1 \end{bmatrix}}_{\mathbf{A}_a} \mathbf{x}_a(k), \quad \text{where } \mathbf{x}_a(k) = \begin{bmatrix} \mathbf{x}(k) \\ u(k) \end{bmatrix}, \quad \mathbf{x}_{\text{ini}} = \mathbf{x}(0)
$$

$$
y(k) = \underbrace{\begin{bmatrix} \mathbf{C} & D \end{bmatrix}}_{\mathbf{C}_a} \mathbf{x}_a(k).
$$

(3.4)

The eigenvalues $\lambda$ of the augmented autonomous system are found using

$$
|\lambda \mathbf{I} - \mathbf{A}_a| = \left| \lambda \mathbf{I} - \begin{bmatrix} \mathbf{A} & \mathbf{B} \\ 0 & 1 \end{bmatrix} \right| = |\lambda \mathbf{I} - \mathbf{A}| (\lambda - 1) = 0.
$$

Therefore, the eigenvalues (poles) of the augmented autonomous system (3.4) are the eigenvalues, poles, of the LTI system, with the additional eigenvalue $\lambda = 1$, pole at $(1, 0)$.

Since the input $u(k+1) = u(k)$, for $k \geq 0$, is an augmented state of the autonomous system, and the system is known, a state estimator is sufficient to estimate the input. In these conditions, the Kalman filter estimates recursively the input value.

## 3.2. Step input estimation without system model

If a model of the sensor is not available, it might be needed to identify a model using the inputs and outputs to design later a compensator using the identified model. However, the input is unknown and the model should be identified using only the sensor output.

A feasible method can be one that identifies a model of the sensor from the step response, assuming we have exact data, and later estimates the input step level using the identified sensor model. The model identification consists in the estimation of the matrices $\widehat{\mathbf{A}}_a$ and $\widehat{\mathbf{C}}_a$, and the initial conditions $\widehat{\mathbf{x}}(0)$. To do this, consider that the Hankel matrix $\mathcal{H}(y) \in \mathbb{R}^{n \times n}$, constructed from any linearly independent $n$ autonomous responses from the sensor's initial conditions, is full

column rank. Then, we can express the following equality

$$
\underbrace{\begin{bmatrix} y(0) & y(1) & \cdots & y(n-1) \\ y(1) & y(2) & \cdots & y(n) \\ \ddots & \ddots & \ddots \\ y(n-1) & y(n) & \cdots & y(2n-2) \end{bmatrix}}_{\mathcal{H}(y)} = \underbrace{\begin{bmatrix} \mathbf{C}_a \\ \mathbf{C}_a \mathbf{A}_a \\ \vdots \\ \mathbf{C}_a \mathbf{A}_a^{n-1} \end{bmatrix}}_{\mathcal{O}_a} \underbrace{\begin{bmatrix} \mathbf{x}_a(0) & \mathbf{x}_a(1) & \cdots & \mathbf{x}_a(n-1) \end{bmatrix}}_{\mathbf{X}_{\mathrm{ini}}},
$$

(3.5)

where $\mathbf{X}_{\mathrm{ini}}$ is a matrix with the initial conditions of the *n* free responses. A singular value decomposition of $\mathcal{H}(y)$

$$
\mathbf{U}\boldsymbol{\Sigma}\mathbf{V} = \mathcal{H}(y), \tag{3.6}
$$

permits the estimation of the observability matrix $\mathcal{O}_a$ and the initial conditions $\mathbf{X}_{\mathrm{ini}}$, for example, by choosing

$$
\widehat{\mathcal{O}}_a = \mathbf{U}\sqrt{\boldsymbol{\Sigma}}, \quad \text{and} \quad \widehat{\mathbf{X}}_{\mathrm{ini}} = \sqrt{\boldsymbol{\Sigma}}\mathbf{V}. \tag{3.7}
$$

The matrices $\widehat{\mathbf{A}}_a$ and $\widehat{\mathbf{C}}_a$ can be estimated, from $\widehat{\mathcal{O}}_a$, by solving a system of equations. In order to estimate the input, it is necessary to find a minimal representation of the autonomous system, by doing a linear transformation that removes the pole at $(1,0)$, and recovers the matrices $\widehat{\mathbf{A}}, \widehat{\mathbf{B}}, \widehat{\mathbf{C}}$, and $\widehat{\mathbf{D}}$.

A second method can estimate the step input when the model of the LTI sensor is unknown but its static gain *G* is given. Using the static gain *G*, we can express $y = Gu$, where *u* is the input exact value and *y* is the exact sensor steady state response. The total response of the system is the sum of the transient and the steady-state responses. Thus, considering the augmented autonomous model, we can write

$$
y = G\,u + \mathcal{O}_a\,\mathbf{x}_a(0), \tag{3.8}
$$

which in matrix form is

$$
\underbrace{\begin{bmatrix} y(0) \\ y(1) \\ \vdots \\ y(N) \end{bmatrix}}_{\mathbf{y}} = \underbrace{\begin{bmatrix} G & \mathbf{C}_a \\ G & \mathbf{C}_a \mathbf{A}_a \\ \vdots & \vdots \\ G & \mathbf{C}_a \mathbf{A}_a^N \end{bmatrix}}_{\mathbf{K}} \begin{bmatrix} u \\ \mathbf{x}_a(0) \end{bmatrix}. \tag{3.9}
$$

Then, it is necessary to estimate the observability matrix of the augmented system, followed by the estimation of the input *u*, and the initial conditions, using least-squares

$$
\begin{bmatrix} \widehat{u} \\ \widehat{\mathbf{x}}_{a(0)} \end{bmatrix} = \left( \mathbf{K}^\top \mathbf{K} \right)^{-1} \mathbf{K}^\top \mathbf{y}. \tag{3.10}
$$

A third method can directly estimate the input step level from the step response, without identifying a sensor model. To derive this method, we use the first difference operator $\Delta$, defined as $\Delta y(k) = y(k+1) - y(k)$. Applying the first difference operator to the system state-space representation (3.1) results in the autonomous system

$$\Delta \mathbf{x}(k+1) = \mathbf{A}\Delta \mathbf{x}(k), \quad \Delta y(k) = \mathbf{C}\Delta \mathbf{x}(k), \quad \text{with} \quad \Delta \mathbf{x}_{\text{ini}} = \Delta \mathbf{x}(0), \qquad (3.11)$$

where $\Delta u(k) = \mathbf{0}$, for $k \geq 0$, and $\Delta \mathbf{x}(0) = (\mathbf{A} - \mathbf{I})\mathbf{x}(0) + \mathbf{B}u$.

If the response $\Delta y$ of this autonomous system is persistently exciting of order $L$, then the rank of the Hankel matrix $\mathcal{H}_{L+1}(\Delta y)$ of $L+1$ block rows constructed from $\Delta y$ satisfies

$$\text{rank}\left(\mathcal{H}_{L+1}\left(\Delta y\right)\right) = \text{rank}\left(\begin{bmatrix} \Delta y(1) & \Delta y(2) & \cdots & \Delta y(n) \\ \Delta y(2) & \Delta y(3) & \cdots & \Delta y(n+1) \\ \cdot\cdot & \cdot\cdot & \cdot\cdot & \\ \Delta y(L+1) & \Delta y(L+2) & \cdots & \Delta y(L+n) \end{bmatrix}\right) \leq L, \quad (3.12)$$

and the Hankel matrix $\mathcal{H}_{L+1}(\Delta y)$ is a linear map to the natural responses of the augmented autonomous system (3.4)

$$\mathbf{y}_{\text{natural}} = \mathcal{H}\left(\Delta y\right)\boldsymbol{\ell}, \qquad (3.13)$$

from any vector $\boldsymbol{\ell} \in \mathbb{R}^n$. The total response of the system is the sum of the forced response, due to the applied input $u$ and the natural response

$$\mathbf{y} = \mathbf{y}_{\text{forced}} + \mathbf{y}_{\text{natural}} = Gu + \mathcal{H}\left(\Delta y\right)\boldsymbol{\ell}, \qquad (3.14)$$

that is equivalent to

$$\underbrace{\begin{bmatrix} y(n+1) \\ \vdots \\ y(N) \end{bmatrix}}_{\mathbf{y}} = \underbrace{\begin{bmatrix} G & \Delta y(1) & \Delta y(2) & \cdots & \Delta y(n) \\ G & \Delta y(2) & \Delta y(3) & \cdots & \Delta y(n+1) \\ \vdots & \cdot\cdot & \cdot\cdot & \cdot\cdot & \\ G & \Delta y(N-n) & \Delta y(N-n+1) & \cdots & \Delta y(N-1) \end{bmatrix}}_{\mathbf{K}} \underbrace{\begin{bmatrix} u \\ \boldsymbol{\ell} \end{bmatrix}}_{\boldsymbol{\theta}}, \qquad (3.15)$$

where $N$ is the number of samples. From this point of view, the vector $\boldsymbol{\ell}$ is a linear transformation of the system's initial conditions. The solution to this system of equations exist and is unique when we have exact data. Nevertheless, in practice, the observations of the sensor step response are perturbed by noise.

Assuming that the observations of the vector $\mathbf{y}$ are perturbed by measurement noise $\epsilon$ of zero mean and given variance $\sigma_\epsilon^2$, we can express

$$\widetilde{\mathbf{y}} = \mathbf{y} + \epsilon, \qquad (3.16)$$

and

$$\widetilde{\mathbf{K}} = \mathbf{K} + \mathbf{E}. \tag{3.17}$$

The matrix $\mathbf{E}$ is constructed with the noise data, and is given as

$$\mathbf{E} = \begin{bmatrix} 0 & \Delta\varepsilon(1) & \Delta\varepsilon(2) & \cdots & \Delta\varepsilon(n) \\ 0 & \Delta\varepsilon(2) & \Delta\varepsilon(3) & \cdots & \Delta\varepsilon(n+1) \\ \vdots & \vdots & \vdots & & \vdots \\ 0 & \Delta\varepsilon(N-n) & \Delta\varepsilon(N-n+1) & \cdots & \Delta\varepsilon(N-1) \end{bmatrix}. \tag{3.18}$$

Therefore, the matrix $\widetilde{\mathbf{K}}$ is expressed as

$$\widetilde{\mathbf{K}} = \begin{bmatrix} G & \Delta\widetilde{y}(1) & \Delta\widetilde{y}(2) & \cdots & \Delta\widetilde{y}(n) \\ G & \Delta\widetilde{y}(2) & \Delta\widetilde{y}(3) & \cdots & \Delta\widetilde{y}(n+1) \\ \vdots & \vdots & \vdots & & \vdots \\ G & \Delta\widetilde{y}(N-n) & \Delta\widetilde{y}(N-n+1) & \cdots & \Delta\widetilde{y}(N-1) \end{bmatrix}. \tag{3.19}$$

The underlying system of equations

$$\widetilde{\mathbf{y}} = \widetilde{\mathbf{K}}\boldsymbol{\theta} \tag{3.20}$$

is another representation of the minimization problem

$$\widehat{\boldsymbol{\theta}} = \underset{\boldsymbol{\theta}}{\operatorname{argmin}} \; \left\| \widetilde{\mathbf{y}} - \widetilde{\mathbf{K}}\boldsymbol{\theta} \right\|_2^2. \tag{3.21}$$

where $\widetilde{\mathbf{y}} = \begin{bmatrix} \widetilde{y}(n+1) & \dots & \widetilde{y}(N) \end{bmatrix}^\top$, and $\widehat{\boldsymbol{\theta}} = \begin{bmatrix} \widehat{u} & \widehat{\boldsymbol{\ell}}^\top \end{bmatrix}^\top$. This minimization problem is an errors-in-variables (EIV) problem with Hankel structure, and correlation between the regression matrix $\widetilde{\mathbf{K}}$ and the regressor vector $\widetilde{\mathbf{y}}$.

The data-driven step input estimation method converts the output-error simultaneous model identification and input estimation problem into an errors-in-variables (EIV) input estimation problem. The cost of avoiding the parametric sensor modeling is to deal with a more difficult stochastic framework.

The problem (3.20) admits a least-squares (LS) solution with normal equations given by

$$\widetilde{\mathbf{K}}^\top \widetilde{\mathbf{K}}\boldsymbol{\theta} = \widetilde{\mathbf{K}}^\top \widetilde{\mathbf{y}}. \tag{3.22}$$

The closed form of the LS solution can be expressed as

$$\widehat{\boldsymbol{\theta}} = \widetilde{\mathbf{K}}^\dagger \widetilde{\mathbf{y}} = (\widetilde{\mathbf{K}}^\top \widetilde{\mathbf{K}})^{-1} \widetilde{\mathbf{K}}^\top \widetilde{\mathbf{y}}, \tag{3.23}$$

where $\widetilde{\mathbf{K}}^{\dagger}$ is the pseudo-inverse matrix of $\widetilde{\mathbf{K}}$. As the number of samples $N$ increases, the number of rows of the matrix $\widetilde{\mathbf{K}}$ grows, making the pseudo-inverse computation inefficient since it requires larger flops, memory and time.

For metrology applications, it is desired to have a fast solution that can be obtained in real-time. The recursive algorithm (RLS) is a least-squares alternative to implement the step input estimation method in real-time. The RLS recursively updates the solution of the system of equations, for each newly acquired sensor response sample, considering the previous value of the estimation, instead of performing a matrix inversion. An expression of the RLS equations is given in Kailath et al. [2000] as

$$\widehat{\boldsymbol{\theta}}(k) = \widehat{\boldsymbol{\theta}}(k-1) + \boldsymbol{\kappa}_k \left( \widetilde{y}(k) - \widetilde{\mathbf{k}}_k \widehat{\boldsymbol{\theta}}(k-1) \right),$$

$$\boldsymbol{\kappa}_k = \boldsymbol{\Psi}(k-1)\widetilde{\mathbf{k}}_k^{\top} / \left( 1 + \widetilde{\mathbf{k}}_k \boldsymbol{\Psi}(k-1)\widetilde{\mathbf{k}}_k^{\top} \right) \qquad (3.24)$$

$$\boldsymbol{\Psi}(k) = \left( \mathbf{I} - \boldsymbol{\kappa}_k \widetilde{\mathbf{k}}_k \right) \boldsymbol{\Psi}(k-1),$$

for $k = 2n+1, 2n+2, \ldots$, where $\widetilde{\mathbf{k}}_k$ represents the row of $\widetilde{\mathbf{K}}$ that corresponds to the $k$−th sample, $\boldsymbol{\kappa}_k$ is a gain scalar, and $\boldsymbol{\Psi}(k)$ is a covariance matrix. The estimates and the covariance matrix are initialized using the first $n+1$ samples, i.e., $\widehat{\boldsymbol{\theta}}(2n+1) = \left( \widetilde{\mathbf{K}}_{n+1}^{\top} \widetilde{\mathbf{K}}_{n+1} \right)^{-1} \widetilde{\mathbf{K}}_{n+1}^{\top} \widetilde{\mathbf{y}}_{n+1}$ and $\boldsymbol{\Psi}(2n+1) = \left( \widetilde{\mathbf{K}}_{n+1}^{\top} \widetilde{\mathbf{K}}_{n+1} \right)^{-1}$, where $\widetilde{\mathbf{K}}_{n+1}$ is the matrix $\widetilde{\mathbf{K}}$ with the first $n+1$ rows, and $\widetilde{\mathbf{y}}_{n+1}$ is the vector $\widetilde{\mathbf{y}}$ with the first $n+1$ elements. Since the RLS is a recursive implementation of the least-squares computation, the RLS solution is equivalent to the LS solution. Moreover, the statistical analysis of the LS solution is valid also for the RLS solution, and is preferred since it is simpler to express the statistics using the closed form of the LS solution.

The computational complexity of the RLS algorithm solution to the system of equations (3.15) is $O\left((n+1)^2\right)$. The largest computational requirement is for the initialization of the algorithm, where a matrix inverse is required when the number of samples is just enough to have a square matrix $\widetilde{\mathbf{K}}_{n+1}$. From there on, the RLS algorithm updates the solution with linear complexity. Therefore, even though a large number of samples $N$ makes the matrix in the system of equations (3.15) increase in the number of rows, the estimation of the solution does not increase in complexity. The data-driven step input estimation method is then scalable for any sensor of order $n$, and can be executed in devices with limited computational resources, provided that the computation of the $n+1 \times n+1$ inverse matrix is feasible.

The LS solution is used even though it might exhibit bias due to the correlation of the perturbation in $\widetilde{\mathbf{K}}$ with the perturbation in $\widetilde{\mathbf{y}}$. To conduct the statistical

analysis of the step input estimation method, it is more convenient to use the standard least-squares terminology. The statistical analysis results obtained from LS treatment are fully compatible with the RLS estimation results. The well known bias and covariance results for the LS estimator cannot be invoked because they assume that the additive perturbation only affects the regressor, and that there is no correlation between the regressor and the regression matrix.

# 4. Statistical Analysis

*The results of this chapter were published in Quintana Carapia, G., Markovsky, I. Pintelon, R., Csurcsia, P.Z., and Verbeke, D., "Bias and covariance of the least-squares estimate in a structured errors-in-variables problem", Computational Statistics & Data Analysis journal, Vol. 144, 2020, ISSN 0167-9473, doi:10.1016/j.csda.2019.106893.*

The linear estimation problems with perturbation in both the regression matrix and the regressor are errors-in-variables (EIV) problems. The formulation of the data-driven step input estimation problem is an EIV problem. This formulation gives a Hankel structure to the perturbed regression matrix, which is correlated with the regressor vector. The solution to the structured EIV problem is proposed by means of a recursive least squares algorithm to benefit from its simplicity for online implementations in devices with small computational resources. The properties of this least-squares (LS) approximation cannot be inferred from classical results. The statistical analysis aims to calculate the statistical moments of the least-squares estimate to evaluate these properties. The statistical analysis of the LS estimate demands an additional effort when the regression matrix is structured, and when it is correlated with the regressor, in a EIV problem.

The total least-squares methods reviewed in Markovsky and Van Huffel [2007] are not appropriate to solve structured EIV problems. To overcome the challenges imposed by the structure, methods such as the structured total least-squares described in Lemmerling and Van Huffel [2002] and the structured total maximum likelihood presented in Beck and Eldar [2010] are proposed. Nevertheless, the structured total least-squares requires optimization and even the recursive alternatives such as the one developed by Rhode et al. [2014] are not suitable for online applications in devices with reduced computational resources. Moreover, current versions of the structured total maximum likelihood method consider uncorrelated cases only. The instrumental-variables methods described in Söderström [2018] are other alternatives to implement recursive algorithms that solve EIV problems. The generalized instrumental-variables estimator is one example of them, that is mainly used in the identification of linear systems from observed input and output data. However, it is not straightforward to use the generalized instrumental-variables estimator to implement the direct estimation of the input from the observed output bypassing the model identification, like the data-driven input estimation method does. Thus, the recursive LS method is proposed in Markovsky [2015a] to get a real-time approximation to the structured EIV problem solution. Even though this estimation is suboptimal, we benefit from its simplicity and suitability for implementation in devices with limited computational resources.

As it is described in the works of Ferrero and Salicone [2006] and Hessling [2013], and in the review of Hack and ten Caten [2012], the measurement results are meaningful only when the input estimation is provided together with an assessment of its uncertainty. For an unbiased estimator, the uncertainty is assessed from the estimation variance. On the other hand, for a biased estimator the mean-

squared error is the main metric used to describe the uncertainty. Therefore, it is necessary to know the first two statistical moments of the estimation.

This chapter describes a methodology to study the statistical moments of the LS solution for the structured EIV problem introduced in Markovsky [2015a,b] for the data-driven step input estimation method. The described statistical analysis obtains the statistical moments of the LS solution, and they allow to assess the estimation uncertainty in terms of the mean-squared error. The statistical analysis results provide insight into the impact that the structure of the regression matrix and its correlation with the regressor has on the uncertainty of the RLS estimate.

## 4.1. Statistical analysis of the data-driven step input estimation method

For an overdetermined system of linear equations, constructed by the data-driven step input estimation method (3.21), the least-squares (LS) solution is given by 3.23. The objective of the statistical analysis is to obtain the bias and the covariance of the solution $\widehat{\theta}$ to the structured and correlated EIV problem (3.20). The bias and the covariance are computed using the mathematical expectation operator $\mathbb{E}\{\cdot\}$. First we substitute the expressions (3.16) and (3.17) in Equation (3.23) to obtain

$$\widehat{\theta} = \left( (\mathbf{K}+\mathbf{E})^\top (\mathbf{K}+\mathbf{E}) \right)^{-1} (\mathbf{K}+\mathbf{E})^\top (\mathbf{y}+\boldsymbol{\epsilon}),$$

which is equivalent to

$$\widehat{\theta} = \left( \left( \mathbf{K}^\top \mathbf{K} \right) \left( \mathbf{I} + \left( \mathbf{K}^\top \mathbf{K} \right)^{-1} \left( \mathbf{K}^\top \mathbf{E} + \mathbf{E}^\top \mathbf{K} + \mathbf{E}^\top \mathbf{E} \right) \right) \right)^{-1} (\mathbf{K}+\mathbf{E})^\top (\mathbf{y}+\boldsymbol{\epsilon}),$$

and

$$\widehat{\theta} = (\mathbf{I}+\mathbf{M})^{-1} \mathbf{Q}^{-1} (\mathbf{K}+\mathbf{E})^\top (\mathbf{y}+\boldsymbol{\epsilon}), \qquad (4.1)$$

where

$$\mathbf{Q} = \mathbf{K}^\top \mathbf{K}, \quad \text{and} \quad \mathbf{M} = \mathbf{Q}^{-1}(\mathbf{K}^\top \mathbf{E} + \mathbf{E}^\top \mathbf{K} + \mathbf{E}^\top \mathbf{E}). \qquad (4.2)$$

Applying a second-order Taylor expansion of the inverse matrix

$$(\mathbf{I}+\mathbf{M})^{-1} \approx \mathbf{I} - \mathbf{M} + \mathbf{M}^2, \qquad (4.3)$$

that is valid when the SNR is sufficiently high, and therefore $\mathbf{E}$ and $\mathbf{M}$ are small, satisfying the constraint on the spectral radius $\|\mathbf{M}\| < 1$. The neglected term in the Taylor series expansion is of the order $O(\|M\|^3)$. We can express the estimate as

$$\widehat{\theta} \approx \left( \mathbf{I} - \mathbf{M} + \mathbf{M}^2 \right) \mathbf{Q}^{-1} (\mathbf{K}+\mathbf{E})^\top (\mathbf{y}+\boldsymbol{\epsilon}). \qquad (4.4)$$

Now that the perturbation variables $\epsilon$ and $\mathbf{E}$ are no longer inside an inverse matrix, we can compute the mathematical expectation of expressions derived from the Taylor series approximation (4.4) of $\widehat{\boldsymbol{\theta}}$. The bias of the estimate $\widehat{\boldsymbol{\theta}}$ is obtained from

$$\mathbf{b}\left(\widehat{\boldsymbol{\theta}}\right) = \boldsymbol{\mu}\left(\widehat{\boldsymbol{\theta}}\right) - \boldsymbol{\theta}, \tag{4.5}$$

where $\boldsymbol{\mu}\left(\widehat{\boldsymbol{\theta}}\right) = \mathbb{E}\left\{\widehat{\boldsymbol{\theta}}\right\}$, and $\boldsymbol{\theta} = \mathbf{K}^{\dagger}\mathbf{y} = \mathbf{Q}^{-1}\mathbf{K}^{\top}\mathbf{y}$ is the true value. The covariance of the estimate $\widehat{\boldsymbol{\theta}}$ is obtained from

$$\mathbf{C}\left(\widehat{\boldsymbol{\theta}}\right) = \mathbb{E}\left\{\left(\widehat{\boldsymbol{\theta}} - \boldsymbol{\mu}\left(\widehat{\boldsymbol{\theta}}\right)\right)\left(\widehat{\boldsymbol{\theta}} - \boldsymbol{\mu}\left(\widehat{\boldsymbol{\theta}}\right)\right)^{\top}\right\}. \tag{4.6}$$

The terms derived from (4.4) that do not contribute to the bias and to the covariance are filtered out by the mathematical expectation operator, described in Papoulis and Pillai [2002], considering the following general rules that are valid regardless of the existence of structure in the regression problem:

- the expected values $\mathbb{E}\{\mathbf{E}\} = \mathbf{0}$, and $\mathbb{E}\{\epsilon\} = \mathbf{0}$, since $\mathbf{E}$ and $\epsilon$ are zero-mean random variables, and

- the expected values of odd order moments, such as $\mathbb{E}\{\mathbf{E}^{\top}\mathbf{E}\mathbf{E}^{\top}\}$, are zero.

Moreover, the second-order approximation disregards moments of order four and higher.

The normality assumption of the perturbation noise is necessary to provide more prior information into the method formulation. The second order Taylor series expansion (4.4) is developed considering the perturbation noise that gets into the regression matrix from the sensor transient response. Assuming only that the perturbation noise is distributed with zero mean and variance $\sigma_{\epsilon}^{2}$ is not enough. If we additionally assume normality for the perturbation noise, then we benefit from the knowledge of the third moment equal to zero due to symmetry, and the fourth moment equal to three times the squared variance, ~~which can be disregarded since $3\sigma_{\epsilon}^{4} \ll \sigma_{\epsilon}^{2}$.~~

After removing the terms with negligible expected value, we have expressions that are approximations of the LS estimation bias and covariance. These expressions are different depending on the type of EIV problem considered. Subsections 3.1 and 3.2 describe the resulting expressions for the unstructured and structured EIV problems, respectively. The perturbations in the considered unstructured EIV problem are independent. Comparing the expressions that result from the statistical analysis, we get an insight of what is the impact that the structure and the correlation have on the LS solution of the structured EIV problem.

## 4.1.1. Bias and covariance of the LS estimator for an unstructured EIV problem with uncorrelated noise

First, the statistics of the least-squares estimator (3.23) of an unstructured EIV problem is discussed, provided that the perturbations of the regression matrix and the regressor are i.i.d. normally distributed with zero mean, and variances $\sigma_{\mathbf{E}}^2$ and $\sigma_\epsilon^2$, respectively. Therefore, the terms in the Taylor series expansion that contain products of $\mathbf{E}$ and $\epsilon$ have zero expected value. After removing the terms without contribution to the bias, and to the covariance, with the mathematical expectation operator, the analytic approximation of the bias (4.5) is given by

$$\mathbf{b}_{\mathrm{p}}\left(\widehat{\boldsymbol{\theta}}\right) \approx \sigma_{\mathbf{E}}^2 \left(2 + 2n - N\right) \mathbf{Q}^{-1} \boldsymbol{\theta}, \tag{4.7}$$

and the covariance (4.6) is approximated by

$$\mathbf{C}_{\mathrm{p}}\left(\widehat{\boldsymbol{\theta}}\right) \approx \sigma_\epsilon^2 \, \mathbf{Q}^{-1} + \sigma_{\mathbf{E}}^2 \, \mathrm{trace}\left(\boldsymbol{\theta}\boldsymbol{\theta}^\top\right) \mathbf{Q}^{-1} - \sigma_{\mathbf{E}}^4 \left(2 + 2n - N\right)^2 \mathbf{Q}^{-1} \boldsymbol{\theta}\boldsymbol{\theta}^\top \mathbf{Q}^{-1}, \tag{4.8}$$

where the subscript p stands for prediction of the bias and covariance. The derivation of equations (4.7) and (4.8) is described in Appendix 1. We use the results described in Vaccaro [1994] §3 and Stewart [1990] §2.1 for the expected values of products of unstructured matrices with perturbations. Equations (4.7) and (4.8) depend on the unobservable true values $\boldsymbol{\theta}$, $\mathbf{K}$, and on the variance of the perturbations. The observed variables are $\widetilde{\mathbf{y}}$, $\widetilde{\mathbf{K}}$, and from them we compute $\widehat{\boldsymbol{\theta}}$. It is proposed to directly substitute the observed variables in the analytic expressions. The substitution gives an approximation of the estimation bias and covariance using the observed data. We have then

$$\widetilde{\mathbf{b}}_{\mathrm{p}}\left(\widehat{\boldsymbol{\theta}}\right) \approx \sigma_{\mathbf{E}}^2 \left(2 + 2n - N\right) \widetilde{\mathbf{Q}}^{-1} \widehat{\boldsymbol{\theta}}, \tag{4.9}$$

$$\widetilde{\mathbf{C}}_{\mathrm{p}}\left(\widehat{\boldsymbol{\theta}}\right) \approx \sigma_\varepsilon^2 \, \widetilde{\mathbf{Q}}^{-1} + \sigma_{\mathbf{E}}^2 \, \mathrm{trace}\left(\widehat{\boldsymbol{\theta}}\widehat{\boldsymbol{\theta}}^\top\right) \widetilde{\mathbf{Q}}^{-1} - \sigma_{\mathbf{E}}^4 \left(2 + 2n - N\right)^2 \widetilde{\mathbf{Q}}^{-1} \widehat{\boldsymbol{\theta}}\widehat{\boldsymbol{\theta}}^\top \widetilde{\mathbf{Q}}^{-1}. \tag{4.10}$$

In order to have a prediction of the estimation bias and covariance, the variances $\sigma_{\mathbf{E}}^2$ and $\sigma_\epsilon^2$ and the observed variables $\widetilde{\mathbf{y}}$, $\widetilde{\mathbf{K}}$, and $\widehat{\boldsymbol{\theta}}$ are needed.

## 4.1.2. Bias and covariance of the LS estimator for a structured EIV problem with noise correlation

This subsection describes the statistics of a structured EIV problem with correlation between the perturbations of the regression matrix and the regressor. The

structured EIV problem is given by the step input estimation method (3.21). The correlation is a consequence of the construction of the block-Hankel matrix in the regression matrix $\widetilde{\mathbf{K}}$ with the first difference of the elements in the regressor $\widetilde{\mathbf{y}}$.

The mathematical expectation operator is applied to the Taylor series expansion of the LS estimate (4.4). After removing the terms with negligible expected value, and considering the structure of matrix $\mathbf{K}$, the estimation bias (4.5) is approximated by

$$\mathbf{b}_p\left(\widehat{\boldsymbol{\theta}}\right) \approx \mathbf{Q}^{-1}\left(\left(\mathbf{K}^\top \mathbf{B}_1 - \mathbf{B}_2\right)\mathbf{x} - \left(\mathbf{K}^\top \mathbf{B}_3 - \mathbf{B}_4\right)\right), \tag{4.11}$$

whereas, the estimation covariance (4.6) is approximated by

$$\mathbf{C}_p\left(\widehat{\boldsymbol{\theta}}\right) \approx \mathbf{K}^\dagger\left(\sigma_\epsilon^2 \mathbf{I}_{N-n} + \mathbf{C}_1 - \mathbf{C}_2 - \mathbf{C}_2^\top\right)\mathbf{K}^{\dagger\top} - \mathbf{b}_p\left(\widehat{\boldsymbol{\theta}}\right)\mathbf{b}_p^\top\left(\widehat{\boldsymbol{\theta}}\right), \tag{4.12}$$

where $\mathbf{B}_1 = \mathbb{E}\left\{\mathbf{E}\mathbf{K}^\dagger\mathbf{E}\right\}$, $\mathbf{B}_2 = \mathbb{E}\left\{\mathbf{E}^\top\mathbf{P}_\perp\mathbf{E}\right\}$, $\mathbf{B}_3 = \mathbb{E}\left\{\mathbf{E}\mathbf{K}^\dagger\boldsymbol{\epsilon}\right\}$, $\mathbf{B}_4 = \mathbb{E}\left\{\mathbf{E}^\top\mathbf{P}_\perp\boldsymbol{\epsilon}\right\}$, $\mathbf{C}_1 = \mathbb{E}\left\{\mathbf{E}\boldsymbol{\theta}\boldsymbol{\theta}^\top\mathbf{E}^\top\right\}$, $\mathbf{C}_2 = \mathbb{E}\left\{\mathbf{E}\boldsymbol{\theta}\boldsymbol{\epsilon}^\top\right\}$, $\mathbf{P} = \mathbf{K}\mathbf{K}^\dagger$, and $\mathbf{P}_\perp = \mathbf{I} - \mathbf{P}$. The derivation of equations (4.11) and (4.12) is described in Appendix 1. The expected values $\mathbf{B}_1$, $\mathbf{B}_2$, $\mathbf{B}_3$, $\mathbf{B}_4$, $\mathbf{C}_1$ and $\mathbf{C}_2$ are obtained using the results of Lemma 1.

**Lemma 1.** *Let* $\mathbf{E} \in \mathbb{R}^{(N-n)\times(n+1)}$ *be the partitioned matrix*

$$\mathbf{E} = \begin{bmatrix} \mathbf{0}_{N-n\times 1} & \mathscr{H}(\boldsymbol{\epsilon})\mathbf{D}_{n+1\times n}^{1,0} \end{bmatrix},$$

*where* $\mathscr{H}(\boldsymbol{\epsilon}) \in \mathbb{R}^{(N-n)\times(n+1)}$ *is the block-Hankel matrix of* $N-n$ *rows and* $n$ *columns*

$$\mathscr{H}(\boldsymbol{\epsilon}) = \begin{bmatrix} \varepsilon(0) & \varepsilon(1) & \cdots & \varepsilon(n) \\ \varepsilon(1) & \varepsilon(2) & \cdots & \varepsilon(n+1) \\ \vdots & \vdots & & \vdots \\ \varepsilon(N-n-1) & \varepsilon(N-n) & \cdots & \varepsilon(N-1) \end{bmatrix},$$

*constructed from samples of the i.i.d. normally distributed random variable* $\boldsymbol{\epsilon} \sim \mathcal{N}(0, \sigma_\epsilon^2)$. *Let* $\mathbf{D}_{r\times c}^{1,d}$ *and* $\mathbf{D}_{r\times c}^{2,d}$ *be the first and second-order finite differences matricial operators of dimensions* $r \times c$ *starting from the subdiagonal* $d$, *for example,*

$$\mathbf{D}_{4\times 3}^{1,-1} = \begin{bmatrix} 0 & 0 & 0 \\ -1 & 0 & 0 \\ 1 & -1 & 0 \\ 0 & 1 & -1 \end{bmatrix}, \; \mathbf{D}_{4\times 3}^{2,0} = \begin{bmatrix} -1 & 0 & 0 \\ 2 & -1 & 0 \\ -1 & 2 & -1 \\ 0 & -1 & 2 \end{bmatrix}.$$

*For a compatible deterministic matrix* $\mathbf{A}$, *or vector* $\mathbf{a}$, *the following expected values hold.*

$\mathbb{E}\{\mathbf{EAE}\} = \mathbf{Z}$, *where* $\mathbf{z}_{i1} = \mathbf{0}$, *and* $z_{ij} = \sigma_\epsilon^2 \operatorname{Tr}\left(\mathbf{A} \begin{bmatrix} \mathbf{0}_{N-n} & \mathbf{D}_{N-n \times n}^{2,j-i} \end{bmatrix}\right)$,

   *for* $i = 1, \cdots, N-n$, *and* $j = 2, \cdots, n+1$.

$\mathbb{E}\left\{\mathbf{E}^\top \mathbf{AE}\right\} = \mathbf{Z}$, *where* $\mathbf{z}_{1j} = \mathbf{0}$, $\mathbf{z}_{i1} = \mathbf{0}$, *and* $z_{ij} = \sigma_\epsilon^2 \operatorname{Tr}\left(\mathbf{A}\, \mathbf{D}_{N-n \times N-n}^{2,j-i+1}\right)$,

   *for* $i = 2, \cdots, n+1$, *and* $j = 2, \cdots, n+1$.

$\mathbb{E}\left\{\mathbf{EAE}^\top\right\} = \mathbf{Z}$, *where* $z_{ij} = \sigma_\epsilon^2 \operatorname{Tr}\left(\mathbf{A} \begin{bmatrix} 0 & \mathbf{0}_n^\top \\ \mathbf{0}_n & \mathbf{D}_{n \times n}^{2,j-i+1} \end{bmatrix}\right)$,

   *for* $i = 1, \cdots, N-n$, *and* $j = 1, \cdots, N-n$.

$\mathbb{E}\{\mathbf{EA}\boldsymbol{\epsilon}\} = \mathbf{z}$, *where* $z_i = \sigma_\epsilon^2 \operatorname{Tr}\left(\mathbf{A} \begin{bmatrix} \mathbf{0}_{N-n} & \mathbf{D}_{N-n \times n}^{1,n+1-i} \end{bmatrix}\right)$,

   *for* $i = 1, \cdots, N-n$.

$\mathbb{E}\left\{\mathbf{E}^\top \mathbf{A}\boldsymbol{\epsilon}\right\} = \mathbf{z}$, *where* $z_1 = 0$, *and* $z_i = \sigma_\epsilon^2 \operatorname{Tr}\left(\mathbf{A}\, \mathbf{D}_{N-n \times N-n}^{1,n+2-i}\right)$,

   *for* $i = 2, \cdots, n+1$.

$\mathbb{E}\left\{\mathbf{Ea}\boldsymbol{\epsilon}^\top\right\} = \mathbf{Z}$, *where each column* $\mathbf{Z}_j = -\sigma_\epsilon^2\, \mathbf{D}_{N-n \times n+1}^{1,-j} \mathbf{R}_{n+1}\, \mathbf{a}$,

   *for* $j = 1, \cdots, N-n$, *with* $\mathbf{R}_{n+1} = \begin{bmatrix} & \mathbf{R}_n \\ 0 & \end{bmatrix}$,

   *where* $\mathbf{R}_n$ *is a reversal matrix.*

The proof of the lemma is given in Appendix A.2.

The matrices $\mathbf{B}_1$, $\mathbf{B}_2$, $\mathbf{B}_3$, $\mathbf{B}_4$, $\mathbf{C}_1$ and $\mathbf{C}_2$ are considered in the different cases of Lemma 1. Each expected value in the lemma is a matrix, or a vector, whose elements are found following the indicated operations. These operations mainly compute the trace of a product of the corresponding deterministic matrix $\mathbf{A}$, and a matrix constructed from the finite differences matricial operator, which can be of first order $\mathbf{D}^1$ or of second order $\mathbf{D}^2$. The total number of operations in the computation of the bias and the covariance is $O\left(N^3 + n^2\right)$, but this order can be reduced since the $\mathbf{D}$ matrices are sparse.

The formulas for the bias and covariance (4.11) and (4.12) depend on the perturbation variance and on the unobservable variables $\boldsymbol{\theta}$ and $\mathbf{K}$. The substitution of the observed variables in the expression gives an approximation of the estimation bias and covariance based on the observed system response. We have then

$$\mathbf{b}_{\widetilde{\mathbf{p}}}\left(\widehat{\boldsymbol{\theta}}\right) \approx \widetilde{\mathbf{Q}}^{-1}\left(\left(\widetilde{\mathbf{K}}^\top \widetilde{\mathbf{B}}_1 - \widetilde{\mathbf{B}}_2\right)\widehat{\boldsymbol{\theta}} - \left(\widetilde{\mathbf{K}}^\top \widetilde{\mathbf{B}}_3 - \widetilde{\mathbf{B}}_4\right)\right), \tag{4.13}$$

and

$$\mathbf{C}_{\widetilde{\mathbf{p}}}\left(\widehat{\boldsymbol{\theta}}\right) \approx \widetilde{\mathbf{K}}^\dagger \left(\sigma_\epsilon^2 \mathbf{I}_{N-n} + \widetilde{\mathbf{C}}_1 - \widetilde{\mathbf{C}}_2 - \widetilde{\mathbf{C}}_2^\top\right)\widetilde{\mathbf{K}}^{\dagger\top} - \mathbf{b}_{\widetilde{\mathbf{p}}}\left(\widehat{\boldsymbol{\theta}}\right)\mathbf{b}_{\widetilde{\mathbf{p}}}^\top\left(\widehat{\boldsymbol{\theta}}\right), \tag{4.14}$$

where $\widetilde{\mathbf{B}}_1 = \mathbb{E}\left\{\mathbf{E}\widetilde{\mathbf{K}}^\dagger\mathbf{E}\right\}$, $\widetilde{\mathbf{B}}_2 = \mathbb{E}\left\{\mathbf{E}^\top\widetilde{\mathbf{P}}_\perp\mathbf{E}\right\}$, $\widetilde{\mathbf{B}}_3 = \mathbb{E}\left\{\mathbf{E}\widetilde{\mathbf{K}}^\dagger\epsilon\right\}$, $\widetilde{\mathbf{B}}_4 = \mathbb{E}\left\{\mathbf{E}^\top\widetilde{\mathbf{P}}_\perp\epsilon\right\}$, $\widetilde{\mathbf{C}}_1 = \mathbb{E}\left\{\mathbf{E}\widehat{\boldsymbol{\theta}}\widehat{\boldsymbol{\theta}}^\top\mathbf{E}^\top\right\}$, $\widetilde{\mathbf{C}}_2 = \mathbb{E}\left\{\mathbf{E}\widehat{\boldsymbol{\theta}}\epsilon^\top\right\}$, $\widetilde{\mathbf{C}} = \widetilde{\mathbf{K}}^\top\widetilde{\mathbf{K}}$, $\widetilde{\mathbf{P}} = \widetilde{\mathbf{K}}\widetilde{\mathbf{K}}^\dagger$, and $\widetilde{\mathbf{P}}_\perp = \mathbf{I} - \widetilde{\mathbf{P}}$.

## 4.1.3. Cramér-Rao lower bound of the structured errors-in-variables problem

The Cramér-Rao lower bound (CRLB) provides the lower limit on the estimation variance. For a biased estimator of the minimization problem (3.21), the CRLB is given by

$$\mathrm{CRLB_b}(\boldsymbol{\theta}) = \left(\mathbf{I}_{n+1} + \frac{\partial\mathbf{b}\left(\widehat{\boldsymbol{\theta}}\right)}{\partial\boldsymbol{\theta}}\right)^\top \mathbf{Fi}^{-1}(\boldsymbol{\theta}) \left(\mathbf{I}_{n+1} + \frac{\partial\mathbf{b}\left(\widehat{\boldsymbol{\theta}}\right)}{\partial\boldsymbol{\theta}}\right), \qquad (4.15)$$

and for an unbiased estimator it is $\mathrm{CRLB_{ub}}(\boldsymbol{\theta}) = \mathbf{Fi}^{-1}(\boldsymbol{\theta})$, where $\mathbf{b}(\widehat{\boldsymbol{\theta}})$ is the estimation bias and $\mathbf{Fi}(\widehat{\boldsymbol{\theta}})$ is the Fisher information matrix described in Pintelon and Schoukens [2012].

The Fisher information matrix is defined as the expected value of the Hessian of the negative likelihood function

$$\mathbf{Fi}(\boldsymbol{\theta}) = -\mathbb{E}\left\{\frac{\partial^2 l(\widehat{\boldsymbol{\theta}})}{\partial\widehat{\boldsymbol{\theta}}^2}\right\}, \qquad (4.16)$$

where the partial derivatives are evaluated in $\widehat{\boldsymbol{\theta}} = \boldsymbol{\theta}$.

The minimization problem (3.21) can be expressed as a linear in the measurements problem, as it is described in Pintelon and Schoukens [2012],

$$e(\widehat{\boldsymbol{\theta}},\widetilde{\mathbf{z}}) = \mathbf{M}_1(\widehat{\boldsymbol{\theta}})\,\widetilde{\mathbf{z}} = \underbrace{\begin{bmatrix}\mathbf{I}_{N-n} & -\widehat{\boldsymbol{\theta}}^\top\otimes\mathbf{I}_{N-n}\end{bmatrix}}_{\mathbf{M}_1(\widehat{\boldsymbol{\theta}})}\underbrace{\begin{bmatrix}\widetilde{\mathbf{y}}\\\mathrm{vec}(\widetilde{\mathbf{K}})\end{bmatrix}}_{\widetilde{\mathbf{z}}} = 0, \qquad (4.17)$$

where $\widetilde{\mathbf{z}} = \mathbf{z} + \epsilon_{\mathbf{z}}$ is a vector constructed by stacking the perturbation noise of the regressor and the regression matrix, and the true model must satisfy the equality $\mathbf{M}_1(\boldsymbol{\theta})\,\mathbf{z} = 0$. Since the true measurements $\mathbf{z}$ are unknown, they have to be estimated and are parameterized as $\widehat{\mathbf{z}}$. Under the assumption of the measurement

perturbation $\epsilon_{\mathbf{z}}$ being normally distributed with zero mean and covariance matrix

$$\mathbf{C_z} = \sigma_\epsilon^2 \begin{bmatrix} \mathbf{I}_{N-n} & \mathbf{0}_{N-n} & \mathbf{D}^{1,n}_{N-n\times N-n} & \mathbf{D}^{1,n-1}_{N-n\times N-n} & \cdots & \mathbf{D}^{1,1}_{N-n\times N-n} \\ \mathbf{0}_{N-n} & \mathbf{0}_{N-n} & \mathbf{0}_{N-n} & \mathbf{0}_{N-n} & \cdots & \mathbf{0}_{N-n} \\ \left(\mathbf{D}^{1,n}_{N-n\times N-n}\right)^\top & \mathbf{0}_{N-n} & \mathbf{D}^{2,1}_{N-n\times N-n} & \mathbf{D}^{2,0}_{N-n\times N-n} & \cdots & \mathbf{D}^{2,2-n}_{N-n\times N-n} \\ \left(\mathbf{D}^{1,n-1}_{N-n\times N-n}\right)^\top & \mathbf{0}_{N-n} & \mathbf{D}^{2,2}_{N-n\times N-n} & \mathbf{D}^{2,1}_{N-n\times N-n} & \cdots & \mathbf{D}^{2,3-n}_{N-n\times N-n} \\ \vdots & \vdots & \vdots & \vdots & & \vdots \\ \left(\mathbf{D}^{1,1}_{N-n\times N-n}\right)^\top & \mathbf{0}_{N-n} & \mathbf{D}^{2,n}_{N-n\times N-n} & \mathbf{D}^{2,n-1}_{N-n\times N-n} & \cdots & \mathbf{D}^{2,1}_{N-n\times N-n} \end{bmatrix} \quad (4.18)$$

the loglikelihood function of the structured EIV problem is

$$\ln l(\widetilde{\mathbf{z}}, \widehat{\mathbf{z}}, \widehat{\boldsymbol{\theta}}) = -\frac{1}{2}\left(\widetilde{\mathbf{z}} - \widehat{\mathbf{z}}\right)^\top \mathbf{C_z}^{-1} \left(\widetilde{\mathbf{z}} - \widehat{\mathbf{z}}\right) + \text{constant}, \quad (4.19)$$

The size of the Fisher information matrix $\mathbf{Fi}(\boldsymbol{\theta}, \mathbf{z})$ depends on the number of to-be-estimated parameters $\widehat{\mathbf{z}}$, that grows with the sample size. In Chapter 19 of Pintelon and Schoukens [2012] it is shown that the Fisher information matrix $\mathbf{Fi}(\boldsymbol{\theta})$ that depends only on $\boldsymbol{\theta}$ can be obtained after doing inversion by parts, resulting in

$$\mathbf{Fi}(\boldsymbol{\theta}) = \left(\frac{\partial e(\widehat{\boldsymbol{\theta}}, \mathbf{z})}{\partial \boldsymbol{\theta}}\right)^\top \left(\mathbf{M}_1(\boldsymbol{\theta})\, \mathbf{C_z}\, \mathbf{M}_1^\top(\boldsymbol{\theta})\right)^{-1} \left(\frac{\partial e(\widehat{\boldsymbol{\theta}}, \mathbf{z})}{\partial \boldsymbol{\theta}}\right). \quad (4.20)$$

## 4.1.4. Instrumental variables formulation of the data-driven step input estimation method

The errors-in-variables problem formulation (3.21) of the data-driven step input estimation method can be converted into an instrumental-variables problem. A guide to do this conversion is found in Söderström [2018] and in Pintelon and Schoukens [2012]. The instrumental variable $\widetilde{\mathbf{Z}}$ has to be selected so that the normal equations (3.22) are expresed instead as

$$\widetilde{\mathbf{Z}}^\top \widetilde{\mathbf{K}} \boldsymbol{\theta} = \widetilde{\mathbf{Z}}^\top \widetilde{\mathbf{y}}. \quad (4.21)$$

The selection of the instrumental variable has to be done in such a way that is correlated the regression matrix $\widetilde{\mathbf{K}}$, and uncorrelated with the perturbations $\epsilon$. Considering the block-Hankel matrix $\widetilde{\mathbf{K}}$ (3.19) with $N = 2n+1$,

$$\widetilde{\mathbf{K}} = \begin{bmatrix} G & \Delta\widetilde{y}(1) & \Delta\widetilde{y}(2) & \cdots & \Delta\widetilde{y}(n) \\ G & \Delta\widetilde{y}(2) & \Delta\widetilde{y}(3) & \cdots & \Delta\widetilde{y}(n+1) \\ \vdots & \vdots & \vdots & & \vdots \\ G & \Delta\widetilde{y}(n+1) & \Delta\widetilde{y}(n+2) & \cdots & \Delta\widetilde{y}(2n) \end{bmatrix}, \quad (4.22)$$

then, the instrumental variable $\widetilde{\mathbf{Z}}$ should not contain the elements that construct $\widetilde{\mathbf{K}}$, i.e., the elements of the vector $(\widetilde{y}(1), \ldots, \widetilde{y}(2n+1))^{\top}$. A possibility to generalize this ideas is expressing the instrumental variable as

$$
\widetilde{\mathbf{Z}}(t) = \begin{bmatrix} G & \Delta\widetilde{y}(t-4n) & \Delta\widetilde{y}(t-4n+1) & \cdots & \Delta\widetilde{y}(t-3n-1) \\ G & \Delta\widetilde{y}(t-4n+1) & \Delta\widetilde{y}(t-4n+2) & \cdots & \Delta\widetilde{y}(t-3n) \\ \vdots & \vdots & \vdots & & \vdots \\ G & \Delta\widetilde{y}(t-3n) & \Delta\widetilde{y}(t-3n+1) & \cdots & \Delta\widetilde{y}(t-2n-1) \end{bmatrix}, \tag{4.23}
$$

for a regression matrix

$$
\widetilde{\mathbf{K}}(t) = \begin{bmatrix} G & \Delta\widetilde{y}(t-2n+1) & \Delta\widetilde{y}(t-2n+2) & \cdots & \Delta\widetilde{y}(t-n) \\ G & \Delta\widetilde{y}(t-2n+2) & \Delta\widetilde{y}(t-2n+3) & \cdots & \Delta\widetilde{y}(t-n+1) \\ \vdots & \vdots & \vdots & & \vdots \\ G & \Delta\widetilde{y}(t-n+1) & \Delta\widetilde{y}(t-n+2) & \cdots & \Delta\widetilde{y}(t) \end{bmatrix}, \tag{4.24}
$$

for $t = 4n+1, \ldots, N$.

The difference with the EIV formulation is that this implementation of the IV method requires to wait more, until $4n+1$ samples of the sensor response are read, instead of $2n+1$ samples. For sensors of small dynamic order this twice-the-time waiting does not represent a big change, but as the sensor order increases, the need for waiting can turn the method into impractical since a lot of time should pass before starting to estimate the input.

## Recursive generalized instrumental variables method

There exists a generalized instrumental variables method (GIVE) that was proposed to identify dynamic models from input/output data. GIVE is a bias-eliminating method that uses a generalized instrumental vector constructed from delayed values of the input and output signals Söderström [2018]. Since the aim of this thesis is to analyze a method that directly estimates the input from the observed sensor output, without identifying explicitly a dynamic model of the sensor, the GIVE method is out of the scope of this work. Future research can include studying the formulation of a data-driven input estimation method in the spirit of the GIVE method. Nevertheless, a brief description of the recursive GIVE method is given in the following paragraphs.

## Generalized instrumental variables method

For an errors-in-variables problem expressed as

$$
\widetilde{y}(t) = \widetilde{\phi}(t)\boldsymbol{\theta} \tag{4.25}
$$

where $\widetilde{y}(t)$ is the output perturbed by measurement noise, $\boldsymbol{\theta}$ is the vector of to-be-estimated parameters, and $\widetilde{\boldsymbol{\phi}}(t)$ is the regressor vector constructed from delayed samples of the measured input $\widetilde{u}(t)$ and output $\widetilde{y}(t)$. The least-squares estimate $\widehat{\boldsymbol{\theta}}_{\mathrm{LS}}$ is the solution of the normal equation

$$\widehat{\mathbf{R}}_{\widetilde{\phi}}\widehat{\boldsymbol{\theta}}_{\mathrm{LS}} = \widehat{\mathbf{r}}_{\widetilde{\phi}\widetilde{y}}, \tag{4.26}$$

where $\widehat{\mathbf{R}}_{\widetilde{\phi}}$ is the sample covariance matrix of the regressor vector, and $\widehat{\mathbf{r}}_{\widetilde{\phi}\widetilde{y}}$ is the sample cross-covariance matrix of the regressor vector and the output. When the number of samples becomes infinitely large, these covariances matrices can be expressed as a sum of the contributions from exact data and measurement noise contributions

$$\begin{aligned} \lim_{N\to\infty}\widehat{\mathbf{R}}_{\widetilde{\phi}} &= \mathbb{E}\{\widetilde{\boldsymbol{\phi}}\widetilde{\boldsymbol{\phi}}^{\top}\} = \mathbf{R}_{\phi} + \mathbf{R}_{\eta} \\ \lim_{N\to\infty}\widehat{\mathbf{r}}_{\widetilde{\phi}\widetilde{y}} &= \mathbb{E}\{\widetilde{\boldsymbol{\phi}}\widetilde{y}^{\top}\} = \mathbf{r}_{\phi y} + \mathbf{r}_{\eta\epsilon}, \end{aligned} \tag{4.27}$$

where we are assuming that $\widetilde{y} = y + \epsilon$, $\widetilde{\boldsymbol{\phi}} = \boldsymbol{\phi} + \boldsymbol{\eta}$, and $\mathbf{r}_{\phi y} = \mathbf{R}_{\phi}\boldsymbol{\theta}$. The bias of the least-square solution can be expressed as

$$\mathbf{R}_{\widetilde{\phi}}\left(\widehat{\boldsymbol{\theta}}_{\mathrm{LS}} - \boldsymbol{\theta}\right) = \mathbf{r}_{\widetilde{\phi}\widetilde{y}} - \mathbf{R}_{\widetilde{\phi}}\boldsymbol{\theta} = \mathbf{r}_{\widetilde{\eta}\epsilon} - \mathbf{R}_{\eta}\boldsymbol{\theta}, \tag{4.28}$$

If we assume that the measurement noise is white for both the input and output,

$$\mathbf{r}_{\widetilde{\eta}\epsilon} = \mathbb{E}\{\boldsymbol{\eta}\boldsymbol{\epsilon}^{\top}\} = \mathbf{0} \quad \text{and} \quad \mathbf{R}_{\eta} = \begin{bmatrix} \sigma_{\epsilon}^{2}\mathbf{I}_{n_{y}} & \mathbf{0} \\ \mathbf{0} & \sigma_{u}^{2}\mathbf{I}_{n_{u}} \end{bmatrix}, \tag{4.29}$$

where $\sigma_{\epsilon}^{2}$ and $\sigma_{u}^{2}$ are the variances of the output and the input, respectively. The normal equation (4.26) implies that

$$(\mathbf{R}_{\phi} + \mathbf{R}_{\eta})\left(\widehat{\boldsymbol{\theta}}_{\mathrm{LS}} - \boldsymbol{\theta}\right) \neq \mathbf{0}, \tag{4.30}$$

and the estimate $\widehat{\boldsymbol{\theta}}_{\mathrm{LS}}$ is not consistent. Instead, a bias-compensating least squares estimation can be obtained with

$$\widehat{\boldsymbol{\theta}}_{\mathrm{BCLS}} = \left(\mathbf{R}_{\widetilde{\phi}} - \mathbf{R}_{\eta}\right)^{-1}\left(\mathbf{r}_{\widetilde{\phi}\widetilde{y}} - \mathbf{r}_{\eta\epsilon}\right). \tag{4.31}$$

To formulate the generalized instrumental variable estimator, a generalized instrumental vector $\mathbf{z}(t)$ is built from delayed samples of the input and the output

$$\mathbf{z}(t) = (y(t), y(t-1), \ldots, y(t-n_{y}), u(t), u(t-1), \ldots, u(t-n_{u}))^{\top}.$$

The dimension of the generalized instrumental vector should be $n_{\mathbf{z}} \geq \dim(\vartheta) = n_{u} + n_{y} + 2$, because the total parameter vector $\vartheta = \left(\boldsymbol{\theta}^{\top}, \boldsymbol{\rho}^{\top}\right)^{\top}$ considers also the

variances of the measurement noise $\rho = \left(\sigma_\epsilon^2, \sigma_u^2\right)^\top$. Since the generalized instrumental vector $\mathbf{z}(t)$ and the equation error $\widetilde{y}(t) - \widetilde{\phi}(t)\theta$ must be correlated, we can express the system of equations as

$$\left(\mathbf{R}_{\widetilde{\mathbf{z}}\widetilde{\phi}} - \mathbf{R}_{\zeta\eta}\left(\rho\right)\right)\theta = \left(\mathbf{r}_{\widetilde{\mathbf{z}}\widetilde{y}} - \mathbf{r}_{\zeta\epsilon}\left(\rho\right)\right), \tag{4.32}$$

where $\widetilde{\mathbf{z}} = \mathbf{z} + \zeta$.

## Recursive generalized instrumental variables method

If we define

$$\mathbf{h}\left(\rho,\,\theta\right) = \mathbf{r}_{\zeta\epsilon}\left(\rho\right) - \mathbf{R}_{\zeta\eta}\left(\rho\right)\theta = \mathbf{J}\left(\theta\right)\rho,$$

$$\mathbf{R}\left(t\right) = \frac{1}{t}\sum_{\tau-1}^{t}\widetilde{\mathbf{z}}\left(\tau\right)\widetilde{\phi}^\top\left(\tau\right),$$

$$\mathbf{q}\left(t\right) = \frac{1}{t}\sum_{\tau-1}^{t}\widetilde{\mathbf{z}}\left(\tau\right)\widetilde{y}\left(\tau\right) \tag{4.33}$$

$$\mathbf{b}\left(t\right) = \mathbf{q}\left(t\right) - \mathbf{h}\left(\rho,\,\theta\right),$$

then the equation (4.32) is equivalent to

$$\mathbf{R}\left(t\right)\theta = \mathbf{b}\left(t\right). \tag{4.34}$$

This representation allows a recursive form

$$\mathbf{R}\left(t+1\right) = \mathbf{R}\left(t\right) + \frac{1}{t+1}\left(\widetilde{\mathbf{z}}\left(t+1\right)\widetilde{\phi}^\top\left(t+1\right) - \mathbf{R}\left(t\right)\right),$$

$$\mathbf{b}\left(t+1\right) = \mathbf{b}\left(t\right) + \frac{1}{t+1}\left(\widetilde{\mathbf{z}}\left(t+1\right)\widetilde{y}\left(t+1\right) - \mathbf{b}\left(t\right) - \mathbf{h}\left(\rho,\,\theta\right)\right),$$

$$\widehat{\theta}\left(t+1\right) = \left(\mathbf{R}^\top\left(t+1\right)\mathbf{R}\left(t+1\right)\right)^{-1}\mathbf{R}^\top\left(t+1\right)\mathbf{b}\left(t+1\right) \tag{4.35}$$

$$\mathbf{q}\left(t+1\right) = \mathbf{q}\left(t\right) + \frac{1}{t+1}\left(\widetilde{\mathbf{z}}\left(t+1\right)\widetilde{y}\left(t+1\right) - \mathbf{q}\left(t\right)\right)$$

$$\widehat{\rho}\left(t+1\right) = \mathbf{J}^\dagger\left(\widehat{\theta}\left(t\right)\right)\left(\mathbf{q}\left(t\right) - \mathbf{R}\left(t\right)\widehat{\theta}\left(t\right)\right),$$

where $\mathbf{J}^\dagger\left(\widehat{\theta}\left(t\right)\right)$ is the pseudo-inverse of $\mathbf{J}\left(\theta\right)$.

The complexity of this recursive generalized instrumental variables estimator is $O(n^3)$, which is larger than the $O(n^2)$ of the recursive least squares. Another drawback of the recursive generalized IV estimator is that it computes a pseudo-inverse matrix in each iteration step. If we would need to formulate the data-driven step input estimation problem in the generalized IV framework, it would require

to study the formulation in detail because currently the IV framework is based on the assumption that both measurements of the input and output are available, but for the step input estimation problem only the output is available. Therefore, it is not straightforward to implement the recursive generalized IV estimator to estimate the step input, and this can lead to future research.

## 4.2. Simulation results

Two Monte Carlo (MC) simulation studies were conducted to test the obtained bias and variance formulas. There are two sets of formulas. One set was obtained for the unstructured and uncorrelated EIV problem, and, the other set, for the structured and correlated EIV problem. The problem solved by the data-driven step input estimation method (3.21) belongs to the second set. The objective of the MC simulations is to compare the results of the bias and variance formulas in these two cases. The comparison is an evaluation of the effect that the structure and correlation have in the problem solution. To make a fair comparison, the same exact data and the perturbation variance is used in both types of EIV problems.

The exact data is the system of linear equations (3.15) built by the data-driven step input estimation method. To build the system of equations, the processed signal $y$ is the exact response of a sensor to the input $0.1s(t)$, where $s(t)$ is the unit step response. The sensor is modeled as a linear time-invariant mass-spring-damper system of order $n = 2$, that is given by

$$\mathbf{x}(k+1) = \begin{bmatrix} 0 & 1 \\ \dfrac{-k_\mathrm{s}}{m+M} & \dfrac{-k_\mathrm{d}}{m+M} \end{bmatrix} \mathbf{x}(k) + \begin{bmatrix} 0 \\ -g \end{bmatrix} u(k), \quad y(k) = \begin{bmatrix} -1 & 0 \end{bmatrix} \mathbf{x}(k), \quad (4.36)$$

where $m = 0.015$ kg, $k_\mathrm{s} = 500$ kg/m, $k_\mathrm{d} = 0.5$ kg s/m, $M = 0.1$ kg, and $g = 9.81$ m/s$^2$. The exact sensor response is shown in Figure 4.1.

In the simulations, the sample size considered is $N = 200$, since there the transient regime of the sensor model is still evident. In the case of the structured EIV problem, this sample size satisfies the requirements of the data-driven step input estimation method.

The MC simulations performed $N_{MC} = 10^6$ runs of the LS solver with different realizations of the additive perturbations $[\mathbf{E} \quad \epsilon]$. The perturbation variance $\sigma_\epsilon^2$ was selected to have a signal-to-noise ratio (SNR) in the interval [30 dB, 80 dB],
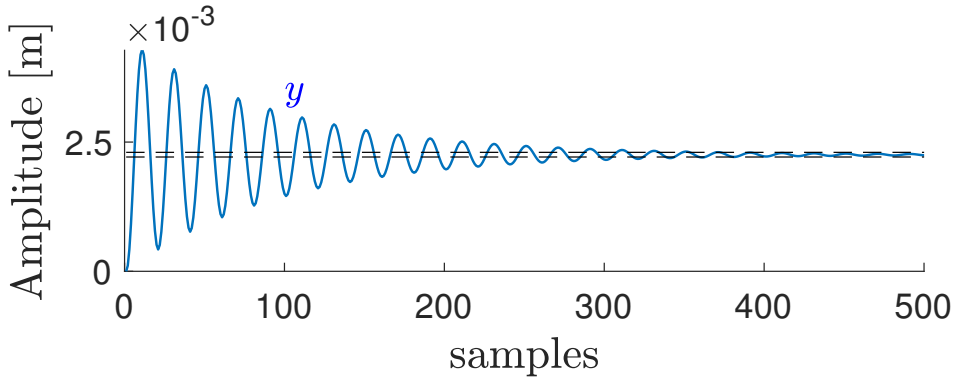
Figure 4.1.: The exact response of the model is used in the simulations of the two EIV problem types. For the structured EIV problem, it is important to consider the transient response. Thus, we use the first 200 samples. The dashed lines show the values of $y$ that are 2% above and below the steady-regime output value.

according to

$$\text{SNR} = 20\log_{10} \frac{\sqrt{\frac{1}{N}\sum\limits_{t=1}^{N} y(t)^2}}{\sigma_\epsilon}. \tag{4.37}$$

The constraint $\|\mathbf{M}\| < 1$ and the Taylor series expansion (4.3) hold for SNR sufficiently high, and in this conditions, the derived expressions predict the LS estimation bias and variance. Thus, it is relevant to monitor the evolution of the largest $\mathbf{M}$ eigenvalue to detect the lower limit of the SNR that allows the validity of the predictions.

The MC simulations provide empirical values of the bias and variance, through the sample mean and sample variance of the LS estimate $\widehat{\boldsymbol{\theta}}$. The results presented in this Section focus the interest in the first element of $\widehat{\boldsymbol{\theta}}$, because in the structured EIV problem, the step input estimate is $\widehat{u} = \widehat{\boldsymbol{\theta}}_{[1]}$.

## 4.2.1. Monte Carlo simulation results for an unstructured EIV problem with uncorrelated perturbations

The MC simulation of the unstructured EIV problem solution was conducted using the following settings. The perturbations $\mathbf{E}$ and $\epsilon$ are normally distributed with zero mean and variances $\sigma_{\mathbf{E}}^2 = 2\sigma_\epsilon^2$. This relationship between the variances is

also present in the structured EIV problem, and then we have similar assumptions. However, for the uncorrelated and unstructured EIV case, the perturbations $\mathbf{E}$ and $\epsilon$ are independent.

The difference between the sample mean of the estimate $\widehat{\boldsymbol{\theta}}_{[1]}$ and its true value $\boldsymbol{\theta}_{[1]}$ is the empirical bias $b_{\mathrm{e}}$.

$$b_{\mathrm{e}} = \frac{1}{N_{\mathrm{MC}}} \sum_{i=1}^{N_{\mathrm{MC}}} \left( \widehat{\boldsymbol{\theta}}_{[1]} \right)_i - \boldsymbol{\theta}_{[1]} \approx \mu \left( \widehat{\boldsymbol{\theta}}_{[1]} \right) - \boldsymbol{\theta}_{[1]}. \tag{4.38}$$

The standard deviation of the estimate $\widehat{\boldsymbol{\theta}}_{[1]}$ is used to obtain the standard error $\sigma_{\mathrm{e,err}}$ of the MC simulation, which decreases with respect to the square root of the number of MC runs $N_{\mathrm{MC}}$ as it is explained in Hammersley and Handscomb [1975]:

$$\sigma_{\mathrm{e,err}} = \frac{\sigma_{\mathrm{e}} \left( \widehat{\boldsymbol{\theta}}_{[1]} \right)}{\sqrt{N_{\mathrm{MC}}}}, \quad \text{where} \quad \sigma_{\mathrm{e}}^2 \left( \widehat{\boldsymbol{\theta}}_{[1]} \right) = \frac{1}{N_{\mathrm{MC}} - 1} \sum_{i=1}^{N_{\mathrm{MC}}} \left( \left( \widehat{\boldsymbol{\theta}}_{[1]} \right)_i - \mu \left( \widehat{\boldsymbol{\theta}}_{[1]} \right) \right)^2. \tag{4.39}$$

In each of the $N_{\mathrm{MC}}$ runs we also obtain the aproximations of the estimation bias $\mathbf{b}_{\widetilde{\mathrm{p}}[1]}$ and variance $\mathbf{C}_{\widetilde{\mathrm{p}}[1,1]}$ from observed data, using Equations (4.9), and (4.10). Similarly as before, we get the sample mean of the aproximations to have bias and variance predictions from observed data

$$b_{\widetilde{\mathrm{p}}} = \frac{1}{N_{\mathrm{MC}}} \sum_{i=1}^{N_{\mathrm{MC}}} \left( \mathbf{b}_{\widetilde{\mathrm{p}}[1]} \right)_i, \quad \text{and} \quad v_{\widetilde{\mathrm{p}}} = \frac{1}{N_{\mathrm{MC}}} \sum_{i=1}^{N_{\mathrm{MC}}} \left( \mathbf{C}_{\widetilde{\mathrm{p}}[1,1]} \right)_i. \tag{4.40}$$

The standard error of the bias prediction $b_{\widetilde{\mathrm{p}}}$ is given by

$$\sigma_{\widetilde{\mathrm{p}},\mathrm{err}} = \sqrt{\frac{1}{N_{\mathrm{MC}} \left( N_{\mathrm{MC}} - 1 \right)} \sum_{i=1}^{N_{\mathrm{MC}}} \left( \left( \mathbf{b}_{\widetilde{\mathrm{p}}[1]} \right)_i - b_{\widetilde{\mathrm{p}}} \left( \widehat{\boldsymbol{\theta}}_{[1]} \right) \right)^2}. \tag{4.41}$$

The predicted bias $b_{\mathrm{p}} = \mathbf{b}_{\mathrm{p}[1]}$ and variance $v_{\mathrm{p}} = \mathbf{C}_{\mathrm{p}[1,1]}$ from exact data are obtained with one evaluation of the expressions (4.7) and (4.8).

Figure 4.2 shows the empirical bias and the bias predictions, with their corresponding standard errors, for the unstructured EIV problem. The simulation settings for the structured and correlated EIV problem are described in the following subsection. In the figure, it can be observed that the empirical bias $b_{\mathrm{e}}$ is proportional to the perturbation noise variance while the standard error $\sigma_{\mathrm{e,err}}$ is proportional to the perturbation noise standard deviation. The bias predictions $b_{\mathrm{p}}$ and $b_{\widetilde{\mathrm{p}}}$ are accurate since they coincide with the empirical bias $b_{\mathrm{e}}$ in all the SNR interval

for unstructured EIV problems. In both unstructured and structured EIV cases, the standard errors of the MC estimates $\sigma_{e,err}$ and $\sigma_{\tilde{p},err}$ are smaller than the bias estimates $b_e$ and $b_{\tilde{p}}$. The bias estimates are spread near their sample means. The uncertainty is smaller than the bias, therefore, the MC simulation is meaningful.
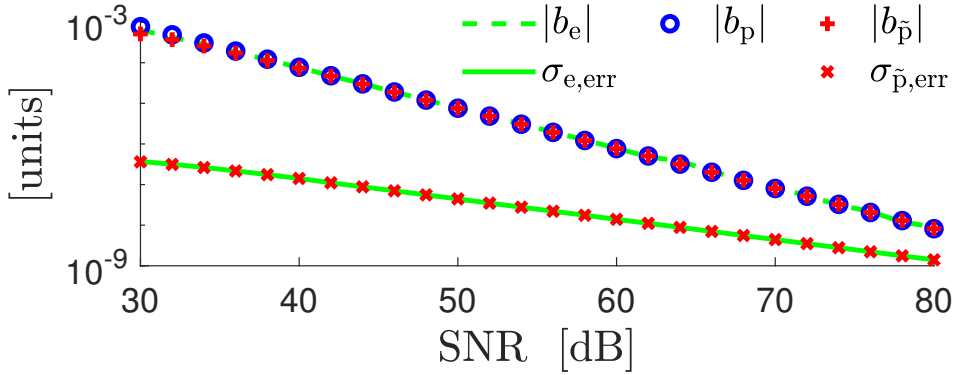


Figure 4.2.: We observe the results of the LS solutions for the unstructured EIV problem. These results are the empirical bias $b_e$, the predicted bias from exact data $b_p$, the predicted bias from observed data $b_{\tilde{p}}$, the empirical standard error $\sigma_{e,err}$, and the standard error from the estimations using observed data $\sigma_{\tilde{p},err}$. The estimation biases are proportional to the perturbation variance and the estimation standard errors are proportional to the perturbation standard deviation. Since the standard errors are smaller than the biases, the MC simulation is meaningful.

The absolute and relative errors between the predicted and the empirical bias are shown in Figure 4.3. The absolute errors decrease with respect to the perturbation variance. The relative errors are lower than 5% for SNR between 30 dB and 70 dB. There is an increment in the relative errors for SNR above 55 dB. As the SNR increases, the empirical and the predicted bias decrease, as well as the bias error between them. In order to reveal the bias error, more Monte Carlo runs are needed to reduce the uncertainty of the Monte Carlo simulation that depends on the square root of $N_{MC}$, see Equation (4.39). If $N_{MC}$ is insufficient, the uncertainty of the Monte Carlo simulation hides the bias error and we see this increasing effect of the relative errors.

The errors between the predicted and the empirical variance are shown in Figure 4.4. The absolute and relative errors decrease with respect to the perturbation variance. The relative errors are lower than 5% for SNR above 40 dB.
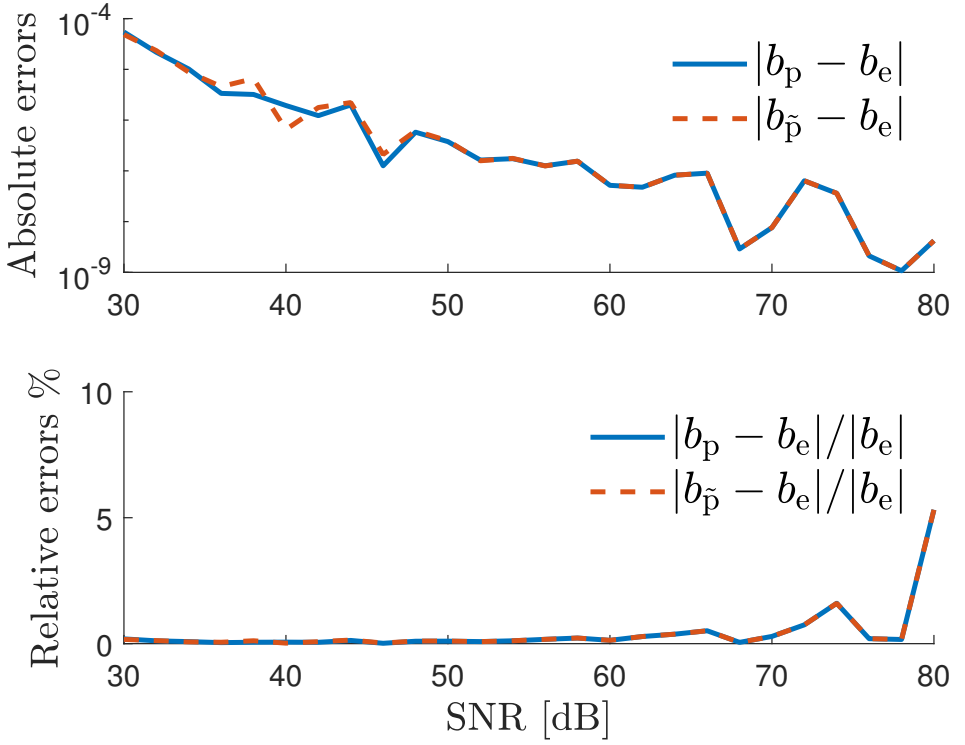
Figure 4.3.: The MC simulation shows that when we solve an unstructured EIV problem with LS, the absolute errors (top) between the predicted bias and the empirical bias are proportional to the perturbation noise variance as it is expected, and the relative errors (bottom) are smaller than 5% for SNR below 70 dB. The bias prediction computed from exact data $b_p$ is very similar to that computed using observed data $b_{\tilde{p}}$.

Figure 4.5 shows the absolute and the relative errors between the predictions computed from observed data and those computed from exact data. The absolute errors between both predictions are proportional to the perturbation noise variance. The bias and variance predictions, from either exact data or observed data, are equivalent for SNR above 35 dB since the relative errors are lower than 5%. The substitution of observed data on the prediction formulas is a valid procedure that allows the prediction of the estimate statistics.
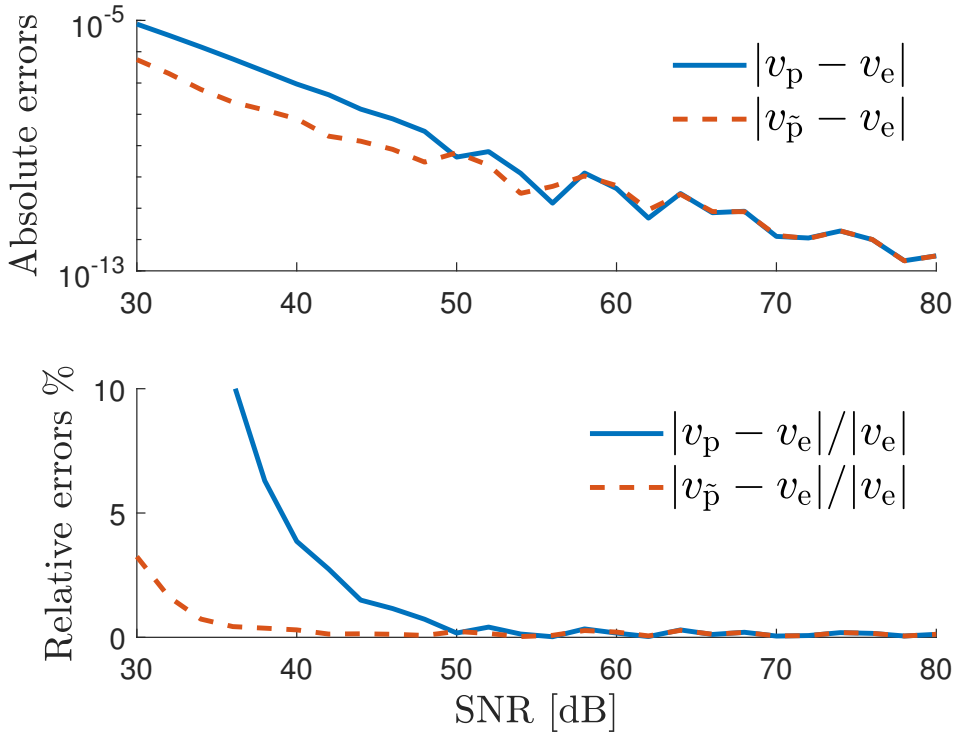
Figure 4.4.: The MC simulation shows that when we solve an unstructured EIV problem with LS, the absolute errors (top) between the predicted variances and the empirical variance are proportional to the perturbation noise variance, and the relative errors (bottom) are smaller than 5% for SNR higher that 40 dB. The variance prediction computed using exact data $v_{\mathrm{p}}$ is very similar to that computed from observed data $v_{\widetilde{\mathrm{p}}}$.

## 4.2.2. Monte Carlo simulation results for a structured EIV problem with correlated perturbations

The MC simulation of the structured EIV problem (3.20) solution was conducted using the step response $\widetilde{y}$ of the sensor model (4.36). We use the same exact data response as for the previous subsection, but in this case the perturbations of the regression matrix $\widetilde{\mathbf{K}}$ have Hankel structure and are correlated with the perturbations of the regressor vector $\widetilde{\mathbf{y}}$. The perturbations $\epsilon$ are normally distributed with zero mean and variance $\sigma_\epsilon^2$, and are also used to build the perturbations $\mathbf{E}$. Due to the Hankel structure in Equation (3.18), the variances of the perturbations $\mathbf{E}$ and $\epsilon$ are related by $\sigma_{\mathbf{E}}^2 \approx 2\sigma_\epsilon^2$.
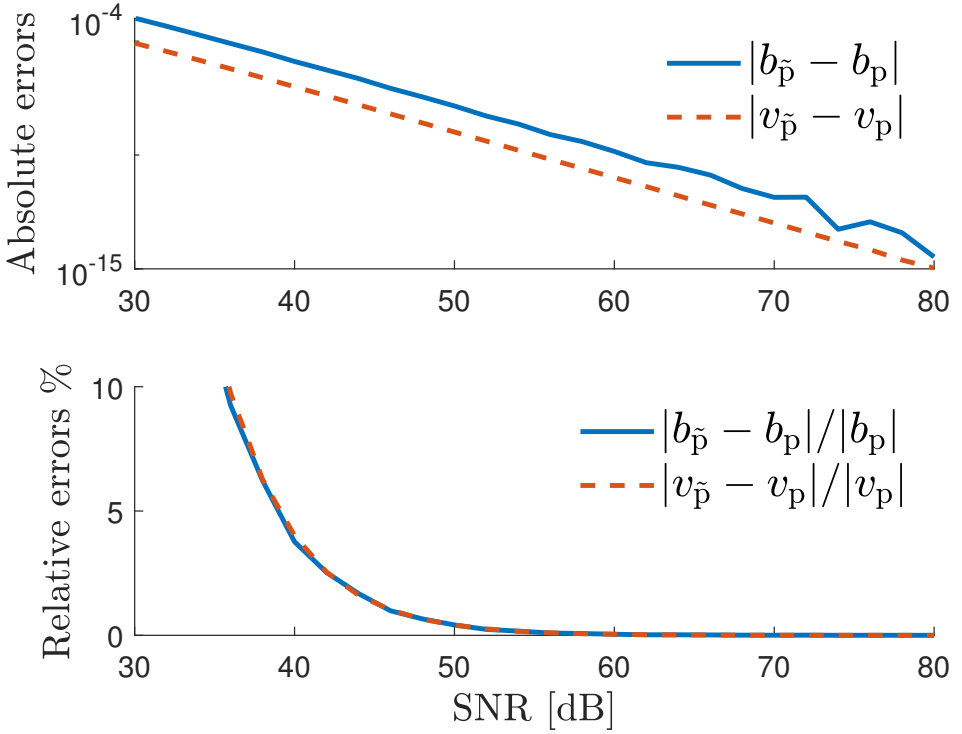
Figure 4.5.: The MC simulation shows that when we solve an unstructured EIV problem with LS, the absolute errors (top) between the prediction with observed data and the prediction with exact data are proportional to the perturbation noise variance. The use of observed data instead of exact data in the prediction formulas is valid when the SNR is above 35 dB since the relative errors (bottom) are smaller than 5%.

The spectral radius of the matrix $\mathbf{K}$ in Equation (4.3) is observed for the SNR values in the interval of interest. As can be observed in Figure 4.6, for SNR values larger than 35 dB, the perturbation levels make the spectral radius $\|\mathbf{M}\| < 1$, and, therefore, ensure the approximation given by the Taylor series expansion of the inverse matrix. Below an SNR of 35 dB, the spectral radius of $\mathbf{K}$ grows above 1. In the rest of this subsection we will evaluate the effect of the error introduced by the approximation.

We are interested in the mean-squared error of the of the step input estimation, obtained empirically with the Monte Carlo simulation. The empirical bias is the
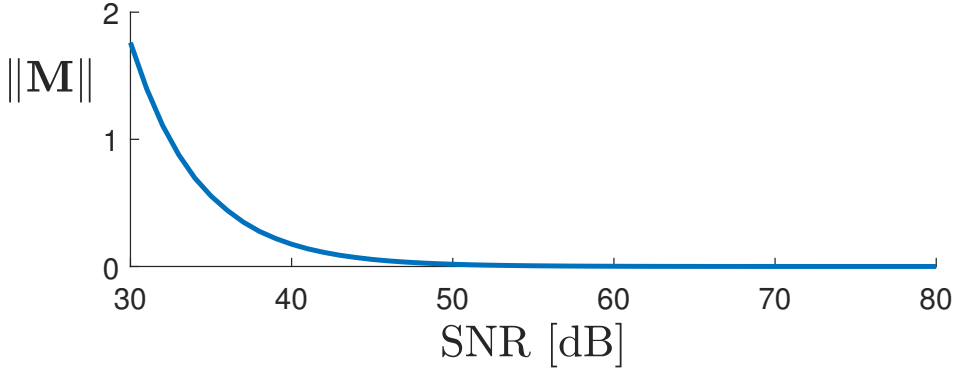
Figure 4.6.: The spectral radius $\|\mathbf{M}\|$ is evaluated for different perturbation levels. The approximation of the inverse matrix with the Taylor series expansion gives small error when $\|\mathbf{M}\| < 1$. The SNR values that increase the spectral radius above one are those below 35 dB.

sample mean of the $N_{\text{MC}}$ estimates minus the true value

$$b_{\text{e}} = \frac{1}{N_{\text{MC}}} \sum_{i=1}^{N_{\text{MC}}} \widehat{u}_i - u \approx \mu\left(\widehat{u}\right) - u. \tag{4.42}$$

The standard error associated to this empirical bias estimation is defined in Hammersley and Handscomb [1975] as

$$\sigma_{\text{e,err}} = \frac{\sigma_{\text{e}}\left(\widehat{u}\right)}{\sqrt{N_{\text{MC}}}}, \quad \text{where} \quad \sigma_{\text{e}}^2\left(\widehat{u}\right) = \frac{1}{N_{\text{MC}} - 1} \sum_{i=1}^{N_{\text{MC}}} \left(\widehat{u}_i - \mu\left(\widehat{u}\right)\right)^2. \tag{4.43}$$

The plots in Figure 4.7 show the empirical bias, the bias predictions (4.11) and (4.13), and their corresponding standard errors, for the structured EIV problem. The empirical bias $b_{\text{e}}$ is proportional to the perturbation noise variance, and the bias predictions $b_{\text{p}}$ and $b_{\widetilde{\text{p}}}$ coincide with the empirical bias $b_{\text{e}}$ only for SNR above 40 dB. This indicates that the SNR drops to a point where the constraint $\|\mathbf{M}\| < 1$ is no longer satisfied. At an SNR of 30 dB the perturbation noise affects the bias prediction from observed data and it is three times smaller than the empirical bias.

The absolute and relative errors between the predicted and the empirical bias are shown in Figure 4.8. It can be seen that the absolute errors are proportional to the perturbation variance, and the relative errors are lower than 5% for SNR higher than 40 dB.
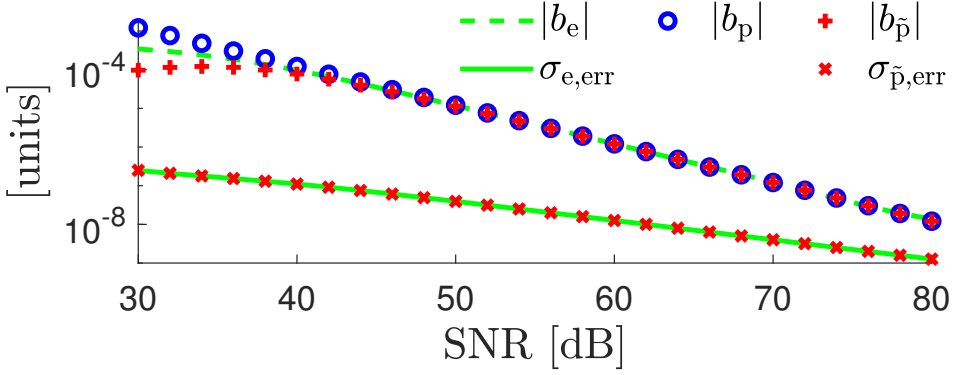
Figure 4.7.: We observe the results of the LS solutions for the structured EIV problem. These results are the empirical bias $b_e$, the predicted bias from exact data $b_p$, the predicted bias from observed data $b_{\tilde{p}}$, the standard error $\sigma_{e,err}$ of the empirical bias, and the standard error $\sigma_{\tilde{p},err}$ of the the estimations bias computed using observed data. The estimation biases are proportional to the perturbation variance and the estimation standard errors are proportional to the perturbation standard deviation. Since the standard errors are smaller than the biases, the MC simulation is meaningful.

The absolute and relative errors between the empirical and the predicted variance, equations (4.12) and (4.14), are shown in Figure 4.9. These absolute errors are proportional to the perturbation noise variance, whereas the relative errors are lower than 5% for SNR higher than 45 dB.

The absolute and relative errors between the two predictions from observed data and from exact data, are shown in Figure 4.10. These absolute errors are also proportional to the perturbation noise variance, and the relative errors show that the bias and variance predictions from either of the two alternatives are equivalent for SNR higher than 45 dB.

The simulation results show that the LS solution of the structured and correlated EIV problem is more sensitive to the perturbation. This represents a low limit in the SNR interval imposed by the noise level. In practical applications it is common to have SNRs of 40 dB and the user needs to be aware of the prediction error that the method has. We measure this prediction error with the mean squared error (MSE), defined as
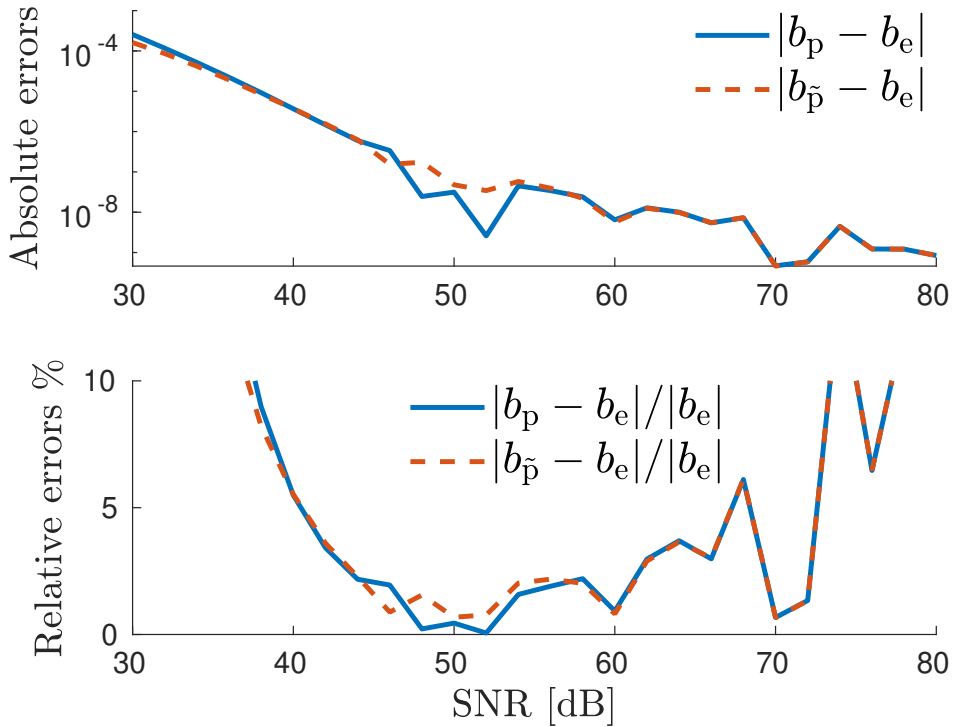
$$\text{MSE} = \sigma^2 + b^2. \tag{4.44}$$

Figure 4.8.: The MC simulation shows that when we solve a structured EIV problem with LS, the absolute errors (top) between the predicted bias and the empirical bias $b_{\mathrm{e}}$ are proportional to the perturbation noise variance, and the relative errors (bottom) are smaller than 5% only for SNR above 40 dB.

By comparing the different MSEs to the CRLB of the structured EIV problem, Figure 5.3 shows that the MSEs has the same proportionality as the CRLB with respect to the disturbing noise variance. The MSEs are three times larger than the CRLB. Since the difference between $\mathrm{MSE}_{\tilde{\mathrm{p}}}$ and the CRLB is lower than one order of magnitude, the LS estimation of the structured EIV problem produces results that are comparable to the ML estimation. The $\mathrm{MSE}_{\tilde{\mathrm{p}}}$ computed from observed data approaches the CRLB for SNR below 40 dB. This is due to the constraint violation of the Taylor series expansion.
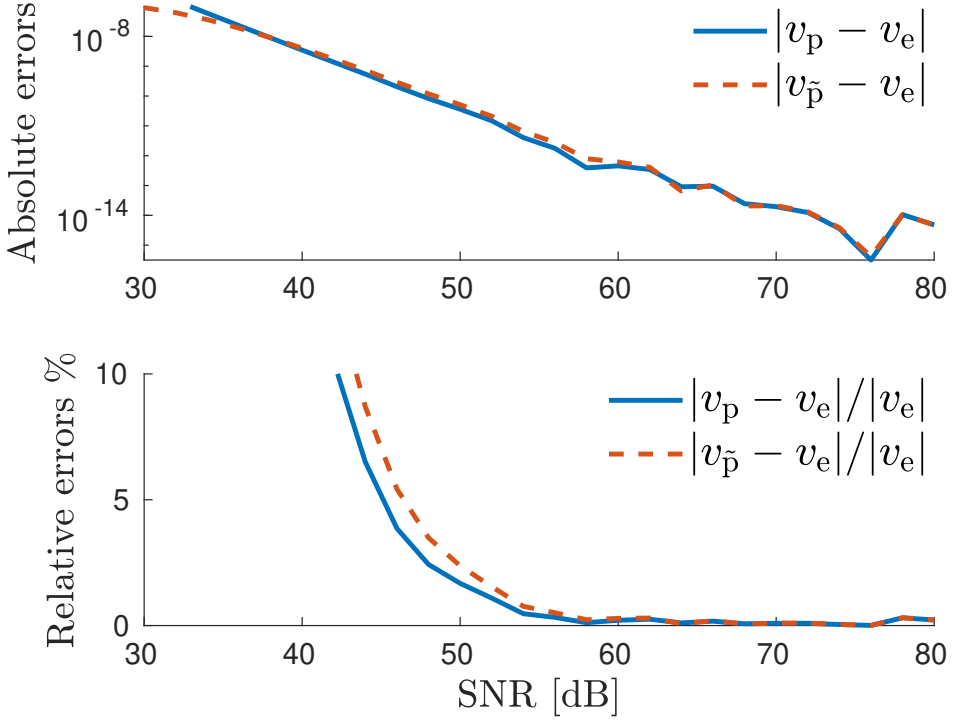
Figure 4.9.: The MC simulation shows that when we solve a structured EIV problem with LS, the absolute errors (top) between the predicted and the empirical variance are proportional to the perturbation variance, and the relative errors (bottom) between the predicted and the empirical variance are smaller than 5% for SNR above 45 dB.

## 4.2.3. Simulation results for the structured IV solution

The structured IV problem, with instrumental variable (4.23), and normal equations (4.21), admits also a recursive least-squares solution. A Monte Carlo simulation was conducted to find the empirical bias and variance of the solution to the IV problem. This simulation is conducted using the same conditions as for the structured EIV problem, in the previous subsection, and aims to compare the EIV and the IV problem solutions. In Figure 4.12 we can observe, for different SNR levels, the empirical bias (top), variance(center), and mean-squared error (bottom) of the solutions to the EIV and the IV problems. The empirical bias the IV solution is two orders of magnitude smaller than that of the EIV solution. Nevertheless,
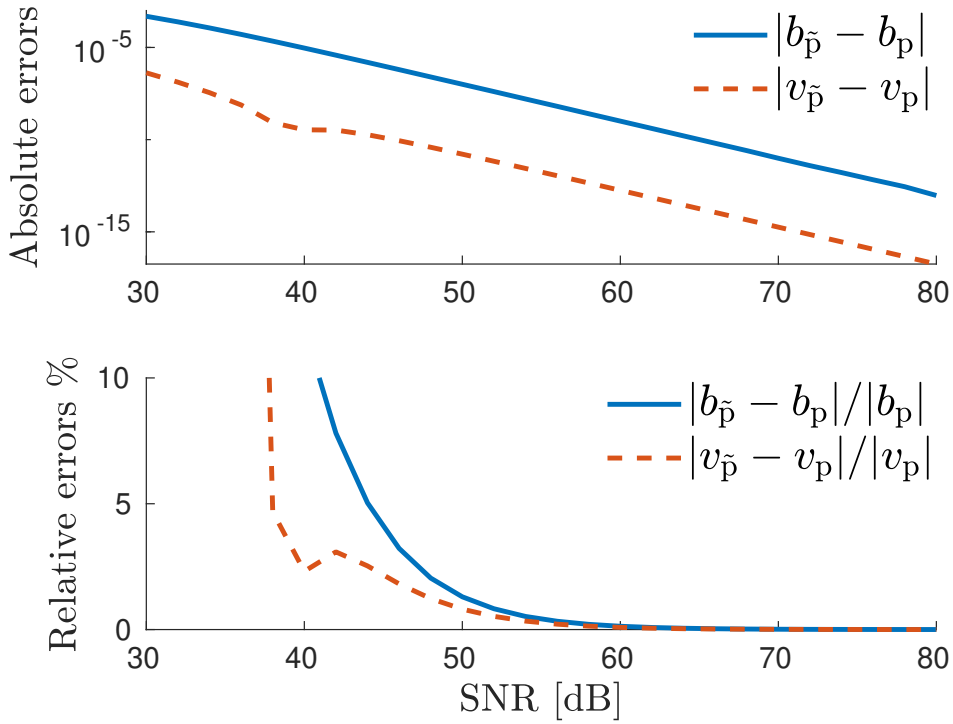
Figure 4.10.: The MC simulation shows that when we solve a structured EIV problem with LS, the absolute errors (top) between the predictions computed from observed data and those from exact data are proportional to the perturbation noise variance. According to the relative errors (bottom), the substitution is valid for SNR higher than 45 dB.

the empirical variance of the two solutions are very close together, making the mean-squared error almost identical.
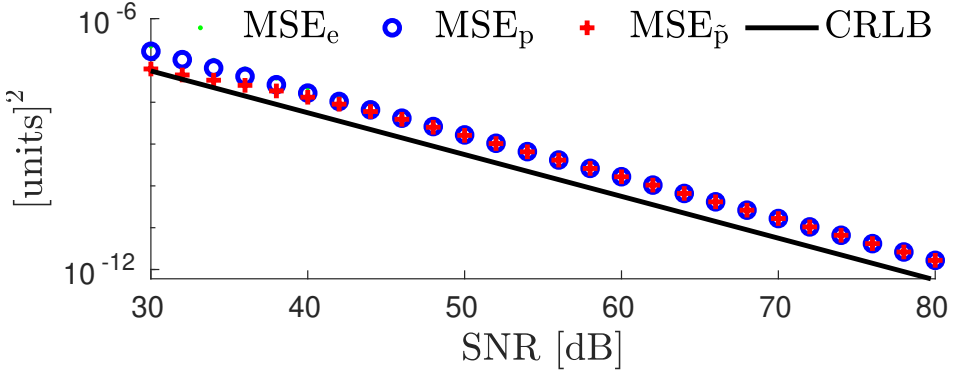
Figure 4.11.: The mean squared errors of the LS estimate are close to the Cramér-Rao lower bound. This is a positive indication of the goodness of the LS estimator for the structured EIV problem. The mean squared error of the empirical estimates is represented by $\mathrm{MSE_e}$, and those of the predictions are $\mathrm{MSE_p}$ and $\mathrm{MSE_{\tilde{p}}}$. The $\mathrm{MSE_{\tilde{p}}}$ is smaller than CRLB below 40 dB of SNR because of the introduced bias error, but the difference between $\mathrm{MSE_{\tilde{p}}}$ and the CRLB is lower than one order of magnitude.
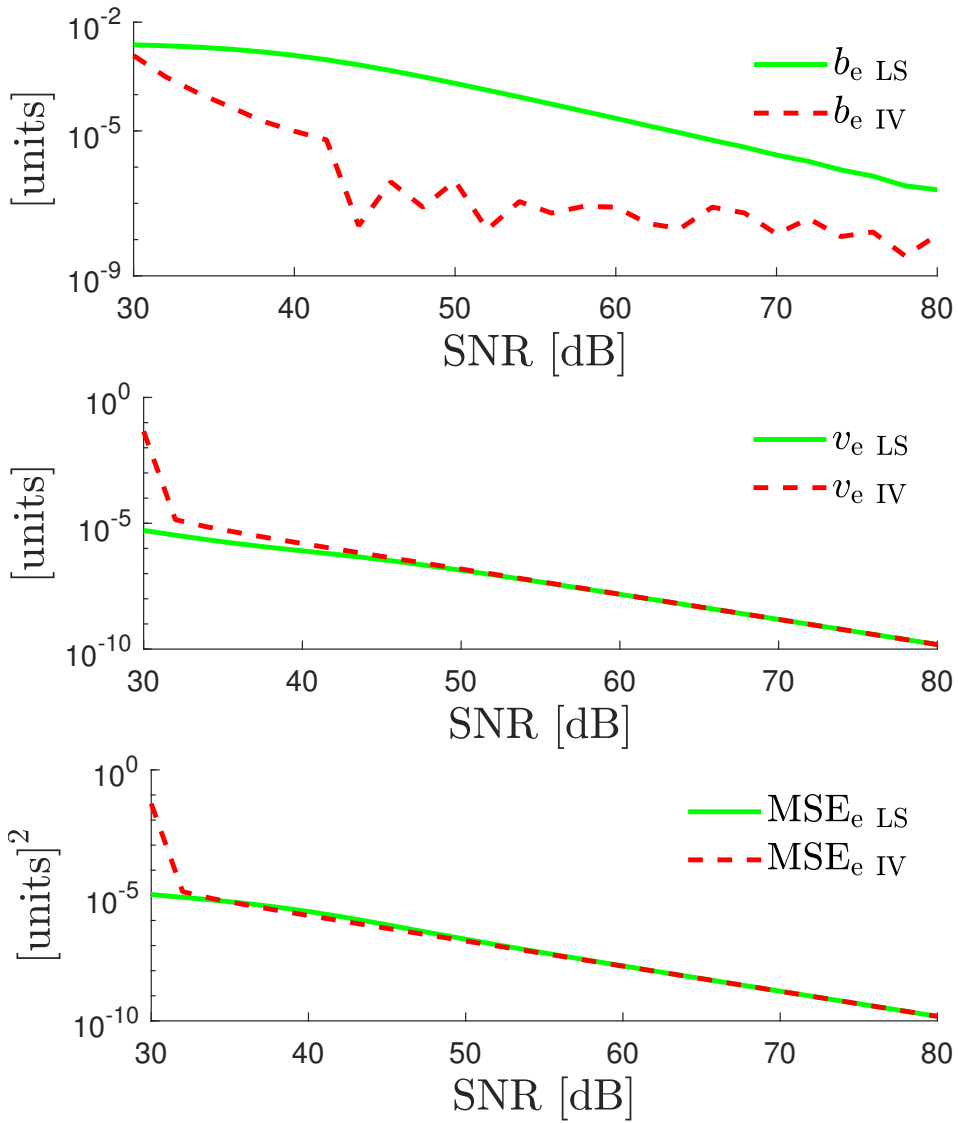
Figure 4.12.: In a simulation, the solutions of the structured EIV and IV problems are empirically compared. The bias from solving the IV problem is noticeable smaller, by two orders of magnitude, than the one from solving the EIV problem. This argument is valid for SNRs higher that 35 dB. The obtained variances, on the other hand, are very similar in the same SNR interval. As a consequence, the mean-squared errors almost coincide.

# 4.3. Conclusions

We conducted a statistical analysis of a structured errors-in-variables (EIV) estimation problem with correlation to find the first and second moments of its least-squares solution. This estimation problem occurs in metrology when we estimate the value of a measurand directly from the sensor transient response. The data-driven estimation of the physical quantity is formulated as a structured EIV problem with correlation that uses the observed transient response to construct both the regression matrix and the regressor. The real-time implementation of the method uses a recursive least-squares algorithm that is simple and has low computational complexity. The assessment of the uncertainty is done using the estimation bias and variance.

The conducted statistical analysis produced expressions that predict the estimation bias and variance for given sample size and perturbation level of the observed response. The Monte Carlo simulation validated the predictions. We compared the results of solving an unstructured and uncorrelated EIV problem with a structured and correlated EIV problem to understand how the structure and the correlation impacts in the estimation. We found that the predictions in the structured case are more susceptible to perturbations. This is due to the two approximations involved, a second-order Taylor series expansion of the estimate, and the substitution of perturbed data on the prediction expressions. The relative error results indicate that the estimation bias, and variance are predicted using the derived expressions, and the observed data. The mean squared error of the estimate is close to the results of the maximum likelihood estimate given by the Cramér-Rao lower bound.

The bias and variance can be accurately predicted, provided that the Taylor series expansion is valid. This constraint has to be taken into account to ensure the effectiveness of the method in practical applications. In the example, it was observed that when the SNR lies outside the validity region, the bias and variance estimation was at most three times larger than the empirical values.

The methodology presented in this chapter can be applied to estimate the uncertainty of the solutions to other structured EIV problems. The bias and variance expressions obtained after the statistical analysis depend on each specific structure.

# 5. Experimental validation of the step input estimation method

A measurement is a dynamic process and a sensor is a dynamic system that is excited by the unknown and to-be-measured input. The input application drives the sensor into a transient regime response. The input excitation influences the sensor output, and the input has to be estimated using the sensor transient response. If the sensor reached its steady-state, the input would be straightforwardly estimated from the sensor output making use of the sensor static gain. As is discussed in Dienstfrey and Hale [2014], the lower is the sensor bandwidth the higher is the need for methods based on processing the sensor transient response to obtain fast input estimation.

A common approach is to filter the sensor transient response with another dynamic system that inverts the sensor dynamics, aiming to compensate the sensor transient time. Examples of this compensation approach are the FIR filter described in Elster et al. [2007], the time-varying continuous-time filter conceived in Piskorowski and Barcinski [2008], and the IIR filters presented in Link and Elster [2009] and Eichstädt et al. [2010]. The main drawback of the common approach is that the compensator design needs to be based on a sensor model. The sensor model requirement implies that the uncertainty on the parameters contributes to the uncertainty budget, as it is explained in Hessling [2011]. The uncertainty propagation through the compensation systems has been studied in Elster et al. [2007]; Link et al. [2007] for the estimated model parameters, in Eichstädt et al. [2016] for a Kalman filter estimator, and in D'Emilia et al. [2016] considering the models of the different elements in the measurement system.

An approach different to compensation uses digital signal processing methods that are independent of the sensor model. This is especially relevant when the measurement system is inaccessible as the temperature sensor on board of a spatial probe described in Saggin et al. [2001], or when the formulation of the estimation method bypasses the model identification and estimates directly the input as in the method introduced in Markovsky [2015a] that estimates the unknown level of step inputs. This data-driven method step input estimation method did not have a method describe its uncertainty, but in the previous chapter of this work is described a methodology to obtain the bias and the variance of the step input estimation. The methodology yields expressions for the bias and variance, and the expressions are validated via Monte Carlo simulation as is suggested in the work of Cox and Siebert [2006]. The estimation uncertainty is then described with the estimation first two statistical moments. This chapter describes the experiments performed to assess the uncertainty of the data-driven step input estimation method under real life data. The estimation method processed step responses from a weighing sensor experimental setup. The experimental results are put in perspective to the simulations and validate the data-driven step input

estimation method, showing which intervals of SNR and sample size ensure the reliability of the method.

The weighing system is constructed using a load cell as the sensing element. The load cell is a popular and versatile device that has been used in weighing sistems in the works of Piskorowski and Barcinski [2008], Boschetti et al. [2013], Kesilmiş and Bar [2016], and Guo et al. [2018]. Other magnitudes can also be measured with load cell, examples of these are found in the works of Rossander et al. [2015] that measure forces in the blades of a wind turbine, Hernandez [2006] that improve the quality of confort of bus seats measuring the forces they are subjet to, Alaziz et al. [2017] and Zahradka et al. [2018] that monitor the quality of sleep by sensing the body motion on the bed, Ballo et al. [2016] that measure accelerations on a dummy in frontal impact tests.

## 5.1. Simulation results

A Monte Carlo (MC) simulation was conducted to test the bias and covariance expressions (4.13) and (4.14). The MC simulation performed $N_{MC} = 10^4$ runs of the data-driven step input estimation with different realizations of the measurement noise $\epsilon$. The MC simulation was conducted processing $N = 5000$ samples of a simulated transient step response $\widehat{\mathbf{y}}$ generated by a stable linear time-invariant (LTI) system of order $n = 5$, with a sampling frequency of $f_s = 4$ kHz. This system is a state-space model obtained with the System Identification Toolbox using the measured step response of the actual sensor described in the Practical Implementation Section. This model represents a weighing sensor, and in the simulations the sensor is excited with a mass of 138.32 g following a step input profile. As can be seen in Figure 5.1, the steady state response of the weighing sensor model is practically reached after 500 samples because from there on the relative error between the transient response and the steady-state response is smaller than 0.2%.

A sensor is a dynamic system, therefore, a fast measurement process must necessarily cope with the system transient response. In that respect we must distinguish between the transient response of the system under test, and the transient phase of the measurement process (i.e. before the process has settled on a final measurement outcome). Notice that the transient phase of the measurement process is considerably smaller than the settling time of the system under test, and this is a major advantage of the step input estimation method.
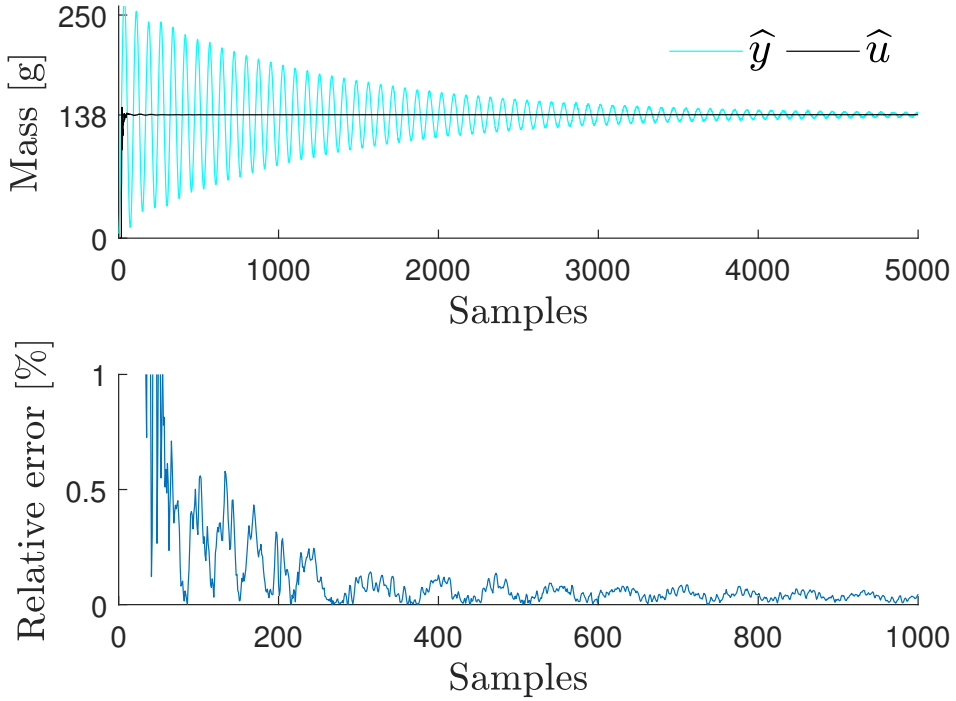
Figure 5.1.: Above: example of a simulated response $\widehat{\mathbf{y}}$ and its step input estimation $\widehat{u}$ assuming measurement Gaussian noise with 50 dB of SNR. Below: the relative error $|\widehat{u} - u|/u$ is below 1% after 100 samples. We take the estimate at 500 samples because there the relative error is smaller than 0.2%.

We are interested in the first element of $\widehat{\boldsymbol{\theta}}$, which is the input estimate $\widehat{u}$. The measurement noise variance was selected to have a signal-to-noise ratio (SNR) in the interval [30 dB, 80 dB], according to (4.37).

The difference between the sample mean $\widehat{\mu}_u$ of the step input estimates and the true value $u$ is the empirical bias $b_{\mathrm{e}}$.

$$b_{\mathrm{e}} = \frac{1}{N_{MC}} \sum_{i=1}^{N_{MC}} \widehat{u}_i - u = \widehat{\mu}_u - u. \tag{5.1}$$

The sample variance $\widehat{\sigma}_u^2$ of the step input estimates is used to obtain the standard error of the MC simulation $\sigma_{\mathrm{e}}$, which decreases with respect to the square root of

the number of MC runs $N_{MC}$.

$$\sigma_{\text{e}} = \frac{\widehat{\sigma}_u}{\sqrt{N_{MC}}}, \text{ where } \widehat{\sigma}_u^2 = \frac{1}{N_{MC}-1} \sum_{i=1}^{N_{MC}} (\widehat{u}_i - \widehat{\mu}_u)^2. \tag{5.2}$$

In each of the $N_{MC}$ runs, we compute the predictions of the step input estimation bias and variance from measured data using Equations (4.13) and (4.14). The step input bias and variance predictions from observed data $b_{\widetilde{\text{p}}}$ and $v_{\widetilde{\text{p}}}$, and the associated standard error $\sigma_{\widetilde{\text{p}},\text{err}}$, are obtained from

$$b_{\widetilde{\text{p}}} = \frac{1}{N_{MC}} \sum_{i=1}^{N_{MC}} \mathbf{b}_{\widetilde{\text{p}}}^i \left( \widehat{\boldsymbol{\theta}} \right) \big|_{[1]}, \ v_{\widetilde{\text{p}}} = \frac{1}{N_{MC}} \sum_{i=1}^{N_{MC}} \mathbf{C}_{\widetilde{\text{p}}}^i \left( \widehat{\boldsymbol{\theta}} \right) \big|_{[1,1]},$$

$$\text{and} \quad \sigma_{\widetilde{\text{p}},\text{err}} = \sqrt{\frac{\sum_{i=1}^{N_{MC}} \left( \mathbf{b}_{\widetilde{\text{p}}}^i \left( \widehat{\boldsymbol{\theta}} \right) \big|_{[1]} - b_{\widetilde{\text{p}}} \right)^2}{N_{MC} (N_{MC}-1)}}, \tag{5.3}$$

where $\widetilde{\mathbf{b}}_{\text{p}}^i \left( \widehat{\boldsymbol{\theta}} \right) \big|_{[1]}$ is the first element in the bias vector and $\widetilde{\mathbf{C}}_{\text{p}}^i \left( \widehat{\boldsymbol{\theta}} \right) \big|_{[1,1]}$ is the first element in the covariance matrix obtained in the $i-$th approximations. The predicted bias and variance from exact data are obtained with one evaluation of the expressions (4.11) and (4.12)

$$b_{\text{p}} = \frac{1}{N_{MC}} \sum_{i=1}^{N_{MC}} \mathbf{b}_{\text{p}} \left( \widehat{\boldsymbol{\theta}} \right) \big|_{[1]}, \text{ and } v_{\text{p}} = \frac{1}{N_{MC}} \sum_{i=1}^{N_{MC}} \mathbf{C}_{\text{p}} \left( \widehat{\boldsymbol{\theta}} \right) \big|_{[1,1]}. \tag{5.4}$$

The uncertainty of the step input estimate is defined as the spread of the estimates that is given by the predicted variance $v_{\text{p}}$.

Figure 5.2 shows the empirical bias, the bias predictions and the standard errors of the MC simulation. It can be seen that the empirical bias $b_{\text{e}}$ and the predicted bias $b_{\widetilde{\text{p}}}$ are proportional to the perturbation noise variance while the standard errors $\sigma_{\text{e},\text{err}}$ and $\sigma_{\widetilde{\text{p}},\text{err}}$ are proportional to the perturbation noise standard deviation. For SNR below 40 dB there is a difference of a small order of magnitude between the empirical bias $b_{\text{e}}$ and the bias prediction $b_{\widetilde{\text{p}}}$.

The standard errors of the MC simulation $\sigma_{\text{e},\text{err}}$ and $\sigma_{\widetilde{\text{p}},\text{err}}$ are smaller than $b_{\text{e}}$ and $b_{\widetilde{\text{p}}}$. The estimates are spread near the sample mean and the uncertainty is smaller than the bias. Therefore, the empirical bias of the MC simulation is meaningful.

The mean squared error (MSE) of the step input estimate, defined as

$$\text{MSE} = b^2 + v, \tag{5.5}$$

where $b$ and $v$ are the bias and the variance of the step input estimate, can be applied to the obtained empirical and predicted results and can be compared to
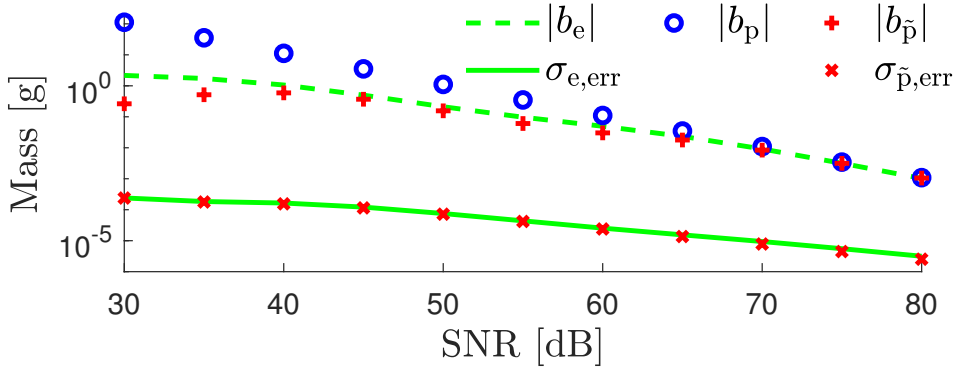
Figure 5.2.: The results of the Monte Carlo simulation of the step input estimation method are the empirical bias $b_e$, the predicted bias using exact data $b_p$, the predicted bias using measured data $b_{\tilde{p}}$, the empirical standard error $\sigma_{e,err}$, and the predicted standard error $\sigma_{\tilde{p},err}$. The estimation biases are proportional to the perturbation variance and the estimation standard errors are proportional to the perturbation standard deviation. Since the standard errors are smaller than the biases, the MC simulation is meaningful.

the Cramér-Rao lower bound (CRLB). Figure 5.3 shows that $\mathrm{MSE}_e = b_e^2 + v_e$ and $\mathrm{MSE}_{\tilde{p}} = b_{\tilde{p}}^2 + v_{\tilde{p}}$ have the same proportionality with respect to the measurement noise variance as the bound for an unbiased estimator $\mathrm{CRLB}_{ub}$. For SNR above 35 dB, $\mathrm{MSE}_e$ and $\mathrm{MSE}_{\tilde{p}}$ are equivalent, and below 35 dB the difference between them is of less than a factor of 10.

We obtained an approximation of the $\mathrm{CRLB}_b$ for our biased estimator using the partial derivative of the bias in expression (4.13). Figure shows that the bounds for the unbiased and biased estimators are almost equal because the partial derivatives of the bias are negligible w.r.t. 1 in Equation (4.15). By adding the square of the predicted bias to the biased estimator bound $\mathrm{CRLB}_b$ we obtain an approximation of the minimum MSE that the biased estimator can achieve. This minimum MSE is close to the CRLBs for large SNR but the square of the bias causes an increase of the MSE around 35 dB. The differences between the CRLBs and $\mathrm{MSE}_e$ and $\mathrm{MSE}_{\tilde{p}}$ are of one order of magnitude for large SNR and become small for SNR lower than 40 dB. This difference is the cost of solving a structured EIV problem with a simple LS method.

There are two features of the system step response that make the CRLB small. One is the measurement noise variance and the second is sample size. The estimation
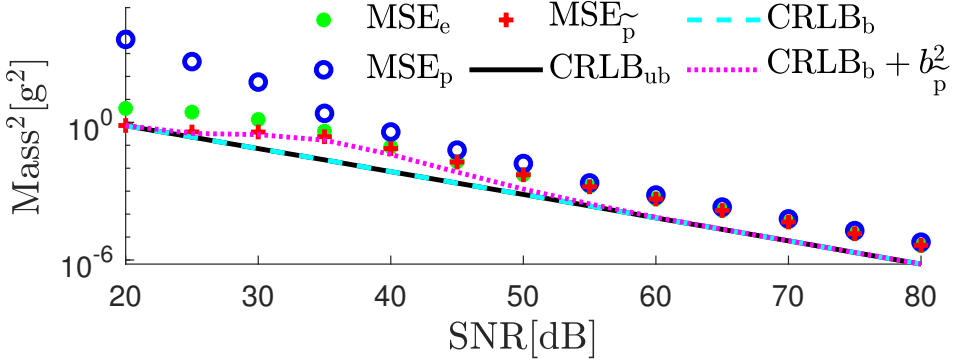
Figure 5.3.: The observation instant is fixed at 500 samples. The bias and the MSEs decrease for large SNR. The empirical $MSE_e$ and the predicted $MSE_{\widetilde{p}}$ of the step input estimation are one order of magnitude larger than the Cramér-Rao lower bound. Adding the CRLB for a biased estimator with the predicted bias squared we have the minimum MSE, that grows in the interval [25 dB, 45 dB]. Below 35 dB the difference between $MSE_{\widetilde{p}}$ and the CRLB is less than a factor of 10.

from step response perturbed with small noise variance has lower uncertainty. Also, using larger sample size to perform the estimation boils down to smaller estimation uncertainty.

In order to get more insight into the step input estimation method we conducted another simulation study. The step input estimation method assumes the order $n$ is given in (3.21). In this simulation, the step input estimation method processed the step response generated by a $5-th$ order system using different values of $n$ in the interval from 2 to 100.

The step response is perturbed with Gaussian white noise with SNR values in the interval [20 dB, 80 dB]. For each order $n$ and SNR value, 100 step input estimations are performed from independent noise realizations. Figure 5.4 shows the average of the squared biases and the variances, and the MSEs of the input estimate using the first 500 samples. It is evident that the estimation variance and MSE depend on the SNR.

Increasing the order $n$ is equivalent to adding more regressors in the regression problem. It is well known that increasing the order $n$ causes a monotonic decrement of the estimation bias and increment of the variance. This is the asymptotic behavior of the estimation statistical moments with respect to the number of regressors. Nevertheless, the simulation results presented in Figure 5.4 show

that the variance first increases for small values of $n$, followed by a decrement and finally after $n \approx 40$ the variances exhibit a slow and steady increment. This apparent contradiction does not prove the invalidity of the estimation method since the results presented correspond to a finite sample size and the asymptotic results cannot be applied. The theoretical explanation of the estimation statistics for finite sample sizes is out of the scope of this document.

There is a bias-variance tradeoff and the MSEs exhibit local minima with respect to $n$. The principal contribution to the MSE is the squared bias for the smaller values of $n$ and the variance for the larger values of $n$. However, the higher orders do not produce overfitting since the MSEs do not grow fast and remain close to the minimum values.

The optimum value of $n$ is not necessarily equal to the order of the generating system and varies for each SNR. According to the plots in Figure 5.4, there are orders that provide local minima of the step input estimation MSEs. From the right hand side of Figure 5.4, the orders that give the first two MSE minima were identified and those values are listed in Table 5.1. For each SNR, there is a first minimum at a low order and a second minimum at a high order. For SNR of 30 and 40 dB, it is recommended to use the order that gives the first minimum since the MSE at the second minimum is less than one order of magnitude smaller than at the first minimum. Depending on the requirements, the user can choose between the simplicity of an estimation with a low order or an estimation with higher computational complexity and a smaller MSE. In a calibration stage, during the setup of the estimation method, the user can search and set the order that enables the estimation method to provide a required MSE.

Table 5.1.: Orders $n$ that provide local minima for the MSE of the step input estimate. It is recommended to use the order that gives the first minimum when there is a difference of small order of magnitude with respect to the MSE at the second minimum.

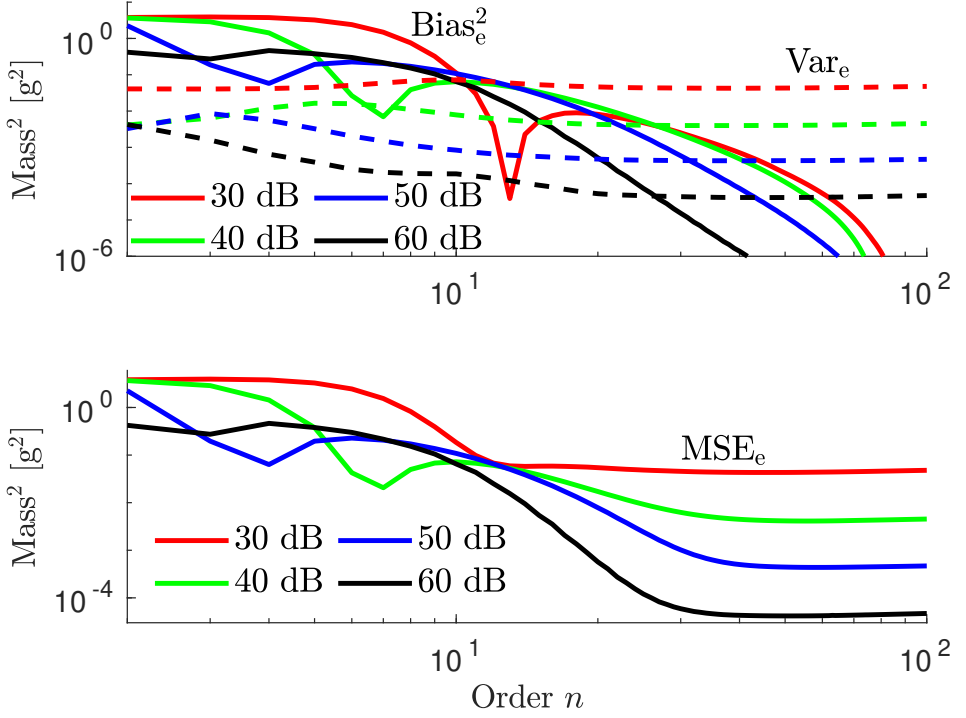| SNR [dB] | 30 | 40 | 50 | 60 |
|---|---|---|---|---|
| order at first minimum | 11 | 7 | 4 | 3 |
| order at second minimum | 40 | 35 | 40 | 31 |

Figure 5.4.: The simulated step responses of a $5-th$ order system are processed by the step input estimation method using different orders $n$ and independent noise realizations. The perturbation of the step responses is Gaussian white noise with SNRs of 30, 40, 50, and 60 dB. The square of the empirical bias (solid) and the empirical variance (dashed) are shown on the left hand side and the MSE is shown on the right hand side, for $n$ between 2 and 100. These results suggest that, during the setup of the estimation method, we have to search the order that gives the minimum MSE without increasing unnecessarily the complexity of the estimation method.

## 5.2. Practical implementation

An experimental setup was constructed to test the step input estimation method. The implementation is a weighing system that uses a load cell Tedea Huntleigh 1004, whose specifications are found in Tedea-Huntleigh [2015]. The maximum rating of the load cell is 600 g. A cylindrical aluminium object of 138.32 g of mass was used to excite the load cell. This value was found by calibration using a balance KERN PCB 200-2 that has an uncertainty of 0.01 g. The step input excitation was provided by a magnet that holds and releases a mass from above the load cell. The magnet is located sufficiently far from the load cell to avoid magnetic interference in the sensor response.
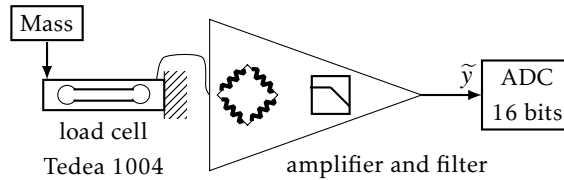


Figure 5.5.: Diagram of the load cell and the conditioning amplifier that provide the sensor response.

A two-stage linear conditioning amplifier performs amplification and filtering of the load cell signal. The first stage is a precision instrumentation amplifier INA114 that has high common mode rejection ratio. The second stage is a third-order low-pass Butterworth filter with cut-off frequency of 100 Hz. The low-pass filter prevents the aliasing noise in the measured transient response. The signal obtained from the conditioning amplifier is considered to be the response of the sensor. The sensor responses to step excitations were sampled with a frequency of $f_s = 4$ kHz, and therefore the Nyquist frequency is 2 kHz. The step responses were collected and stored as datasets for further analysis. The datasets, and the code used to generate the results in this section are publicly available in the sense of reproducible research research in the following url: https://drive.google.com/drive/folders/1EfQb4nccg6x4kGcZropKRug3WkeNGX-m?usp=sharing. The number of samples collected for each step response is $N = 20000$. For practical purposes, we consider that the last 10000 samples correspond to the steady state response.

The step input estimation method processed 100 measured sensor step responses, assuming the sensor is of $7-th$ order. Figure 5.6 shows a typical measured transient response $\widetilde{y}$ and an example of the estimated input $\widehat{u}$.
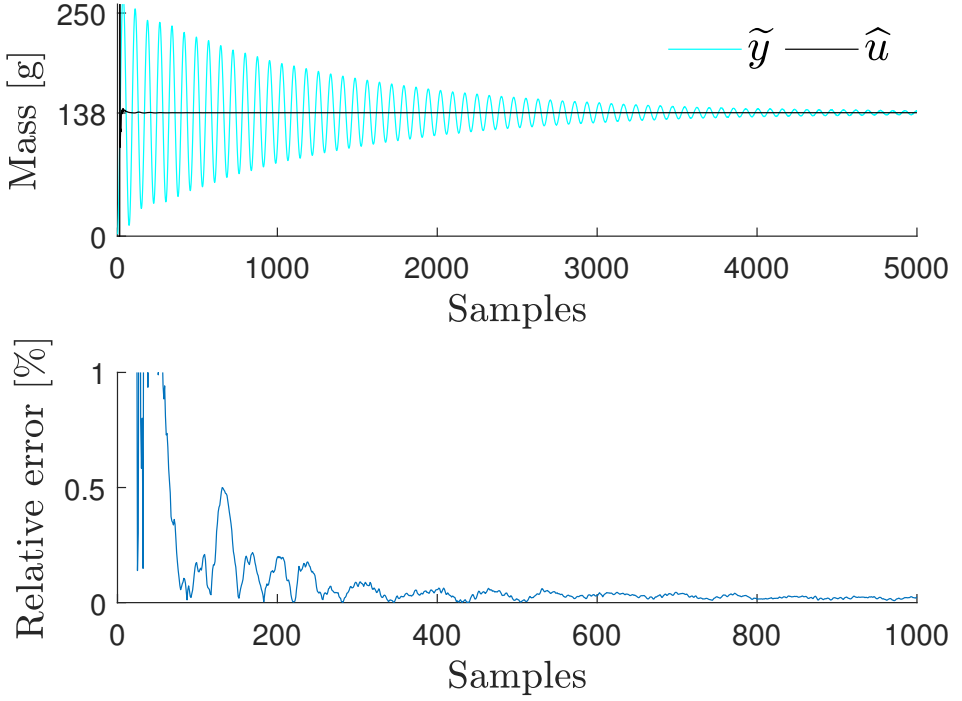
Figure 5.6.: Above: a typical measured sensor transient response $\widetilde{y}$ takes more than 1.25 s (5000 samples, $f_s = 4$ kHz) to converge to the steady state response. Below: the relative error of the input estimate $\widehat{u}$ is smaller than 0.2% from 300 samples. We consider that at 500 samples the relative error of the estimate $\widehat{u}$ is small enough to consider that $\widehat{u}$ is close to its expected value $u$.

The empirical bias $b_e$ is the difference between the average of the 100 estimates $\widehat{u}$ and the mass calibration value $u = 138.32$ g, at each instant of time, and the standard error $\sigma_{e,err}$ is the standard deviation of the mean estimate of the responses processed, i.e.,

$$\widehat{\mu}_e = \frac{1}{100}\sum_{i=1}^{100}\widehat{u}_i, \quad b_e = \widehat{\mu}_e - u, \quad \text{and}$$

$$\sigma_{e,err} = \frac{\widehat{\sigma}_e}{\sqrt{100}}, \quad \text{where } \widehat{\sigma}_e{}^2 = \frac{1}{99}\sum_{i=1}^{100}(\widehat{u}_i - \widehat{\mu}_e)^2. \tag{5.6}$$

The bias $\widetilde{b}_p$ and variance $\widetilde{v}_p$ predictions from the measured data were obtained by processing off-line the 100 measured sensor transient step responses with

expressions (4.13) and (4.14). These expressions require the measurement noise variance $\sigma_\varepsilon^2$ to obtain the bias and variance prediction. One way to estimate the measurement noise variance is computing the variance of each sensor steady state response, see Figure 5.7. Later in this section we will explore another way to estimate the measurement noise variance. Computing the noise variance from the steady state response we observed that the SNR of the measured step responses is 55 dB in average.
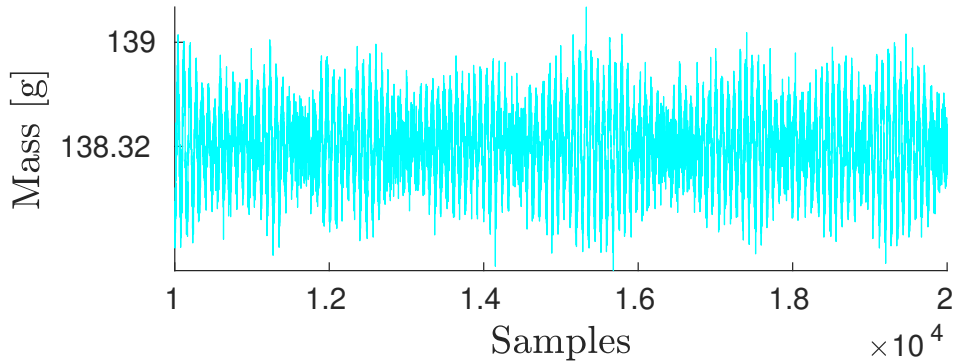


Figure 5.7.: From the sensor steady-state response an estimation of the measurement noise variance is obtained.

Figure 5.8 shows the empirical bias $b_e$ and the standard error $\sigma_{e,err}$ that result after processing the first $N = 500$ samples of the 100 measured step responses $\widetilde{\mathbf{y}}$. The standard error is smaller than the bias. As it was observed in the MC simulation, this is the uncertainty of the estimation method. The oscillations observed in the bias are mainly due to the transient response and not to the measurement noise. The measurement noise effects are partially removed since we averaged the 100 transient responses, which is a small number compared with the $N_{MC}$ runs averaged in the simulation section.

It is expected that the empirical bias is large when a small number of samples is processed. The data-driven input estimation method is recursive and it is implemented in real-time. The estimation errors decrease as more data is processed.

The measurement noise is not white since there is evidence of frequency components in the sensor steady state response that are observed as oscillations in Fig 5.7. To get insight into the properties of the measured sensor response $\widetilde{\mathbf{y}}$, a $7-th$ order model was identified from input-output data assuming that the input is a step of level $u$. A response $\widehat{\mathbf{y}}$ was simulated from the identified model and the residual $\mathbf{r} = \widetilde{\mathbf{y}} - \widehat{\mathbf{y}}$ was obtained. We can observe these signals in the frequency domain
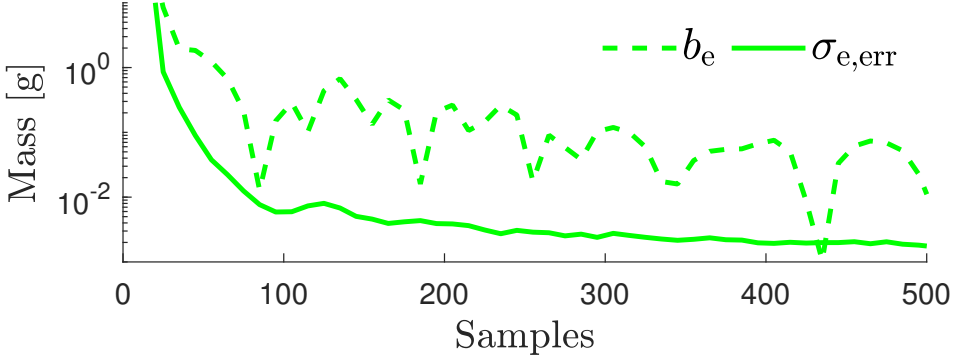
Figure 5.8.: The results of estimating the step input level after processing 100 measured step responses are the empirical bias $b_e$ and the empirical standard error $\sigma_{e,err}$. The estimation bias and the estimation standard error decrease as more samples are processed. The estimation bias is affected by the transient effects of the sensor response. The values of $b_e$ and $\sigma_e$ provide the estimate accuracy and uncertainty for a given sample size.

using the discrete Fourier transform, that for the signal $\widetilde{\mathbf{y}}$ is defined as

$$\widetilde{Y}(f) = \frac{1}{\sqrt{N}} \sum_{k=0}^{N-1} \widetilde{y}(k) e^{-j2\pi k f/N} \tag{5.7}$$

where $f = 1, \ldots, N/2$ are the frequency lines and $N$ is the total number of samples. The power spectrum of the signal $\widetilde{\mathbf{y}}$ is given in decibels by $\widetilde{\mathbf{Y}}_{dB} = 20\log_{10}|\widetilde{\mathbf{Y}}|$. Figure 5.9 shows the corresponding power spectra of the sensor response $\widetilde{\mathbf{Y}}_{dB}$, the simulated response $\widehat{\mathbf{Y}}_{dB}$, and the residual $\mathbf{R}_{dB}$. There are frequency components near the main resonance peak in the magnitude spectrum of the residual. The presence of frequency components near the main resonance peak is commonly found in mechanical devices. The vibrations captured from the environment explain the accumulation of energy near the main resonance modes.

Even when the residual $\mathbf{r}$ is not white, it provides an alternative way to estimate the measurement noise variance. The average of the residual power spectrum approximates the measurement noise variance as follows

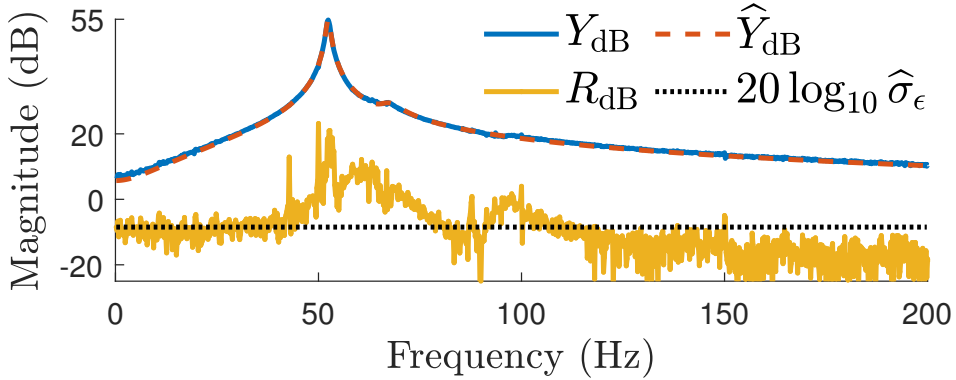$$\widehat{\sigma}_\varepsilon^2 \approx \frac{2}{N} \sum_{f=1}^{N/2} |R(f)|^2. \tag{5.8}$$

Figure 5.9.: The power spectra of a measured response $\widetilde{\mathbf{Y}}_{\mathrm{dB}}$, a simulated response $\widehat{\mathbf{Y}}_{\mathrm{dB}}$, and the residual $\mathbf{R}_{\mathrm{dB}}$ is not flat and then the measurement noise is not white. The average of the residual power spectrum provides a conservative estimate of the measurement noise variance $\widehat{\sigma}_{\varepsilon}^2$, represented with the dotted line.

The dotted line in Figure 5.9 indicates the $10\log_{10}\left(\widehat{\sigma}_{\varepsilon}^2\right)$ level of the measurement noise variance estimated from the residual. This level is higher than the mean value of the residual power spectrum $\mathbf{R}_{\mathrm{dB}}$ in the frequencies above 120 Hz.

Using the residual power spectra that correspond to the measured step responses, we obtained the measurement noise variance and the SNR for each experiment. Figure 5.10 shows the estimated SNRs from the residual power spectra. The SNR mean value is 50 dB. Therefore, we assume that the SNR of the measured transient responses is 50 dB instead of 55 dB, as it was estimated from the steady state response.

The 5 dB difference provides a conservative bound since the bias and variance computed from 50 dB of SNR are higher than those obtained using the variance estimation from the steady-state response. Figure 5.11 shows a comparison of the results obtained with both measurement noise variance estimations after processing the first $N = 500$ samples of the step response $\widetilde{\mathbf{y}}$. Using expression (4.13), the bias prediction $b_{\widetilde{\mathrm{p}}2}$ obtained using an SNR of 50 dB approximates more closely the empirical bias than $b_{\widetilde{\mathrm{p}}1}$ obtained using an SNR of 55dB. In accordance, the standard error of the bias predictions $\sigma_{\widetilde{\mathrm{p}},\mathrm{err}2}$ is larger than $\sigma_{\widetilde{\mathrm{p}},\mathrm{err}1}$ and is a conservative measure of the input estimation uncertainty. In conclusion, using the noise variance estimated from the residual prevents underestimating the step input estimation uncertainty.
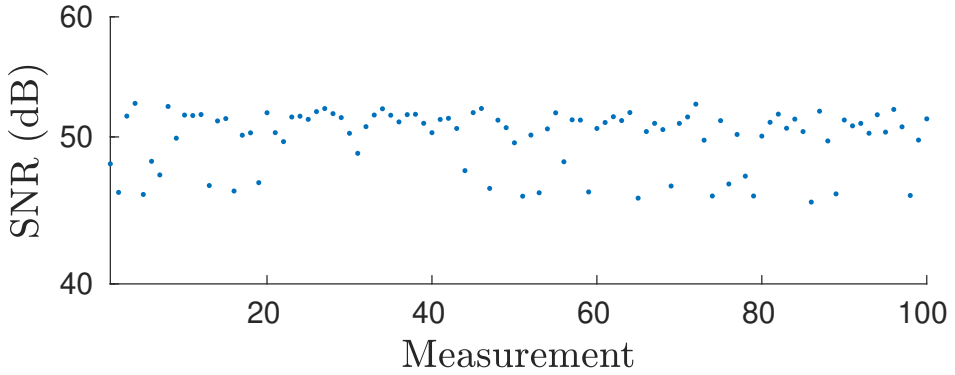
Figure 5.10.: The mean value of the signal-to-noise ratios estimated from the residual power spectra is 50 dB. We consider that this is the estimated SNR of the measured step responses.
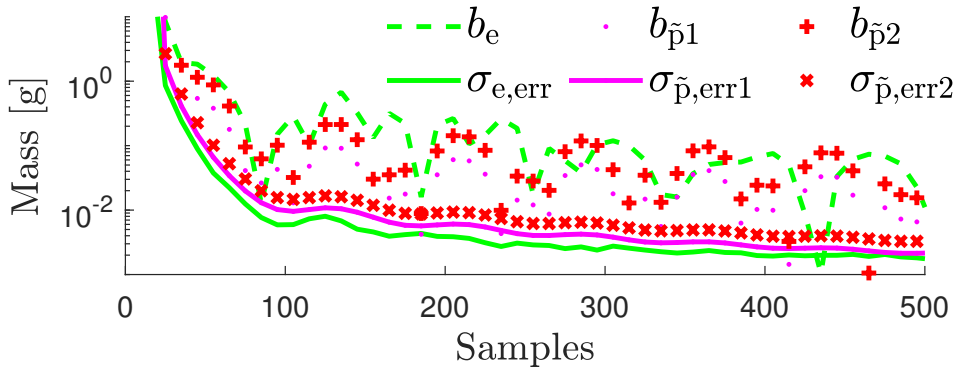


Figure 5.11.: Comparative view of the bias prediction using two different noise variance estimations. Estimating the variance from the step response residual gives a bias prediction $b_{\tilde{p}2}$ and a standard error $\sigma_{\tilde{p},\mathrm{err}2}$ that are slightly higher than $b_{\tilde{p}1}$ and $\sigma_{\tilde{p},\mathrm{err}1}$ which correspond to computations that use the noise variance estimated from the steady state response. The bias prediction $b_{\tilde{p}2}$ approximates better the empirical bias. The standard error $\sigma_{\tilde{p},\mathrm{err}2}$ provides a conservative value of the input estimation uncertainty.

We investigated another aspect of the step input estimation method performance when processing measured step responses. The step input estimation method requires an assumption of the generating system order in the formulation of the estimation problem (3.21). The estimation method performance is assessed under

different assumptions of the values of $n$ in the interval from 2 to 100. For each value of $n$, 100 step input estimations are computed from measured transient responses and the empirical MSEs are compared. Figure 5.12 shows that, similar to the observations made in the simulation study, the MSEs have two local minima at $n = 7$ and $n = 48$. It is recommended to use $n = 7$ in the estimation method to provide a small estimation MSE without the higher computational complexity that $n = 48$ implies.
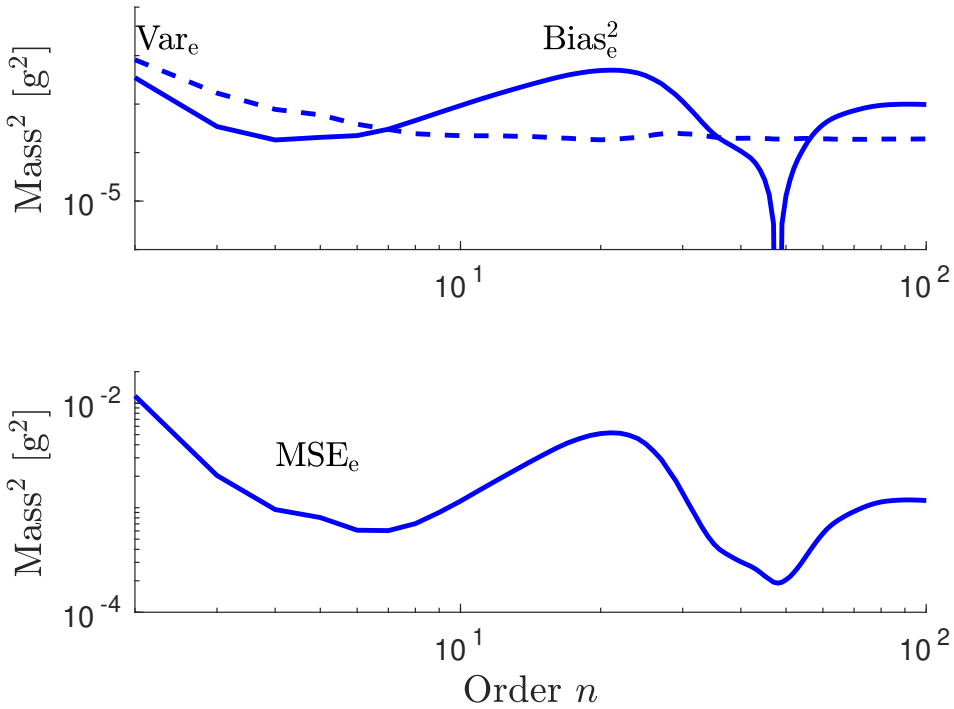


Figure 5.12.: The hundred measured sensor step responses are processed by the step input estimation method for different values of the order $n$. The empirical squared bias (solid) and the empirical variance (dashed) are shown on the left and the empirical MSE on the right. The MSE has a local minimum at $n = 7$ and another at $n = 48$. It is recommended to use the estimation method with $n = 7$ because at $n = 48$ the decrement of the MSE is not significant.

# 5.3. Conclusions

In this chapter we investigated the statistical properties of a data-driven step input estimation method in a real-life application. The step input estimation method is a structured and correlated errors-in-variables problem that is solved with recursive least-squares. A statistical analysis was conducted using the ordinary least-squares condensed notation. This statistical analysis of the input estimate provides expressions that approximate the estimation bias and variance assuming that the measurement noise is Gaussian white noise. The variance approximation is useful to assess the uncertainty of the input estimate. In simulation we observed that the mean squared error of the input estimate is close to the theoretical minimum that uses the Cramér-Rao lower bound for biased estimators. Since the data-driven step input estimation method is not statistically efficient, there is room for improvement. This is a topic for future research. In the practical experiments, the measurement noise is not white. The noise variance obtained from the sensor steady state response underestimates the measurement noise variance, that was observed 5 dB larger in the power spectrum due to nonlinearities of the sensor. Considering this difference in the measurement noise variance, we introduced a conservative bound of the measurement noise variance so that the first and second moments of the input estimate are more accurately predicted. Using the variance approximation, we can assess the uncertainty of the input estimate with respect to the number of samples processed by the data-driven step input estimation method. The step input estimation method is useful in practical applications where the whiteness assumption of the measurement noise is not fulfilled.

# 6. Affine input estimation method

In this thesis ~~document~~ we have discussed that a measurement estimates the unknown value of a physical quantity, also called measurand. The physical quantity of interest is applied as an input signal to a dynamic system, the sensor, and its state changes from the initial conditions into a transient state. The input value is estimated using the sensor response in transient state. A dynamic measurement occurs when the input fluctuations impacts on the input value estimation. A typical example of a dynamic measurement problem is a low-bandwidth sensor excited with a fast changing input as is explained in Dienstfrey and Hale [2014]. In this case, the sensor transient response is slower than the variation of the input, makih difficult to track the input evolution. The variation of some input characteristics, like the minimum or maximum or the effects of the environment, are considered in applications such as measurements of temperature in Saggin et al. [2001], pressure in Matthews et al. [2014], acceleration in Link et al. [2007], force in Vlajic and Chijioke [2016]; Hessling [2008], and mass in Shu [1993]; Boschetti et al. [2013].

The data-driven step input estimation method, introduced by Markovsky [2015a] and described in Chapter 3, estimates the unknown step level of an input directly from the sensor step response. Since most inputs have variations, contrary to the step response that is constant after its application, sets the need for methods for estimating more input models. One of such input models are affine inputs that vary at a constant rate, and they are found in applications where the measurand activates the sensor gradually. An example of gradual activation is the mass measurement of objects in motion, that exists in along conveyor belts.

Current solutions to the weighing in motion are low pass filters that estimate the mass using a saturated ramp as it is proposed by Tasaki et al. [2007], and by Niedźwiecki and Pietrzak [2016], and also time varying filters are developed in Piskorowski and Barcinski [2008] and in Pietrzak et al. [2014]. Nevertheless, the signal processing affine input estimation methods are motivated by the need to obtain the mass of the object from the ramp before it reaches saturation. The ramp is parameterized as a straight line model where the slope and the interception are the parameters of interest of an affine input model. This chapter describes two methods for the estimation of the affine input parameters.

One method is an extension of the data-driven step input estimation method, and then it is a recursive algorithm of low computational cost that can be implemented in real-time. The second method is a maximum-likelihood (ML) estimation method based on local-optimization that is proposed for off-line processing of the sensor transient response. The ML method is similar to the model predictive control approach, as discussed in Mayne [2014], because a cost function is minimized iteratively to optimize the parameters of a sensor model using the observed sensor

response in a receding time horizon. The difference is that the ML method aims to estimate the unknown value of the affine input parameters instead of identifying a model and controlling the dynamic system. Nevertheless, the ML method can estimate the parameters of the affine input, the parameters of a sensor model, and the initial conditions of the sensor.

The uncertainty of the subspace method is assessed in Quintana-Carapia et al. [2019a] using a Taylor expansion of the estimate and Monte Carlo random sampling approach. The Monte Carlo approach requires a large set of generated random samples, and according to Cox and Siebert [2006], for simple systems it is the recommended method. The uncertainty of the ML method is assessed using the derivatives of the residual error that constructs the to-be-minimized cost function. The covariance of the optimization method estimate is found in Pintelon and Schoukens [2012] using the inverse of the Hessian matrix.

## 6.1. Affine input estimation problem

The affine input is modeled as a straight line $u(t) = at + b$ with parameters the slope $a$ and the intercept $b$. The affine input estimation problem is formulated as a signal processing problem as follows.

**Problem**  Given the sequence of measured output observations $\widetilde{\mathbf{y}} = (\widetilde{y}(1), \ldots, \widetilde{y}(N))$, with $\widetilde{y}(t) \in \mathbb{R}$, of a stable linear time-invariant system of order $n$, and static gain $G$, generated by an affine input $u(t) = at + b$, estimate the parameters of the affine input, *i.e.*, find the values of the parameters $\widehat{a}, \widehat{b} \in \mathbb{R}$ such that $\widehat{u}(t) = \widehat{a}t + \widehat{b}$ approximates $u(t)$. The measured observations $\widetilde{\mathbf{y}} = \mathbf{y} + \boldsymbol{\epsilon}$ are exact sensor responses $\mathbf{y}$ perturbed by additive noise $\boldsymbol{\epsilon}$ assumed to be independent and normally distributed of zero mean and given variance $\sigma_\varepsilon^2$.

**Motivating example**  Dynamic weighing is an application example where the affine input can be observed. The weighing of objects in a conveyor belt gives the sensor input an ideal straight line profile when the conveyor belt moves at a constant speed. The straight line represents the mass coming gradually into the weighing scale sensor in the conveyor belt, and the mass can be estimated from the slope $a$ of the straight line model. The mechanical vibrations of the conveyor belt perturb the input and the sensor response is affected by measurement noise. Estimating the mass of the object using the sensor response observations is the ultimate goal.

Consider the weighing scale modeled as a second order mass-spring-damper system, such as the one shown in the diagram of Figure 6.1.
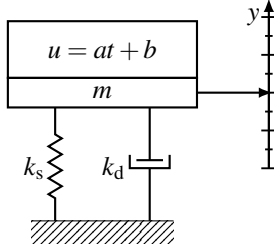


Figure 6.1.: A second order mass-spring-damper model represents the dynamic weighing system. The dynamics of the system depend on the affine input. The weighing system is time-varying when the applied input changes with respect to time.

The application of an affine input turns the linear time-invariant system into a linear time-varying system, whose dynamics depends on the input $u(t) = at + b$, as it is described by the differential equation:

$$\frac{d}{dt}\left( (at+b+m)\frac{dy}{dt} \right) + k_d \frac{dy}{dt} + k_s y = (at+b+m)\,g \tag{6.1}$$

where $m$ is the mass of the scale, $k_d$ is the damping constant, $k_s$ is the elasticity constant, and $g = 9.81 \text{ m/s}^2$ is the gravitational acceleration.

The weighing system admits a state-space representation where the states $x_1 = y$ and $x_2 = \dot{y}$ are the position and the speed of the weighing scale:

$$\dot{\mathbf{x}} = \begin{bmatrix} 0 & 1 \\ \dfrac{-k_s}{at+b+m} & \dfrac{-(k_d+a)}{at+b+m} \end{bmatrix} \mathbf{x} + \begin{bmatrix} 0 \\ g \end{bmatrix}, \quad y = \begin{bmatrix} 1 & 0 \end{bmatrix} \mathbf{x}. \tag{6.2}$$

In this chapter we use the dynamic weighing example to illustrate the implementation of the affine input estimation methods.

## 6.2. Solution methods

This section describes the subspace method for solving the affine input estimation problem. The procedure is motivated by the step input estimation method that is formulated as a structured errors-in-variables (EIV) problem and is solved using

recursive least-squares (RLS). The exponentially weighted recursive least-squares is a generalization of RLS that allows for the extension of the estimation method to reconstruct the affine input.

A maximum-likelihood (ML) method that performs simultaneous system identification and input estimation is described and its results are used as a reference for the subspace method results.

An example of the subspace method is illustrated with a weighing system. An existing time-varying (TV) compensation filter that was designed for weighing applications is described briefly. This TV filter is also used to compare the results of the proposed subspace method.

## 6.2.1. Subspace method

The errors-in-variables (EIV) minimization problem (3.21) is extended to estimate the affine input parameters. The profile of an affine input excitation can be reconstructed by solving the structured EIV problem

$$\widehat{\boldsymbol{\theta}} = \operatorname*{argmin}_{\boldsymbol{\theta}} \left\| \boldsymbol{\Omega}^{1/2} \left( \widetilde{\mathbf{y}} - \widetilde{\mathbf{K}}\boldsymbol{\theta} \right) \right\|_2^2. \tag{6.3}$$

where $\widetilde{\mathbf{y}}$ is the observed affine response, $\widetilde{\mathbf{K}}$ is defined in (3.17), and the matrix $\boldsymbol{\Omega} \in \mathbb{R}^{(N-n)\times(N-n)}$ is a diagonal matrix of descending powers of the weight factor $\omega \in [0,1)$, i.e., $\boldsymbol{\Omega} = \operatorname{diag}\left( \omega^{N-n}, \ldots, \omega^2, \omega^1 \right)$. The weight factor $\omega$ is a data selection forgetting factor since it enables to apply different weights to the residuals $\widetilde{\mathbf{y}} - \widetilde{\mathbf{K}}\boldsymbol{\theta}$.

The exponentially weighted RLS solution to the problem (6.3) is implemented to facilitate the online implementation of the affine input estimation method. The exponentially weighted recursive least-squares (RLS) can solve recursively the estimation problem (6.1). In Kailath et al. [2000] is described the exponentially weighted RLS algorithm, which is as follows

$$\widehat{\boldsymbol{\theta}}(k) = \widehat{\boldsymbol{\theta}}(k-1) + \boldsymbol{\kappa}_k \left( \widetilde{y}(k) - \widetilde{\mathbf{k}}_k \widehat{\boldsymbol{\theta}}(k-1) \right),$$

$$\boldsymbol{\kappa}_k = \omega^{-1} \boldsymbol{\Psi}(k-1)\widetilde{\mathbf{k}}_k^\top / \left( 1 + \omega^{-1}\widetilde{\mathbf{k}}_k \boldsymbol{\Psi}(k-1)\widetilde{\mathbf{k}}_k^\top \right) \tag{6.4}$$

$$\boldsymbol{\Psi}(k) = \omega^{-1} \left( \mathbf{I} - \boldsymbol{\kappa}_k \widetilde{\mathbf{k}}_k \right) \boldsymbol{\Psi}(k-1),$$

for $k = 2n+1, 2n+2, \ldots$, where $\widetilde{\mathbf{k}}_k$ represents the row of $\widetilde{\mathbf{K}}$ that corresponds to the $k$−th sample, $\boldsymbol{\kappa}_k$ is a gain scalar, and $\boldsymbol{\Psi}(k)$ is a covariance matrix. The estimates

and the covariance matrix are initialized using the first $n+1$ samples, i.e.,

$$\widehat{\theta}(2n+1) = \left(\widetilde{\mathbf{K}}_{n+1}^{\top}\Omega\widetilde{\mathbf{K}}_{n+1}\right)^{-1}\widetilde{\mathbf{K}}_{n+1}^{\top}\Omega\widetilde{\mathbf{y}}_{n+1}, \quad \text{and}$$

$$\Psi(2n+1) = \left(\widetilde{\mathbf{K}}_{n+1}^{\top}\Omega\widetilde{\mathbf{K}}_{n+1}\right)^{-1},$$ 

(6.5)

where $\widetilde{\mathbf{K}}_{n+1}$ is the matrix $\widetilde{\mathbf{K}}$ with the first $n+1$ rows, and $\widetilde{\mathbf{y}}_{n+1}$ is the vector $\widetilde{\mathbf{y}}$ with the first $n+1$ elements. When $\omega = 1$, the exponentially weighted RLS solution is identical to that of the RLS. When $\omega < 1$, the older residuals are weighted with lower values than the residuals of recent observations. In this way, the solution of the minimization problem depends more on newer data, and less on older data.

In Figure 6.2 we can see an example of the affine input $\mathbf{u}$ that excites a weighing sensor, and the generated response $\widetilde{\mathbf{y}}$. After the transient effects have diminished, the sensor response is a ramp of the same slope as the input, but with a different intercept due to an offset o. The offset o is explained by the parameter $m$ in the sensor representation given in Figure 6.1. This is the mass of the sensor itself, that is added to the mass of the object under measurement. From the point of view of the subspace method, the value of $m$ is unknown, and there is no interest in its estimation.

The exponentially weighted RLS solution to the problem (6.3) provides an affine input estimation $\widehat{\mathbf{u}}$. The affine input parameters $a$ and $b$ are estimated, in a second step, by fitting $\widehat{\mathbf{u}}$ to a straight line using linear regression, as follows

$$\begin{bmatrix} 1 & 1 \\ \vdots & \vdots \\ N & 1 \end{bmatrix} \begin{bmatrix} \widehat{a} \\ \widehat{b} \end{bmatrix} = \begin{bmatrix} \widehat{u}(1) - \text{o} \\ \vdots \\ \widehat{u}(N) - \text{o} \end{bmatrix},$$

(6.6)

where it is considered the existance of the offset o.

For each new observation $y(t)$, the estimation $\widehat{\mathbf{u}}$ is updated followed by the RLS update of the slope $\widehat{a}$ and the intercept $\widehat{b}$. The values of the tuning parameters $\omega$ and o can be obtained in the calibration of the method using the response of the sensor.

The calibration procedure consists in the measurement of an object with a reference mass. During the calibration, $\omega$ and o are tuned by changing their values aiming to reduce the estimation errors of $\widehat{a}$ and $\widehat{b}$. This reduction of the estimation errors is observed in the convergence of the affine input parameters towards their true values.

The subspace method estimates the input applied to a dynamic system directly from the caused transient response. This is a recursive method that can be implemented in real time to estimate the input using low cost digital signal processors.
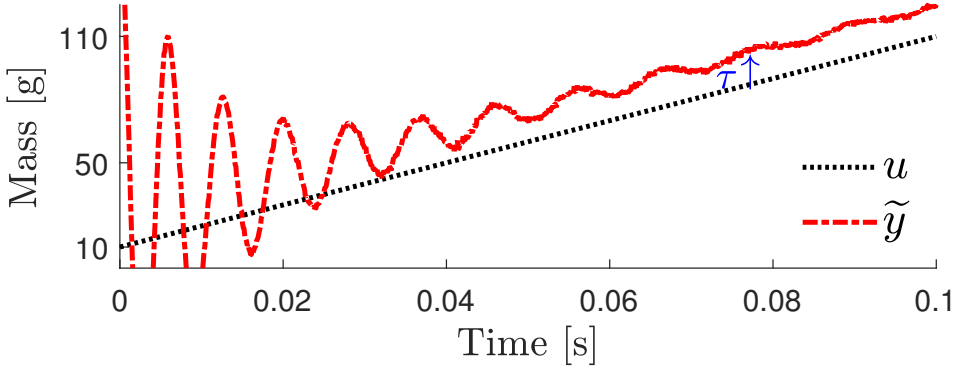
Figure 6.2.: When the transient part of the sensor response $\widetilde{\mathbf{y}}$ asymptotically decreases, a ramp with the same slope $a$ of the affine input $u(t) = at + b$ predominates. The intercept of the prevailing ramp is the intercept $b$ added to and offset o.

The method is a model-free approach and can be used in a variety of physical measurements. The method tracks any arbitrary time-varying input and can estimate the parameters of the input when it is associated to a particular input model.

### Statistical analysis of the subspace method

To obtain the first and second moments of the step input estimate $\widehat{\mathbf{u}}$, we need to study the solution

$$\widehat{\boldsymbol{\theta}} = (\widetilde{\mathbf{K}}^\top \boldsymbol{\Omega} \widetilde{\mathbf{K}})^{-1} \widetilde{\mathbf{K}}^\top \boldsymbol{\Omega} \widetilde{\mathbf{y}}, \tag{6.7}$$

of the overdetermined structured errors-in-variables EIV problem (6.3). Using a second order Taylor series expansion of the inverse matrix we can approximate the LS solution as

$$\widehat{\boldsymbol{\theta}} \approx \left( \mathbf{I} - \mathbf{M} + \mathbf{M}^2 \right) \mathbf{C}^{-1} (\mathbf{K} + \mathbf{E})^\top \boldsymbol{\Omega} (\mathbf{y} + \boldsymbol{\epsilon}). \tag{6.8}$$

where

$$\mathbf{C} = \mathbf{K}^\top \boldsymbol{\Omega} \mathbf{K}, \quad \text{and} \quad \mathbf{M} = \mathbf{C}^{-1} (\mathbf{K}^\top \boldsymbol{\Omega} \mathbf{E} + \mathbf{E}^\top \boldsymbol{\Omega} \mathbf{K} + \mathbf{E}^\top \boldsymbol{\Omega} \mathbf{E}). \tag{6.9}$$

The Taylor series approximation of $\widehat{\boldsymbol{\theta}}$ enables the calculation of the estimation bias and covariance since the measurement noise $\boldsymbol{\epsilon}$ and $\mathbf{E}$ are no more subject to matrix inversion. The bias and the covariance of the estimate $\widehat{\boldsymbol{\theta}}$ are obtained from the

definitions (4.5), and (4.6). Considering the structure of the EIV problem, the bias and the covariance of the estimate approximation (6.8) can be expressed as

$$\mathbf{b}_{\mathrm{p}}\left(\widehat{\boldsymbol{\theta}}\right) \approx \mathbf{C}^{-1}\left(\left(\mathbf{K}^{\top}\boldsymbol{\Omega}\mathbf{B}_1 - \mathbf{B}_2\right)\boldsymbol{\theta} - \left(\mathbf{K}^{\top}\boldsymbol{\Omega}\mathbf{B}_3 - \mathbf{B}_4\right)\right), \tag{6.10}$$

$$\mathbf{C}_{\mathrm{p}}\left(\widehat{\boldsymbol{\theta}}\right) \approx \mathbf{K}^{\dagger}\boldsymbol{\Omega}\left(\sigma_{\varepsilon}^2\mathbf{I}_{N-n} + \mathbf{C}_1 - \mathbf{C}_2 - \mathbf{C}_2^{\top}\right)\boldsymbol{\Omega}\mathbf{K}^{\dagger\top} - \mathbf{b}_{\mathrm{p}}\left(\widehat{\boldsymbol{\theta}}\right)\mathbf{b}_{\mathrm{p}}^{\top}\left(\widehat{\boldsymbol{\theta}}\right), \tag{6.11}$$

where $\mathbf{B}_1 = \mathbb{E}\left\{\mathbf{E}\mathbf{K}^{\dagger}\boldsymbol{\Omega}\mathbf{E}\right\}$, $\mathbf{B}_2 = \mathbb{E}\left\{\mathbf{E}^{\top}\boldsymbol{\Omega}\mathbf{P}_{\perp}\mathbf{E}\right\}$, $\mathbf{B}_3 = \mathbb{E}\left\{\mathbf{E}\mathbf{K}^{\dagger}\boldsymbol{\Omega}\boldsymbol{\epsilon}\right\}$, $\mathbf{B}_4 = \mathbb{E}\left\{\mathbf{E}^{\top}\boldsymbol{\Omega}\mathbf{P}_{\perp}\boldsymbol{\epsilon}\right\}$, $\mathbf{C}_1 = \mathbb{E}\left\{\mathbf{E}\boldsymbol{\theta}\boldsymbol{\theta}^{\top}\mathbf{E}^{\top}\right\}$, $\mathbf{C}_2 = \mathbb{E}\left\{\mathbf{E}\boldsymbol{\theta}\boldsymbol{\epsilon}^{\top}\right\}$, $\mathbf{P}_{\perp} = \mathbf{I} - \mathbf{K}\mathbf{K}^{\dagger}\boldsymbol{\Omega}$, and $\mathbf{K}^{\dagger}$ is the pseudo-inverse matrix of $\mathbf{K}$.

The bias and covariance given by expressions (6.10) and (6.11) depend on the unobservable true values $\boldsymbol{\theta}$ and $\mathbf{K}$. The measured observations are in the sensor step response $\widetilde{\mathbf{y}}$, and from its observations we construct $\widetilde{\mathbf{K}}$ and compute $\widehat{\boldsymbol{\theta}}$. The substitution of the measured data in the expressions gives an approximation of the estimation bias and covariance. We have then

$$\widetilde{\mathbf{b}}_{\mathrm{p}}\left(\widehat{\boldsymbol{\theta}}\right) \approx \widetilde{\mathbf{C}}^{-1}\left(\left(\widetilde{\mathbf{K}}^{\top}\boldsymbol{\Omega}\widetilde{\mathbf{B}}_1 - \widetilde{\mathbf{B}}_2\right)\widehat{\boldsymbol{\theta}} - \left(\widetilde{\mathbf{K}}^{\top}\boldsymbol{\Omega}\widetilde{\mathbf{B}}_3 - \widetilde{\mathbf{B}}_4\right)\right), \tag{6.12}$$

$$\widetilde{\mathbf{C}}_{\mathrm{p}}\left(\widehat{\boldsymbol{\theta}}\right) \approx \widetilde{\mathbf{K}}^{\dagger}\boldsymbol{\Omega}\left(\sigma_{\varepsilon}^2\mathbf{I}_{N-n} + \widetilde{\mathbf{C}}_1 - \widetilde{\mathbf{C}}_2 - \widetilde{\mathbf{C}}_2^{\top}\right)\boldsymbol{\Omega}\widetilde{\mathbf{K}}^{\dagger\top} - \widetilde{\mathbf{b}}_{\mathrm{p}}\left(\widehat{\boldsymbol{\theta}}\right)\widetilde{\mathbf{b}}_{\mathrm{p}}^{\top}\left(\widehat{\boldsymbol{\theta}}\right), \tag{6.13}$$

where $\widetilde{\mathbf{B}}_1 = \mathbb{E}\left\{\mathbf{E}\widetilde{\mathbf{K}}^{\dagger}\boldsymbol{\Omega}\mathbf{E}\right\}$, $\widetilde{\mathbf{B}}_2 = \mathbb{E}\left\{\mathbf{E}^{\top}\boldsymbol{\Omega}\widetilde{\mathbf{P}}_{\perp}\mathbf{E}\right\}$, $\widetilde{\mathbf{B}}_3 = \mathbb{E}\left\{\mathbf{E}\widetilde{\mathbf{K}}^{\dagger}\boldsymbol{\Omega}\boldsymbol{\epsilon}\right\}$, $\widetilde{\mathbf{B}}_4 = \mathbb{E}\left\{\mathbf{E}^{\top}\boldsymbol{\Omega}\widetilde{\mathbf{P}}_{\perp}\boldsymbol{\epsilon}\right\}$, $\widetilde{\mathbf{C}}_1 = \mathbb{E}\left\{\mathbf{E}\widehat{\boldsymbol{\theta}}\widehat{\boldsymbol{\theta}}^{\top}\mathbf{E}^{\top}\right\}$, $\widetilde{\mathbf{C}}_2 = \mathbb{E}\left\{\mathbf{E}\widehat{\boldsymbol{\theta}}\boldsymbol{\epsilon}^{\top}\right\}$, and $\widetilde{\mathbf{P}}_{\perp} = \mathbf{I} - \widetilde{\mathbf{K}}\widetilde{\mathbf{K}}^{\dagger}\boldsymbol{\Omega}$.

The results of the expected values $\mathbf{B}_1$, $\mathbf{B}_2$, $\mathbf{B}_3$, $\mathbf{B}_4$, $\mathbf{C}_1$, and $\mathbf{C}_2$ can be found using Lemma 1, on page 26. The bias and covariance were obtained to extend the previous analysis conducted on EIV estimation problems without an imposed structure in Vaccaro [1994] and Stewart [1990]. It was shown that the bias and variance expressions (6.12) and (6.13) are valid predictions of the first and second moments of the LS estimate of a Hankel structured EIV problem. The problem formulated by the step input estimation method belongs to this type of structured EIV problems and we can use the derived expressions to find the bias and variance of the input estimate $\widehat{u}$. The bias of the estimate $\widehat{\mathbf{u}}$ is the fist element of $\widetilde{\mathbf{b}}_{\mathrm{p}}\left(\widehat{\boldsymbol{\theta}}\right)$ and the variance of $\widehat{\mathbf{u}}$ is the first element in the main diagonal of $\widetilde{\mathbf{C}}_{\mathrm{p}}\left(\widehat{\boldsymbol{\theta}}\right)$.

## 6.2.2. Maximum-likelihood method

Using a model of the sensor, the maximum-likelihood ML method simultaneously estimates the parameters of the applied affine input $u(t) = at + b$, and some of

the sensor model parameters, using the observed sensor response $\widetilde{\mathbf{y}}$. This method fits iteratively the response of the model $\widehat{\mathbf{y}}(\boldsymbol{\theta})$ to the sensor response by searching for the parameters $\boldsymbol{\theta}$ that reduce the error difference between both responses. Algorithm 1 describes the formulation of an objective function $f = \mathbf{r}^\top \mathbf{r}$, where $\mathbf{r}$ is the residual $\mathbf{r}(\boldsymbol{\theta}) = \widetilde{\mathbf{y}} - \widehat{\mathbf{y}}(\boldsymbol{\theta})$, that is minimized through the iterations. The objective function is the sum of the squares of the differences between the samples of both responses. Since the measurement noise is assumed Gaussian distributed with zero mean and variance $\sigma_\epsilon^2$, where the samples of this perturbation are independent and identically distributed, the minimization of the objective function $f$ maximizes the likelihood of fitting the actual sensor response with the model response.

The Jacobian matrix of the residual $\mathbf{J}\boldsymbol{\theta} = \partial\mathbf{r}(\boldsymbol{\theta})/\partial\boldsymbol{\theta}$ can be analytically derived using the sensor model. With the Jacobian matrix, the ML method searches the direction in which the residual decreases towards a local minimum. Unfortunately, this ML method cannot guarantee the global minimum since it depends strongly on the initialization of the optimization parameters, as it is discussed in Nocedal and Wright [2006]. Therefore, it is proposed to initialize the to-be-optimized parameters $a$ and $b$ using the results of the subspace method obtained after a convenient number of samples so that the affine input parameters are set close to the optimal values. The initialization of the remaining model parameters under study can be done using the sensor model representation. An illustrative example of the ML will be provided in a posterior subsection.

---

**Algorithm 1** ML Affine input estimation.

---

**Require:** $\widetilde{\mathbf{y}}$, and required sensor model parameters
   Initialize $\boldsymbol{\theta} = (a, b,$ and the to-be-estimated model parameters$)$
   **for** each $N_s$ observations of $\widetilde{\mathbf{y}}$ **do**
      Simulate model response $\widehat{\mathbf{y}}(\boldsymbol{\theta})$
      Obtain residual $\mathbf{r}(\boldsymbol{\theta}) = \widetilde{\mathbf{y}} - \widehat{\mathbf{y}}(\boldsymbol{\theta})$
      Minimize $f = \mathbf{r}^\top \mathbf{r}$ over $\boldsymbol{\theta}$
         using analytic Jacobian matrix $\mathbf{J}\boldsymbol{\theta} = \partial\mathbf{r}(\boldsymbol{\theta})/\partial\boldsymbol{\theta}$
      Update $\boldsymbol{\theta}$
   **end for**
**Ensure:** Optimized parameters $\widehat{a}$, $\widehat{b}$, and estimated model parameters.

---

## Covariance of the ML method estimates

The ML method simulates a dynamic system, and computes the Jacobian of the residual error in each iteration. The analytic formulation of the Jacobian benefits

the estimation method in two ways: it speeds up the minimization and gives direct access to the variance of the estimates. The covariance matrix of the ML estimates can be expressed as in Pintelon and Schoukens [2012]

$$\mathbf{C}\left(\widehat{\boldsymbol{\theta}}\right) = \sigma_\epsilon^2 \left( \left( \frac{\partial \mathbf{r}}{\partial \boldsymbol{\theta}} \right)^\top \left( \frac{\partial \mathbf{r}}{\partial \boldsymbol{\theta}} \right) \right)^{-1}. \tag{6.14}$$

The ML estimation method is asymptotically efficient, and the ML estimation variance values are the mininum values that any estimator can attain. Therefore, the variance of the ML method estimates should be smaller than the CRLB of the structured EIV minimization problem (4.20).

## ML affine input estimation example

The previously described dynamic weighing system is used to illustrate the ML method implementation. In this case, the problem can be formulated as:

$$\text{Minimize} \quad \text{over } a, b, \mathbf{x}_{\text{ini}} \quad \mathbf{r}^\top \mathbf{r}, \text{ subject to:}$$

$$\dot{\mathbf{x}} = \begin{bmatrix} 0 & 1 \\ \frac{-k_s}{at+b+m} & \frac{-(a+k_d)}{at+b+m} \end{bmatrix} \mathbf{x} + \begin{bmatrix} 0 \\ g \end{bmatrix}, \tag{6.15}$$

$$\widehat{\mathbf{y}} = \begin{bmatrix} 1 & 0 \end{bmatrix} \mathbf{x}.$$

where the optimization variables $\boldsymbol{\theta} = (a, b, \mathbf{x}_{\text{ini}})$ are the affine input parameters $a$, $b$, and the sensor model's initial conditions.

The model parameters $m$, $k_d$, and $k_s$ cannot be estimated simultaneously due to identifiability issues. In the state equation of the time-varying sensor model, the parameters $k_d$ and $a$ are entangled and cannot be explicitly separated. The same occurs for the parameters $m$ and $b$, and for $k_s$ with respect to $a$ and $b$.

To define the initial value of the optimization variables $a$, $b$, the subspace estimation method can be used with, at least, the first $2n+2$ transient response samples, where $n = 2$ is the order of the sensor model. With the initial affine input parameters, a sensor response can be simulated, and, since we are using few samples, the first samples of the simulated response also are an approximation of the initial conditions $\mathbf{x}_{\text{ini}}$. The optimization variables are updated every $N_s$ new observations. The minimization algorithm can be, for example, the Levenberg-Marquardt algorithm described in Nocedal and Wright [2006].

The analytic Jacobian matrix $\mathbf{J}$ of the residual $\mathbf{r}(\boldsymbol{\theta})$ can be obtained from the first derivative of the state-space representation (6.15), with respect to the optimization variables $\boldsymbol{\theta}$. The residual $\mathbf{r}(\boldsymbol{\theta}) = \widetilde{\mathbf{y}} - \widehat{\mathbf{y}}(\boldsymbol{\theta})$ is the error difference between the

observed sensor response $\widetilde{\mathbf{y}}$ and the simulated sensor response $\widehat{\mathbf{y}}(\boldsymbol{\theta})$ to the affine input. More details of the Jacobian matrix calculation, for the sensor model under study, are given in the appendix.

### 6.2.3. Time-varying compensation filter

The time-varying (TV) filter described in Pietrzak et al. [2014] was designed to compensate the measured responses of a conveyor weighing system, considering they are modeled as a saturated ramp. The TV filter consists of three low-pass infinite impulse response (IIR) filters in cascade, where the $i-$th IIR filter is given by

$$\widehat{y}_i(t) + k_1(t)\widehat{y}_i(t-1) = k_2(t)\left(\widehat{y}_{i-1}(t) + \widehat{y}_{i-1}(t-1)\right) \tag{6.16}$$

for $i = 1, \ldots, 3$ and $t = 0, \ldots, N$. The sensor response is fed to the filter, then $\widehat{y}_0(t) = \widetilde{y}(t)$, and the output of the TV filter $\widehat{u}_{\text{ltv}}(t) = \widehat{y}_3(t)$ is an estimation of the affine input. Since in our case we are processing only the ramp without the saturation, the estimates $\widehat{a}_{\text{ltv}}$ and $\widehat{b}_{\text{ltv}}$ of the input parameters are obtained by fitting a straight line to the estimated input $\widehat{u}_{\text{ltv}}$ using linear regression.

The time-varying coefficients $k_1(t)$ and $k_2(t)$ are computed in Pietrzak et al. [2014] from

$$k_1(t) = \frac{f_c(t) - \frac{k_3}{\pi T_s}}{f_c(t) + \frac{k_3}{\pi T_s}}, \quad k_2(t) = \frac{1 + k_1(t)}{2}, \quad k_3 = \sqrt{\sqrt[3]{2} - 1} \tag{6.17}$$

where $T_s$ is the sampling time and $f_c(t)$ is a heuristic "cutoff" frequency

$$f_c(t) = f_u + (f_l - f_u)\,\beta^{\frac{t-1}{\alpha(N-1)}} \tag{6.18}$$

that changes between the lower $f_l$ and upper $f_u$ limits, where the coefficient $\beta$ is lower than one, and $\alpha$ is the decay rate. The lower frequency value $f_l$ and the coefficient $\beta$ are fixed and the variables $f_u$ and $\alpha$ are optimized off-line by solving the minimization problem

$$\text{minimize} \quad \text{over } f_u, \alpha \quad \max\left(\frac{\mu_{\widetilde{a}_{\text{ltv}}}}{\mu_{\text{spec}}}, \frac{\mu_{\widetilde{b}_{\text{ltv}}}}{\mu_{\text{spec}}}, \frac{\sigma_{\widetilde{a}_{\text{ltv}}}}{\sigma_{\text{spec}}}, \frac{\sigma_{\widetilde{b}_{\text{ltv}}}}{\sigma_{\text{spec}}}\right) + \max\left(\frac{\eta_i}{N}\right) \tag{6.19}$$

where $\mu_{\widetilde{a}_{\text{ltv}}}$, $\mu_{\widetilde{b}_{\text{ltv}}}$, $\sigma_{\widetilde{a}_{\text{ltv}}}$ and $\sigma_{\widetilde{b}_{\text{ltv}}}$ are the mean values and the standard deviations of the estimation errors $\widetilde{a}_{\text{ltv}} = \widehat{a}_{\text{ltv}} - a$, and $\widetilde{a}_{\text{ltv}} = \widehat{b}_{\text{ltv}} - b$, and where $a$ and $b$ are the true values of the input parameters. The values $\mu_{\text{spec}}$ and $\sigma_{\text{spec}}$ are specified in the OIML recommendation R51 defined in International Recommendation OIML R 51 1 [2006] for mass measurements that use a conveyor belt.

## 6.3. Simulation results

The results of the affine input parameters estimation are discussed in this section. We performed a simulation study using the weighing system presented as an example. We compared the performance of the proposed subspace method to a conventional time-varying (TV) filter, that was conceived for weighing applications, and to the maximum-likelihood (ML) method.

A second order weighing system was excited with an affine input to get the transient response. The parameters of the weighing system are $m = 15$ g, $k_d = 5.5$ Ns/m and $kg_s = 10250$ N/m. The applied affine input $u(t) = 100t + 10$ represents a mass that changes from 10 g to 110 g, at a constant rate, in a time interval of 0.1 s. This change of mass represents one example of the weighing input in a conveyor weighing system when an object of 100 g is measured while it is moving at constant speed. A total of 1000 samples of the sensor response are acquired with sampling time $T_s = 0.1$ ms. In Figure 6.3 the input $\mathbf{u}$ is represented with the black dotted line, the red oscillatory curve is the corresponding sensor ramp response $\widetilde{\mathbf{y}}$, and the blue curve $\widehat{\mathbf{u}}$ is a typic al input estimate obtained with the subspace method.
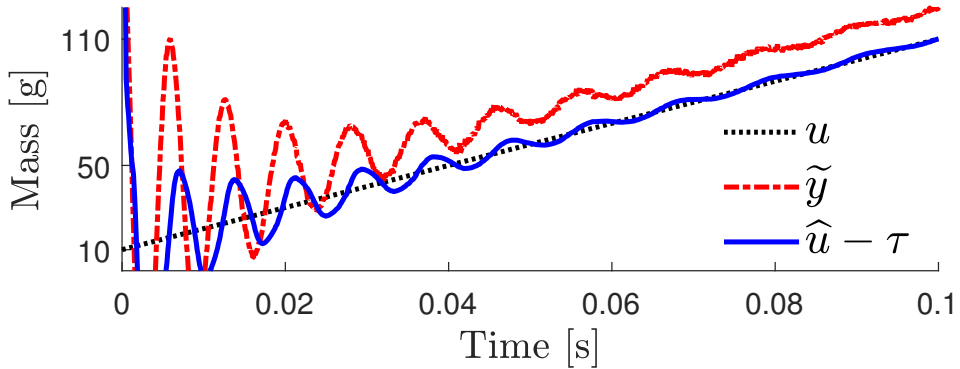


Figure 6.3.: The sensor transient response $\widetilde{y}$ to an affine input excitation $u(t) = at + b$ is processed by the estimation methods to estimate the parameters $a$ and $b$. In the figure we observe an example of the input estimate $\widehat{\mathbf{u}}$ obtained with the subspace method. The input parameters are calculated from $\widehat{\mathbf{u}} - o$ using linear regression.

In each simulation, the sensor response was perturbed with an independent realization of additive normally distributed measurement noise. The added perturbation noise has signal-to-noise ratio (SNR) in the interval [20 dB, 60 dB]. These

SNR values are realistic in practical applications. The SNR is defined as the ratio of signal power to the noise power, that is equivalent to the root-mean-square (RMS) value of the true signal to the standard deviation of the perturbation noise, and in dB is given by (4.37).

## 6.3.1. Results of the subspace method

The subspace method processed online the sensor transient response. The first estimation was obtained with $2n+1$ samples, where $n=2$ is the assumed order of the sensor. The method updated recursively the value of the estimated parameters for each new collected sample, using the forgetting factor $\omega$ listed in Table 6.1. In Figure 6.4 we observe the relative errors of the estimates $\widehat{a}$ and $\widehat{b}$ obtained when SNR = 40 dB. The relative errors are smaller than 5 % after 400 and 500 samples are processed, i.e., 0.04 s and 0.05 s, respectively. As more samples are collected, the parameter estimation improves. Figure 6.5 shows the final value of the relative errors, found at $t=0.1$ s, for the different SNR values considered. The relative errors are smaller than 2 % regardless of the measurement noise level.

Table 6.1.: Here are listed the selected values of the forgetting factor $\omega$ and the offset o that configure the subspace method for the different values of SNR. These values were obtained after calibration of the method and were fixed during the simulation study.

| SNR [dB] | 20 | 30 | 40 | 50 | 60 |
|---|---|---|---|---|---|
| $\omega$ | 0.939 | 0.940 | 0.955 | 0.959 | 0.959 |
| o [g] | 15 | 15 | 17 | 14 | 20 |

The Cramér-Rao lower bound (CRLB) of the errors-in-variables problem formulated by the subspace method was numerically computed for different sample size using Equation (4.20). The CRLB is the minimum variance that the estimates $\widehat{a}$ and $\widehat{b}$ can have from the solution of the structured EIV minimization problem. The average of $10^4$ runs with independent noise realizations allows to find the empirical mean squared error (MSE) of the estimates, defined as

$$\mathrm{MSE}_{\widehat{a}} = \left(b_{\mathrm{p}}\left(\widehat{a}\right)\right)^2 + v_{\mathrm{p}}\left(\widehat{a}\right), \quad \text{and} \quad \mathrm{MSE}_{\widehat{b}} = (b_{\mathrm{p}}(\widehat{b}))^2 + v_{\mathrm{p}}(\widehat{b}), \tag{6.20}$$

where $b_{\mathrm{p}}\left(\widehat{a}\right)$ and $b_{\mathrm{p}}(\widehat{b})$ are the bias, and $v_{\mathrm{p}}\left(\widehat{a}\right)$ and $v_{\mathrm{p}}(\widehat{b})$ are the variances of the input parameters. Figure 6.6 shows that the mean squared errors $\mathrm{MSE}_{\widehat{a}}$ and $\mathrm{MSE}_{\widehat{b}}$ are near to their theoretical minimum $\mathrm{CRLB}_a$ and $\mathrm{CRLB}_b$ within two orders of magnitude, when SNR = 40 dB. Figure 6.7 shows the final value of the Cramér-Rao

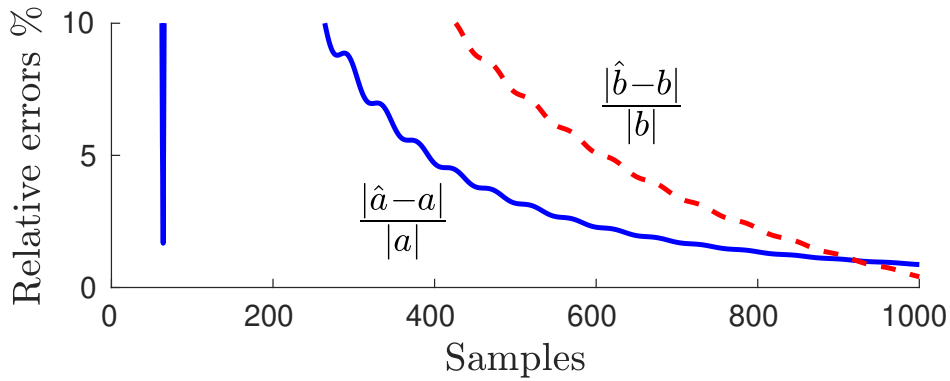Figure 6.4.: The relative errors of the affine input parameters estimates decrease as the subspace method processes more samples. The relative errors of the estimates $\hat{a}$ and $\hat{b}$ are smaller than 5 % after 400 and 500 samples, respectively ($T_s = 0.1$ ms).
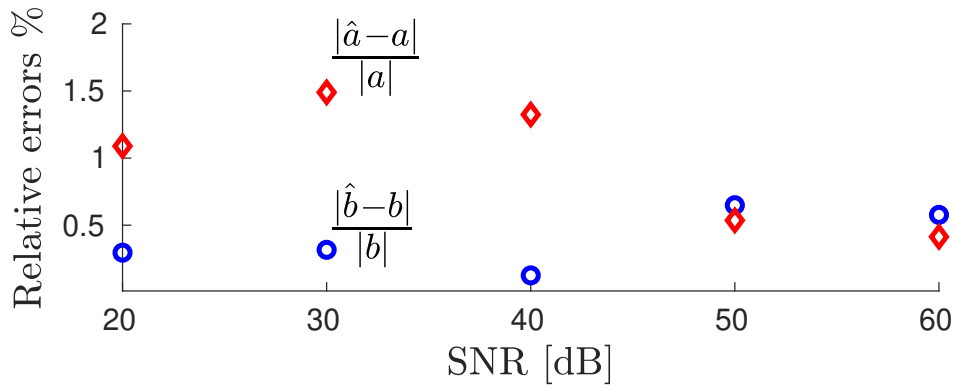


Figure 6.5.: The minimum value of the estimation relative errors obtained with the subspace method is less than 2 % regardless of the SNR between 20 dB and 60 dB.

lower bounds and the empirical mean-squared errors, found at $t = 0.1$ s, for the different SNR values considered. Both $\text{MSE}_{\hat{a}}$ and $\text{MSE}_{\hat{b}}$ are less than one order of magnitude near to $\text{CRLB}_a$ and $\text{CRLB}_b$, respectively, for SNR $\leq 30$ dB. The difference increases for larger SNR but the maximum is two orders of magnitude for SNR = 60 dB.

Table 6.2 shows a comparative view of the estimation mean-squared-errors maximum values when the ramp that excites the sensor corresponds to different masses and time durations. For each mass and duration, the sensor responses were perturbed with measurement noise of SNR in the interval [20 dB, 60 dB]. The sensor parameters and sampling frequency are fixed and are the same described in the first paragraph of this section. The maximum values of the MSE are mainly found at low SNR values between 20 and 40 dB. The higher levels of noise increase the uncertainty of the estimation defined in terms of the MSE. For fast ramp excitations, the MSE's increase considerably. The used sampling frequency constrains the estimation method effectiveness for the ramp input duration of 0.05 s or shorter and there it is recommended to use a higher sampling frequency that will reduce the estimation MSE.
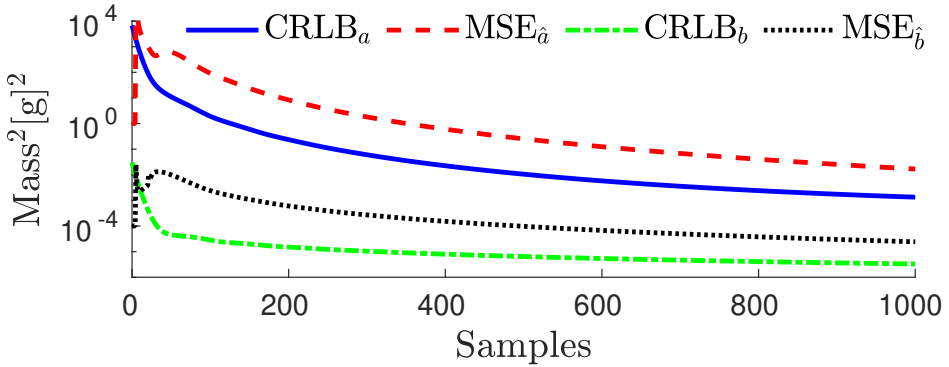


Figure 6.6.: When the SNR of the sensor response is 40 dB, the mean squared errors of the slope estimate $\hat{a}$ and the intercept estimate $\hat{b}$, obtained by the subspace method, are two orders of magnitude above the theoretical minimum variance given by the Cramér-Rao lower bound.

A numerical sensitivity analysis of the subspace method was conducted by adding uncertainty to ramp input generation and looking into the estimation results. The uncertainty $\sigma_s$ of the speed in which the ramp increases, and the uncertainties of the input parameters, represented by $\sigma_{a,b}$, were selected to be 0%, 5% and 10% of their true values. A Monte Carlo simulation with $10^4$ runs was performed for each SNR and the maximum values of the estimation uncertainty are shown in Table

Figure 6.7.: The Cramér-Rao lower bounds of the estimates $CRLB_a$ and $CRLB_b$ determine the minimum uncertainty that can be achieved and increases with the measurement noise. The empirical mean squared errors $MSE_{\hat{a}}$ and $MSE_{\hat{b}}$ are near to the Cramér-Rao lower bounds within one order of magnitude for SNR smaller than 30 dB, and within two orders of magnitude for SNR between 40 dB and 60 dB.

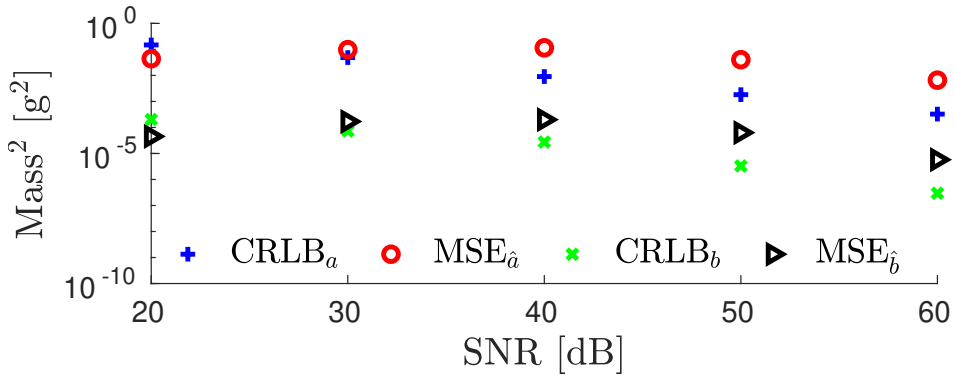Table 6.2.: The maximum values of the estimation mean squared errors observed when the subspace method processed the sensor transient responses caused by ramp excitations of masses 0.1, 0.3, 0.5, and 1.0 kg, that last 0.05, 0.1 and 0.5 s, with signal to noise ratios in the interval [20 dB, 60 dB] occur mainly at 40 dB and for lower SNR. There is an increment in the MSE values when the ramp excitation is faster.

| | Mass | | | |
|---|---|---|---|---|
| Time | 0.1 kg | 0.3 kg | 0.5 kg | 1.0 kg |
| 0.05 s | | | | |
| $MSE_{\hat{a}}$ [g$^2$] | $3.5\text{x}10^0_{(@40\text{ dB})}$ | $13.5\text{x}10^0_{(@50\text{ dB})}$ | $3.8\text{x}10^0_{(@20\text{ dB})}$ | $8.3\text{x}10^0_{(@50\text{ dB})}$ |
| $MSE_{\hat{b}}$ [g$^2$] | $3.1\text{x}10^{-3}_{(@40\text{ dB})}$ | $1.1\text{x}10^{-2}_{(@40\text{ dB})}$ | $1.1\text{x}10^{-2}_{(@40\text{ dB})}$ | $1.9\text{x}10^{-2}_{(@60\text{ dB})}$ |
| 0.1 s | | | | |
| $MSE_{\hat{a}}$ [g$^2$] | $3.1\text{x}10^{-2}_{(@30\text{ dB})}$ | $1.1\text{x}10^0_{(@40\text{ dB})}$ | $8.3\text{x}10^{-1}_{(@60\text{ dB})}$ | $1.3\text{x}10^0_{(@50\text{ dB})}$ |
| $MSE_{\hat{b}}$ [g$^2$] | $6.0\text{x}10^{-5}_{(@30\text{ dB})}$ | $1.2\text{x}10^{-1}_{(@50\text{ dB})}$ | $2.1\text{x}10^{-2}_{(@40\text{ dB})}$ | $3.7\text{x}10^{-2}_{(@40\text{ dB})}$ |
| 0.5 s | | | | |
| $MSE_{\hat{a}}$ [g$^2$] | $3.0\text{x}10^{-2}_{(@20\text{ dB})}$ | $3.0\text{x}10^{-1}_{(@20\text{ dB})}$ | $3.2\text{x}10^0_{(@20\text{ dB})}$ | $8.6\text{x}10^{-2}_{(@20\text{ dB})}$ |
| $MSE_{\hat{b}}$ [g$^2$] | $3.1\text{x}10^{-5}_{(@50\text{ dB})}$ | $9.8\text{x}10^{-4}_{(@40\text{ dB})}$ | $2.0\text{x}10^{-5}_{(@50\text{ dB})}$ | $1.7\text{x}10^{-5}_{(@20\text{ dB})}$ |

6.3. According to these results, the input parameters uncertainties $\sigma_{a,b}$ affect more the uncertainty of the estimation than the speed uncertainty $\sigma_s$. The parameter that is more affected by the input parameters uncertainty is the intercept $\widehat{b}$, since the uncertainty of the slope $\widehat{a}$ is smaller.

Table 6.3.: A sensitivity analysis of the subspace method was conducted by adding uncertainty to the ramp input. The speed $\sigma_s$, and the input parameters $\sigma_s$ uncertainties are 0%, 5%, and 10% of their true values. The table shows the maximum values of the estimation uncertainty. The speed uncertainty causes a smaller spread of the estimates than the input parameters uncertainty.

| $\sigma_{a,b}$ | $\sigma_s$: 0% | 5% | 10% |
|---|---|---|---|
| 0% | | | |
| $\widehat{a}$ [kg/s] | $1.0 \pm 9.6\%_{(@50 \text{ dB})}$ | $1.0 \pm 8.2\%_{(@20 \text{ dB})}$ | $1.0 \pm 8.2\%_{(@50 \text{ dB})}$ |
| $\widehat{b}$ [g] | $10.0 \pm 10.3\%_{(@20 \text{ dB})}$ | $9.9 \pm 14.2\%_{(@30 \text{ dB})}$ | $10.0 \pm 21.7\%_{(@60 \text{ dB})}$ |
| 5% | | | |
| $\widehat{a}$ [kg/s] | $1.0 \pm 9.7\%_{(@50 \text{ dB})}$ | $1.0 \pm 11.3\%_{(@20 \text{ dB})}$ | $1.0 \pm 8.0\%_{(@50 \text{ dB})}$ |
| $\widehat{b}$ [g] | $10.0 \pm 22.4\%_{(@50 \text{ dB})}$ | $10.0 \pm 33.2\%_{(@30 \text{ dB})}$ | $9.9 \pm 16.6\%_{(@50 \text{ dB})}$ |
| 10% | | | |
| $\widehat{a}$ [kg/s] | $1.0 \pm 20.3\%_{(@40 \text{ dB})}$ | $1.0 \pm 22.0\%_{(@50 \text{ dB})}$ | $1.0 \pm 17.7\%_{(@40 \text{ dB})}$ |
| $\widehat{b}$ [g] | $9.9 \pm 46.8\%_{(@40 \text{ dB})}$ | $9.8 \pm 58.8\%_{(@50 \text{ dB})}$ | $9.9 \pm 41.6\%_{(@40 \text{ dB})}$ |

## 6.3.2. Results of the maximum-likelihood method

The maximum-likelihood (ML) method estimates the affine input parameters from the sensor model transient response. A total of 100 runs of the method were obtained, using different realizations of the measurement noise. The measurement noise variance was set to have an SNR of 40 dB. The ML method used the first 50 samples to initialize the optimization variables and updated the variables every $N_s = 5$ samples. Figure 6.8 shows the average of the observed relative errors in the estimation of the parameters $\widehat{a}$, $\widehat{b}$, $\widehat{x}_{\text{ini},1}$, and $\widehat{x}_{\text{ini},2}$. The convergence of the ML estimates gives relative errors below 5 % after three iterations. The largest relative error observed is in the scale velocity $\widehat{x}_{\text{ini},2}$ estimate, which is more sensitive than the other optimization variables.

The estimation covariance was computed using the analytic Jacobian and the Equation (6.14). Figure 6.9 shows the average of the variances that were observed on the diagonal of the covariance matrix $\mathbf{J}$. We can see that the estimation variances
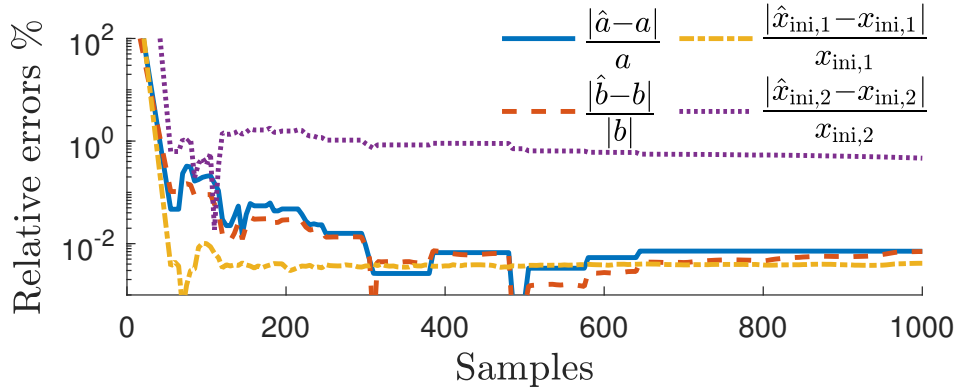
Figure 6.8.: The affine input parameters and the sensor's initial conditions are estimated with the ML method. After three iterations the average of the relative error is smaller than 5 % for each and everyone of the estimates. The estimate $\hat{x}_{\text{ini},2}$ has the larger relative error near to 1 %.

decrease as more samples are processed. Moreover, the estimation variances of $\hat{a}$ and $\hat{b}$ obtained with the ML method are lower than the corresponding estimation MSE errors obtained from a Monte Carlo simulation of the subspace method (see Figure 6.7).
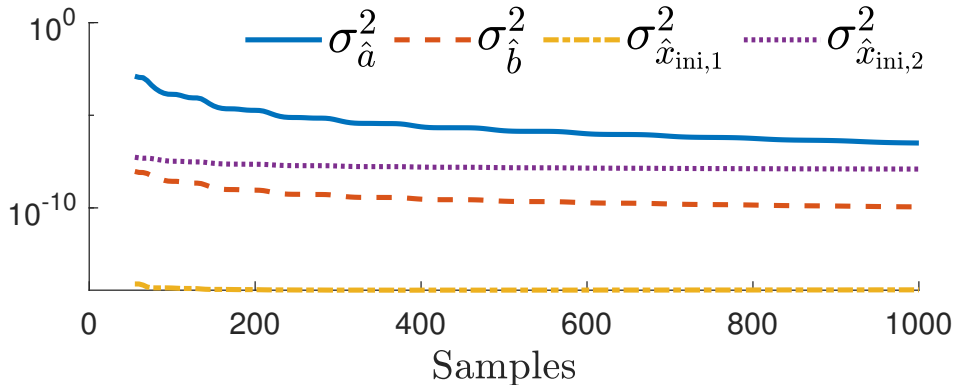


Figure 6.9.: The variances of the ML estimates are calculated using the information provided by the analytic Jacobian. The estimates $\hat{x}_{\text{ini},1}$ and $\hat{a}$ have the smaller and larger variances, respectively.

The ML method is computationally more expensive than the subspace method because the ML method simulates the response of a sensor model to optimize the input parameters and the sensor's initial conditions.

A typical run of the ML method takes 30 s to complete. With this execution time, the ML estimation can only be performed offline. Nevertheless, the ML method objectives are to give the best estimation possible and to serve as a reference to assess the results of the other methods. An efficient implementation of the ML method to make it feasible for real-time implementation is not trivial and requires additional research that is considered a topic for future research.

A numerical sensitivity analysis of the ML method was conducted by adding uncertainty to the ramp input, and to the parameters of the time-varying model. The ramp input was perturbed with uncertainty of the speed in which the ramp increases $\sigma_s$, and with uncertainty on the input parameters $\sigma_{a,b}$. The perturbation uncertainty of the model parameters $m$, $d$, and $k$ is represented by $\sigma_{m,d,k}$. The perturbation uncertainty was simulated by adding normally distributed random noise with standard deviation equal to 0%, 5% and 10% of the corresponding true values of the perturbed parameters. A Monte Carlo simulation with $10^3$ runs was conducted for each SNR in the SNR interval of interest, and in Table 6.4 are shown the maximum values of the observed estimation uncertainties. The results show that the speed uncertainty $\sigma_s$ has a small impact on the estimation uncertainty. On the contrary, the input parameters uncertainties $\sigma_{a,b}$, and the uncertainties of the model parameters $\sigma_{m,d,k}$ cause a large increment in the uncertainty of the estimation.

### 6.3.3. Results of the time-varying filter

We fixed the frequency lower value $f_l = 0.01$ Hz and the base $\beta = 0.01$. The upper value $f_u$ and the decay rate $\alpha$ were found using optimization (6.19). We chose the values $\mu_{\text{spec}} = 0.5$ and $\sigma_{\text{spec}} = 0.24$ as they are specified in the OIML recommendation defined in International Recommendation OIML R 51 1 [2006] for a mass of 100 g measured in a conveyor belt. The optimized values of the frequency upper value and the decay rate, using a dataset of 100 transient responses, were $f_u = 26.94$ Hz and $\alpha = 5.71$.

Figure 6.10 shows the relative errors of the estimates $\widehat{a}$ and $\widehat{b}$ computed with the TV filter after processing the sensor transient response. The relative error of the slope estimate is below 5 % after 300 samples but the relative error of the intercept estimate is near 10 %. The convergence rate of the estimate $\widehat{a}$ was similar to that of the subspace method.
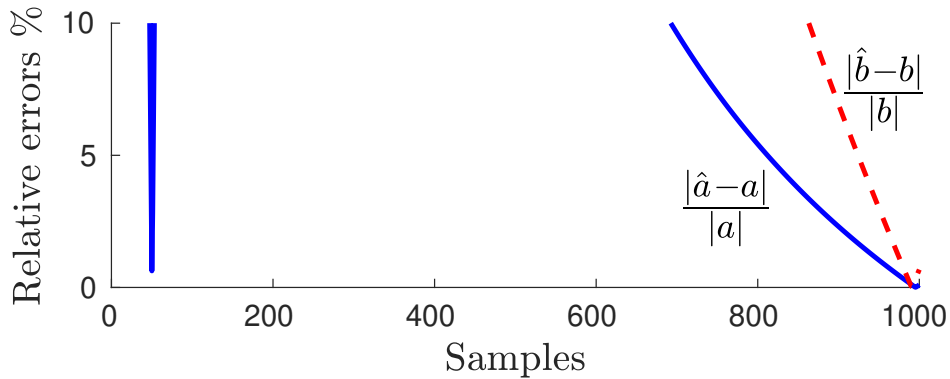
Figure 6.10.: The relative errors of the time-varying filter estimation converge slower than with the subspace method. The relative errors of $\hat{a}$ and $\hat{b}$ are smaller than 5 % only after 800 and 950 samples, respectively. With the subspace method the relative errors are below 5 % after 400 and 500 samples.

## 6.3.4. Discussion of the observed results

The subspace method obtains an estimation of the affine input parameters with a recursive least-squares solution of a structured errors-in-variables problem. Updating the parameter estimates without matrix inversion simplifies the method implementation on digital signal processors of low cost. The price we pay by computing the least-squares solution of an errors-in-variables problem is an increase in the bias of the estimates. Nevertheless, the empirical mean squared errors of the estimates are at most two orders of magnitude larger than the Cramér-Rao lower bound, meaning that the estimation uncertainty is low, even when the SNR is lower than 40 dB.

The proposed subspace method is a general method that can be used in different applications, with realistic signal-to-noise ratios. It is suitable not only for mass measurements. The weighing example shows that the subspace method can be used even when the measurement system is linear time-varying.

It was shown that the time-varying (TV) compensation filter can be modified to estimate the mass only from the increasing section of the saturated ramp, without the need of processing the saturation part. The modified TV filter can be implemented in real-time as the subspace method after a previous off-line coefficients optimization stage with sensor measured data. Nevertheless, the

estimation results of the subspace method are better than the TV filter since they are twice as fast and one order of magnitude more acurate.

The subspace method can estimate the affine input parameters from the sensor response using few parameters, the sensor order $n$, the sensor static gain $G$, and the RLS forgetting factor $\omega$. The subspace method does not necessarily requires optimization of $\omega$ using a dataset of measured sensor responses. It is required to tune $\omega$ online during the calibration of the system and later $\omega$ remains fixed during the measurements.

The results of the sensitivity analysis show how the uncertainty of the subspace method estimates is affected when the ramp input is subject to perturbation. The impact on the uncertainty on the slope $\hat{a}$ and the intercept $\hat{b}$ parameters is different. The ramp speed uncertainty $\sigma_s$ is added to the uncertainty of the parameter $\hat{b}$, but does not contribute to the uncertainty of the parameter $\hat{a}$. On the other hand, the ramp parameters uncertainty ramp speed uncertainty $\sigma_{a,b}$ is added to the uncertainty of the estimates of both parameters $\hat{a}$ and $\hat{b}$. This is not surprising since the estimation parameters are linked to the ramp input parameters.

The maximum-likelihood (ML) method is an approach that requires larger computational resources. This is an iterative method and in each iteration computes a simulation of a dynamic system followed by the evaluation of the residual error Jacobian matrix. The advantage of the ML method is that we can estimate simultaneously sensor parameters and the initial conditions of the sensor. In the weighing case presented as an illustrative example it was not possible to incorporate other parameters of the sensor because they are not identifiable. According to the estimation relative errors, that are lower than 0.01 after 100 samples, from there on the ML method estimates are near to the true values and we may not require to run the method along all the measurement period. With only the first 100 samples we have an accurate parameter estimation and variance assessment.

However, the main drawback of the ML method that prevents online implementations is the required computational power to iteratively simulate the response of a sensor model. It takes an average of 30 s to complete an estimation with the ML method, and this time is too large for fast changing inputs. The development of an efficient ML method, suitable for real-time implementation, is not straightforward, and is proposed for future research.

The results of the sensitivity analysis of the ML method show that the uncertainty of the ramp input speed $\sigma_s$ does not have an impact on the estimation uncertainty. Similar to the subspace case, the uncertainty of the ramp input parameters $\sigma_{a,b}$ is additive to the uncertainty of the estimated parameters $\hat{a}$ and $\hat{b}$, but does not contribute to the uncertainty of the first element of the initial conditions. On the

other hand, the estimation uncertainty is affected by the perturbation on the model parameters $\sigma_{m,d,k}$. It is observed that the uncertainty of the estimated parameters $\widehat{a}$ and $\widehat{b}$ increases two and three times the uncertainty of the model parameters. This implies that we need to have an accurate model of the dynamic system to have a small uncertainty on the estimated input parameters. Unfortunately, the uncertainty of the second element of the inital conditions is always very high and this is not because of the perturbation of the ramp speed or the model parameters. This issue requires more investigation to see if it is due the identifiability of the parameter in the particular example we have.

Table 6.4.: A sensitivity analysis of the ML method was conducted by adding uncertainty to ramp input, and to the model parameters. The perturbation uncertainty was selected with standard deviation of 0%, 5%, and 10% of the parameters true values. The observed maximum estimation uncertainties are shown in the table. The speed uncertainty $\sigma_s$ affects less the input estimation, but the uncertainties of the input parameters $\sigma_{a,b}$, and the model parameters $\sigma_{m,d,k}$ cause an increase of the estimation parameters spread around their mean values.

| $\sigma_{a,b}$ | $\sigma_s$: 0% | 5% | 10% |
|---|---|---|---|
| **0%** | | | |
| $\widehat{a}$ [kg/s] | $1.0 \pm 0.7\%_{(@20\ dB)}$ | $1.0 \pm 0.7\%_{(@20\ dB)}$ | $1.0 \pm 0.4\%_{(@30\ dB)}$ |
| $\widehat{b}$ [g] | $10.0 \pm 1.1\%_{(@20\ dB)}$ | $10.0 \pm 1.1\%_{(@20\ dB)}$ | $10.0 \pm 0.5\%_{(@30\ dB)}$ |
| $\widehat{x}_{ini,1}$ [g] | $0.1 \pm 0.6\%_{(@40\ dB)}$ | $0.1 \pm 0.6\%_{(@20\ dB)}$ | $0.1 \pm 0.2\%_{(@30\ dB)}$ |
| $\widehat{x}_{ini,2}$ [g/s] | $0.1 \pm 122\%_{(@40\ dB)}$ | $0.1 \pm 130\%_{(@40\ dB)}$ | $0.1 \pm 38\%_{(@50\ dB)}$ |
| **5%** | | | |
| $\widehat{a}$ [kg/s] | $1.0 \pm 9.0\%_{(@50\ dB)}$ | $1.0 \pm 5.2\%_{(@40\ dB)}$ | $1.0 \pm 5.6\%_{(@40\ dB)}$ |
| $\widehat{b}$ [g] | $9.9 \pm 25.4\%_{(@50\ dB)}$ | $10.0 \pm 5.2\%_{(@20\ dB)}$ | $10.0 \pm 4.7\%_{(@40\ dB)}$ |
| $\widehat{x}_{ini,1}$ [g] | $0.1 \pm 0.6\%_{(@20\ dB)}$ | $0.1 \pm 0.6\%_{(@20\ dB)}$ | $0.1 \pm 6.2\%_{(@30\ dB)}$ |
| $\widehat{x}_{ini,2}$ [g/s] | $40.1 \pm 116\%_{(@40\ dB)}$ | $0.1 \pm 128\%_{(@40\ dB)}$ | $0.1 \pm 115\%_{(@40\ dB)}$ |
| **10%** | | | |
| $\widehat{a}$ [kg/s] | $1.0 \pm 10.4\%_{(@30\ dB)}$ | $1.0 \pm 10.3\%_{(@20\ dB)}$ | $1.0 \pm 10.3\%_{(@20\ dB)}$ |
| $\widehat{b}$ [g] | $9.9 \pm 10.5\%_{(@20\ dB)}$ | $9.9 \pm 10.4\%_{(@20\ dB)}$ | $10.0 \pm 10.5\%_{(@20\ dB)}$ |
| $\widehat{x}_{ini,1}$ [g] | $0.1 \pm 0.6\%_{(@20\ dB)}$ | $0.1 \pm 0.6\%_{(@20\ dB)}$ | $0.1 \pm 0.6\%_{(@20\ dB)}$ |
| $\widehat{x}_{ini,2}$ [g/s] | $0.1 \pm 108\%_{(@50\ dB)}$ | $0.1 \pm 110\%_{(@40\ dB)}$ | $0.1 \pm 137\%_{(@50\ dB)}$ |
| $\sigma_{m,d,k}$ | $\sigma_s$: 0% | 5% | 10% |
| **0%** | | | |
| $\widehat{a}$ [kg/s] | $1.0 \pm 0.7\%_{(@20\ dB)}$ | $1.0 \pm 0.7\%_{(@20\ dB)}$ | $1.0 \pm 0.3\%_{(@30\ dB)}$ |
| $\widehat{b}$ [g] | $10.0 \pm 1.1\%_{(@20\ dB)}$ | $10.0 \pm 1.1\%_{(@20\ dB)}$ | $10.0 \pm 0.4\%_{(@30\ dB)}$ |
| $\widehat{x}_{ini,1}$ [g] | $0.1 \pm 0.6\%_{(@40\ dB)}$ | $0.1 \pm 0.2\%_{(@30\ dB)}$ | $0.1 \pm 0.2\%_{(@30\ dB)}$ |
| $\widehat{x}_{ini,2}$ [g/s] | $0.1 \pm 122\%_{(@40\ dB)}$ | $0.1 \pm 130\%_{(@40\ dB)}$ | $0.1 \pm 38\%_{(@50\ dB)}$ |
| **5%** | | | |
| $\widehat{a}$ [kg/s] | $1.0 \pm 15.3\%_{(@20\ dB)}$ | $1.0 \pm 0.7\%_{(@20\ dB)}$ | $1.0 \pm 21.5\%_{(@20\ dB)}$ |
| $\widehat{b}$ [g] | $10.3 \pm 79.4\%_{(@20\ dB)}$ | $10.0 \pm 1.2\%_{(@20\ dB)}$ | $9.9 \pm 19.0\%_{(@20\ dB)}$ |
| $\widehat{x}_{ini,1}$ [g] | $0.1 \pm 0.2\%_{(@30\ dB)}$ | $0.1 \pm 0.6\%_{(@20\ dB)}$ | $0.1 \pm 0.2\%_{(@20\ dB)}$ |
| $\widehat{x}_{ini,2}$ [g/s] | $0.1 \pm 113\%_{(@40\ dB)}$ | $0.1 \pm 119\%_{(@40\ dB)}$ | $0.1 \pm 323\%_{(@30\ dB)}$ |
| **10%** | | | |
| $\widehat{a}$ [kg/s] | $1.0 \pm 22\%_{(@30\ dB)}$ | $1.0 \pm 16\%_{(@30\ dB)}$ | $1.0 \pm 28\%_{(@50\ dB)}$ |
| $\widehat{b}$ [g] | $0.1 \pm 26\%_{(@30\ dB)}$ | $9.9 \pm 14.8\%_{(@30\ dB)}$ | $10.4 \pm 93\%_{(@50\ dB)}$ |
| $\widehat{x}_{ini,1}$ [g] | $0.1 \pm 0.6\%_{(@20\ dB)}$ | $0.1 \pm 0.6\%_{(@20\ dB)}$ | $0.1 \pm 0.6\%_{(@20\ dB)}$ |
| $\widehat{x}_{ini,2}$ [g/s] | $0.1 \pm 121\%_{(@40\ dB)}$ | $0.1 \pm 136\%_{(@40\ dB)}$ | $0.1 \pm 111\%_{(@40\ dB)}$ |

## 6.4. Conclusions

An adaptive subspace method was proposed for estimating affine input parameters given the measurement of the caused sensor transient response. The subspace estimation method is a recursive method that allows online implementation. This method tracks the input of a system, using exponential forgetting, to process the system response. The subspace method is model-free and estimates directly the input parameters without identifying a sensor model. Therefore, it can be applied to the measurement of different physical magnitudes. In the specific weighing example described in the manuscript, the input is an affine function. The method is also applicable when the sensor is time-varying. The subspace method is computationally cheap, simple and suitable for implementation on digital signal processor of low computational power.

A maximum-likelihood estimator based on local optimization was designed to obtain a comparative reference for the other methods. The maximum-likelihood method estimates the affine input parameters and also model parameters and the sensor's initial conditions. This method simulates, in a receding horizon scheme, the response of a sensor model to estimate the input and minimizes the sum of the squares of the residual between the measured and the estimated responses. The main drawback of the maximum-likelihood method is its computational cost and efficient implementation of the method is left for future work.

A linear time-invariant weighing system is used as a test example for the estimation methods. The weighing system becomes time-varying when an affine input excites the system. The estimation methods are compared in a simulation study where the time-varying sensor response is perturbed by measurement noise, that is assumed to be white, of zero mean, and with known finite variance. The subspace method results are also compared to those of an existing digital time-varying filter. The coefficients of the time-varying filter require offline optimization. The estimation results obtained with the subspace method converges two times faster and is one order of magnitude smaller than those obtained with the time-varying filter. The empirical mean squared errors of the subspace method estimation is two orders of magnitude larger than the theoretical minimum given by the Cramér-Rao Lower bound.

Future work of this research is the practical implementation of the subspace method for real-time measurements.

# 7. Conclusions and future work

This thesis describes the validation of a signal processing method for metrology applications. The signal processing method takes the transient step response of a linear time-invariant sensor and provides an estimation of the level of the originating step input. The signal processing method is a subspace data-driven estimation method and constitutes an alternative to typical sensor response processing approaches based on compensation filters. Contrary to the compensation filters, this data-driven estimation method is model-independent and reduces the estimation time. The reason for the time reduction is the bypassing of the model parameters estimation, which is not performed previously nor simultaneously to the input estimation. The improvement in speed estimation makes the data-driven method suitable for real-time measurements.

Quantifying the estimation uncertainty was necessary to convince the metrology community of the data-driven method advantages. The uncertainty assessment is not straightforward. The data-driven method formulates a minimization problem that is a block-Hankel structured and correlated errors-in-variables (EIV) problem. The recursive least-squares (RLS) solution to the minimization problem enables the online implementation of the method. The structure and correlation of the EIV problem required research to find the first and second statistical moments of the LS solution.

The first part of the research reported in this thesis deals with the determination of the mean value and the covariance that the LS estimator has when it solves a structured and correlated EIV problem. The Taylor series expansion of the LS solution permits the study of the expected value of the LS estimate. The series expansion takes into account the structure of the regression matrix and the correlation between the regression matrix and the regressor. With the Taylor

series expansion, the element-wise treatment is not a strict requirement for the statistical analysis since it is possible to use matrix form in the computations. As a result, the statistical analysis yielded expressions that approximate the bias and the covariance of the LS estimate for given sample size and perturbation level. These expressions also help to understand the impact that the different matrix structures and the correlation bring into EIV problems and their solutions.

The LS bias and covariance predictions were validated first by Monte Carlo simulations. In the simulations are obtained the empirical statistical moments of the LS estimation, and their predictions calculated using the derived expressions. The simulations used an extensive set of values in the workspace of the step response sample size and perturbation levels. The learning obtained from the simulation results is the operating conditions in which the estimation method is effective. The operation conditions were the data-driven estimation method is effective include a region of signal-to-noise (SNR) near to 40 dB, which is typical in many real-life applications. This effectiveness near an SNR of 40 dB is a positive indication for the usability of the method in metrology. Another encouraging result is that the mean squared error of the data-driven method estimate is considerably near to the minimal theoretical variance that is defined by the Cramér-Rao lower bound of the formulated EIV problem.

The temperature and mass measurements are adequate for testing the implementation of the method. These two physical magnitudes are demanded applications in scientific and industrial fields, and there are available sensors of low cost in the market. The mass measurement demands more effort from the step input estimation method in a real-life application. Mass measurement sensors are affected by environment vibrations. Moreover, the mechanical constructions of the weighing sensors increase the order complexity of the sensor model. A load cell sensor, used as the weighing sensor, has a high order, that in theory, is infinite. A non-surprising observation in the implementation of experimental measurements is that the measurement noise collected from the weighing sensor is not Gaussian white noise. Nevertheless, the implementation of the data-driven step input estimation method showed good performance results under these conditions. The estimation method showed robustness against non-white noise and provided acceptable results for system orders selected between 5 and 7.

A third aspect of the conducted research included the exploration of estimating inputs based on different models with signal processing methods. A first choice is the affine input model, which is one complexity level higher than the step input. The exploration demonstrated that the adaptation of the data-driven method with the exponentially weighted RLS is useful to estimate the affine input. More general

than the RLS estimator, the exponentially weighted RLS uses a tuning parameter to select the data samples relevant for the solution computation.

The affine input estimation problem became more interesting because the application of the affine input to a weighing sensor turns the LTI system into a time-varying (TV) system. The adaptive data-driven affine input estimation method was simulated under different assumptions and showed robustness when processing time-varying sensor responses. Two other estimation methods are used as a reference to compare the results of the adaptive method. These methods are a maximum-likelihood (ML) estimator based on local optimization and a previously reported digital time-varying filter. The adaptive affine input estimation method outperformed the time-varying filter by presenting lower estimation time, and the ML method by requiring less computational effort.

## Future work

The use of model independent signal processing methods is a research field that surely will produce interesting results in the near future. With the increasing power of digital signal processors, the design of new methods is an opportunity that cannot be disregarded.

The data-driven method studied in this thesis is one example of an alternative to dynamic measurements under a different paradigm. With respect to this method, one conclusion of the analysis presented can be that the data-driven step input estimation method is not statistically efficient because the estimation shows bias. A topic for future research is the efficiency increase, perhaps by designing fast and optimal estimators for structured and correlated EIV problems.

On the other hand, for model-based estimation methods, such as the described ML method that has a high computational cost, there is a need also for efficient implementations to enable online optimization in receding-horizon schemes. With such efficient methods, the practical implementation of the ML methods can become feasible for real-time measurements.

# A. Appendices

## A.1. Derivation of bias and covariance expressions

The bias and covariance of the least-squares (LS) estimate (4.4) are obtained using the mathematical expectation in the definitions (4.5) and (4.6). For an unstructured and uncorrelated EIV problem, the expected value, and the covariance of $\widehat{\theta}$ are approximated by

$$
\mathbb{E}\left\{\widehat{\theta}\right\} \approx \theta + \mathbf{Q}^{-1}\mathbb{E}\left\{\mathbf{K}^{\top}\mathbf{E}\mathbf{Q}^{-1}\mathbf{K}^{\top}\mathbf{E} + \mathbf{E}^{\top}\mathbf{K}\mathbf{Q}^{-1}\mathbf{K}^{\top}\mathbf{E} - \mathbf{E}^{\top}\mathbf{E}\right\}\theta, \quad \text{and}
$$

$$
\begin{aligned}
\mathbf{C}\left(\widehat{\theta}\right) \approx{} & \theta\theta^{\top} + \mathbf{Q}^{-1}\mathbb{E}\left\{\mathbf{K}^{\top}\epsilon\epsilon^{\top}\mathbf{K} + \mathbf{K}^{\top}\mathbf{E}\theta\theta^{\top}\mathbf{E}^{\top}\mathbf{K}\right\}\mathbf{Q}^{-1} \\
& + \mathbf{Q}^{-1}\mathbb{E}\left\{\mathbf{K}^{\top}\mathbf{E}\mathbf{Q}^{-1}\mathbf{K}^{\top}\mathbf{E} + \mathbf{E}^{\top}\mathbf{K}\mathbf{Q}^{-1}\mathbf{K}^{\top}\mathbf{E} - \mathbf{E}^{\top}\mathbf{E}\right\}\theta\theta^{\top} \\
& + \theta\theta^{\top}\mathbb{E}\left\{\mathbf{E}^{\top}\mathbf{K}\mathbf{Q}^{-1}\mathbf{E}^{\top}\mathbf{K} + \mathbf{E}^{\top}\mathbf{K}\mathbf{Q}^{-1}\mathbf{K}^{\top}\mathbf{E} - \mathbf{E}^{\top}\mathbf{E}\right\}\mathbf{Q}^{-1} \\
& - \mathbb{E}\left\{\widehat{\theta}\right\}\mathbb{E}\left\{\widehat{\theta}\right\}^{\top},
\end{aligned} \tag{A.1}
$$

where we have considered the second order Taylor series approximation (4.3), and we have removed the terms of zero expected value, and the terms of order higher than 2. After an elementwise evaluation of the corresponding expected values in (A.1), the expressions result in

$$
\begin{aligned}
\mathbb{E}\left\{\widehat{\theta}\right\} &\approx \theta + \mathbf{b}_{\mathrm{p}}\left(\widehat{\theta}\right) = \theta + \sigma_{\mathbf{E}}^{2}\mathbf{Q}^{-1}\left(2\mathbf{I} + 2n\mathbf{I} - N\mathbf{I}\right)\theta, \quad \text{and} \\
\mathbf{C}_{\mathrm{p}}\left(\widehat{\theta}\right) &\approx \sigma_{\epsilon}^{2}\,\mathbf{Q}^{-1} + \sigma_{\mathbf{E}}^{2}\,\mathrm{trace}\left(\theta\theta^{\top}\right)\mathbf{Q}^{-1} - \sigma_{\mathbf{E}}^{4}\left(2 + 2n - N\right)^{2}\mathbf{Q}^{-1}\theta\theta^{\top}\mathbf{Q}^{-1},
\end{aligned} \tag{A.2}
$$

from where equations (4.7) and (4.8) are obtained.

On the other hand, due to the correlation, the expressions that approximate the expected value of the LS estimate of the structured and correlated EIV problem (3.20) have a different form:

$$
\mathbb{E}\left\{\widehat{\boldsymbol{\theta}}\right\} \approx \boldsymbol{\theta} + \mathbf{Q}^{-1}\mathbb{E}\left\{\mathbf{K}^{\top}\mathbf{E}\mathbf{Q}^{-1}\mathbf{K}^{\top}\mathbf{E} + \mathbf{E}^{\top}\mathbf{K}\mathbf{Q}^{-1}\mathbf{K}^{\top}\mathbf{E} - \mathbf{E}^{\top}\mathbf{E}\right\}\boldsymbol{\theta}
$$
$$
+ \mathbf{Q}^{-1}\mathbb{E}\left\{\mathbf{E}^{\top}\boldsymbol{\epsilon} - \mathbf{K}^{\top}\mathbf{E}\mathbf{Q}^{-1}\mathbf{K}^{\top}\boldsymbol{\epsilon} - \mathbf{E}^{\top}\mathbf{K}\mathbf{Q}^{-1}\mathbf{K}^{\top}\boldsymbol{\epsilon}\right\}, \quad \text{and}
$$
$$
\mathbf{C}\left(\widehat{\boldsymbol{\theta}}\right) \approx \boldsymbol{\theta}\boldsymbol{\theta}^{\top}
$$
$$
+ \mathbf{Q}^{-1}\mathbb{E}\left\{\mathbf{K}^{\top}\boldsymbol{\epsilon}\boldsymbol{\epsilon}^{\top}\mathbf{K} + \mathbf{K}^{\top}\mathbf{E}\boldsymbol{\theta}\boldsymbol{\theta}^{\top}\mathbf{E}^{\top}\mathbf{K} - \mathbf{K}^{\top}\mathbf{E}\boldsymbol{\theta}\boldsymbol{\epsilon}^{\top}\mathbf{K} - \mathbf{K}^{\top}\boldsymbol{\epsilon}\boldsymbol{\theta}^{\top}\mathbf{E}^{\top}\mathbf{K}\right\}\mathbf{Q}^{-1}
$$
$$
+ \mathbf{Q}^{-1}\mathbb{E}\left\{\mathbf{K}^{\top}\mathbf{E}\mathbf{Q}^{-1}\mathbf{K}^{\top}\mathbf{E} + \mathbf{E}^{\top}\mathbf{K}\mathbf{Q}^{-1}\mathbf{K}^{\top}\mathbf{E} - \mathbf{E}^{\top}\mathbf{E}\right\}\boldsymbol{\theta}\boldsymbol{\theta}^{\top}
$$
$$
+ \boldsymbol{\theta}\boldsymbol{\theta}^{\top}\mathbb{E}\left\{\mathbf{E}^{\top}\mathbf{K}\mathbf{Q}^{-1}\mathbf{E}^{\top}\mathbf{K} + \mathbf{E}^{\top}\mathbf{K}\mathbf{Q}^{-1}\mathbf{K}^{\top}\mathbf{E} - \mathbf{E}^{\top}\mathbf{E}\right\}\mathbf{Q}^{-1}
$$
$$
- \mathbb{E}\left\{\widehat{\boldsymbol{\theta}}\right\}\mathbb{E}\left\{\widehat{\boldsymbol{\theta}}\right\}^{\top}
$$
$$
+ \mathbf{Q}^{-1}\mathbb{E}\left\{\mathbf{E}^{\top}\boldsymbol{\epsilon} - \mathbf{K}^{\top}\mathbf{E}\mathbf{Q}^{-1}\mathbf{K}^{\top}\boldsymbol{\epsilon} - \mathbf{E}^{\top}\mathbf{K}\mathbf{Q}^{-1}\mathbf{K}^{\top}\boldsymbol{\epsilon}\right\}\boldsymbol{\theta}^{\top}
$$
$$
+ \boldsymbol{\theta}\mathbb{E}\left\{\boldsymbol{\epsilon}^{\top}\mathbf{E} - \boldsymbol{\epsilon}^{\top}\mathbf{K}\mathbf{Q}^{-1}\mathbf{E}^{\top}\mathbf{K} - \boldsymbol{\epsilon}^{\top}\mathbf{K}\mathbf{Q}^{-1}\mathbf{K}^{\top}\mathbf{E}\right\}\mathbf{Q}^{-1}.
$$

(A.3)

These expressions have the non zero expected value terms, up to the second order. We have then

$$
\mathbb{E}\left\{\widehat{\boldsymbol{\theta}}\right\} = \boldsymbol{\theta} + \mathbf{b}_{\mathrm{p}}\left(\widehat{\boldsymbol{\theta}}\right)
$$
$$
\approx \boldsymbol{\theta} + \mathbf{Q}^{-1}\mathbf{K}^{\top}\underbrace{\mathbb{E}\left\{\mathbf{E}\mathbf{Q}^{-1}\mathbf{K}^{\top}\mathbf{E}\right\}}_{\mathbf{B}_1} - \mathbf{Q}^{-1}\underbrace{\mathbb{E}\left\{\mathbf{E}^{\top}\left(\mathbf{I} - \mathbf{K}\mathbf{Q}^{-1}\mathbf{K}^{\top}\right)\mathbf{E}\right\}}_{\mathbf{B}_2}\boldsymbol{\theta}
$$
$$
- \mathbf{Q}^{-1}\mathbf{K}^{\top}\underbrace{\mathbb{E}\left\{\mathbf{E}\mathbf{Q}^{-1}\mathbf{K}^{\top}\boldsymbol{\epsilon}\right\}}_{\mathbf{B}_3} + \mathbf{Q}^{-1}\underbrace{\mathbb{E}\left\{\mathbf{E}^{\top}\left(\mathbf{I} - \mathbf{K}\mathbf{Q}^{-1}\mathbf{K}^{\top}\right)\boldsymbol{\epsilon}\right\}}_{\mathbf{B}_4}, \quad \text{and}
$$
$$
\mathbf{C}\left(\widehat{\boldsymbol{\theta}}\right) \approx \mathbf{Q}^{-1}\mathbf{K}^{\top}\left(\underbrace{\mathbb{E}\left\{\boldsymbol{\epsilon}\boldsymbol{\epsilon}^{\top}\right\}}_{\sigma_{\epsilon}^2\mathbf{I}_{N-n}} + \underbrace{\mathbb{E}\left\{\mathbf{E}\boldsymbol{\theta}\boldsymbol{\theta}^{\top}\mathbf{E}^{\top}\right\}}_{\mathbf{C}_1} - \underbrace{\mathbb{E}\left\{\mathbf{E}\boldsymbol{\theta}\boldsymbol{\epsilon}^{\top}\right\}}_{\mathbf{C}_2} - \underbrace{\mathbb{E}\left\{\boldsymbol{\epsilon}\boldsymbol{\theta}^{\top}\mathbf{E}^{\top}\right\}}_{\mathbf{C}_2^{\top}}\right)\mathbf{K}\mathbf{Q}^{-1}
$$
$$
- \mathbf{b}_{\mathrm{p}}\left(\widehat{\boldsymbol{\theta}}\right)\mathbf{b}_{\mathrm{p}}^{\top}\left(\widehat{\boldsymbol{\theta}}\right).
$$

(A.4)

from where the expressions (4.11) and (4.12) are obtained.

## A.2. Proof of Lemma 1

**Proof** In the first case considered in the lemma, the elements of the expected value $\mathbf{Z} = \mathbb{E}\{\mathbf{EAE}\}$ are

$$z_{ij} = \mathbb{E}\{\mathbf{EAE}\}_{ij} = \mathbb{E}\{\mathbf{e}_i\mathbf{AE}_j\} = \text{tr}\left(\mathbf{A}\,\mathbb{E}\{\mathbf{E}_j\mathbf{e}_i\}\right), \qquad (A.5)$$

where $\mathbf{e}_i$, and $\mathbf{E}_j$ are the $i$-th row, and the $j$-th column of $\mathbf{E}$, for $i = 1,\ldots,N-n$, and $j = 2,\ldots,n+1$. The matrix $\mathbb{E}\{\mathbf{E}_j\mathbf{e}_i\}$ is the product of $\sigma_\epsilon^2$ times a matrix whose elements are 0 in the first column, 2 in the $(j-i-1)$-th diagonal, and -1 in the $(j-i-2)$-th, and $(j-i)$-th diagonals, with zeros elsewhere. By using the definition of the second differential operator, we express

$$\mathbb{E}\{\mathbf{E}_j\mathbf{e}_i\} = \sigma_\epsilon^2 \begin{bmatrix} \mathbf{0}_{N-n} & \mathbf{D}_{N-n\times n}^{2,j-i} \end{bmatrix}. \qquad (A.6)$$

The proof of the other cases in the Lemma is similar. For the second case, the elements of the expected value $\mathbf{Z} = \mathbb{E}\{\mathbf{E}^\top\mathbf{AE}\}$ are

$$z_{ij} = \mathbb{E}\left\{\mathbf{E}^\top\mathbf{AE}\right\}_{ij} = \mathbb{E}\{\mathbf{e}_i\mathbf{AE}_j\} = \text{tr}\left(\mathbf{A}\,\mathbb{E}\{\mathbf{E}_j\mathbf{e}_i\}\right), \qquad (A.7)$$

where now $\mathbf{e}_i$ is the $i$-th row of $\mathbf{E}^\top$, and $\mathbf{E}_j$ is the $j$-th column of $\mathbf{E}$, for $i = 2,\ldots,n+1$, and $j = 2,\ldots,n+1$. The matrix $\mathbb{E}\{\mathbf{E}_j\mathbf{e}_i\}$ is $\sigma_\epsilon^2$ times a matrix whose elements are 2 in the $(j-i)$-th diagonal, and -1 in the $(j-i-1)$-th and $(j-i+1)$-th diagonals, with zeros elsewhere. Therefore we have

$$\mathbb{E}\{\mathbf{E}_j\mathbf{e}_i\} = \sigma_\epsilon^2\mathbf{D}_{N-n\times N-n}^{2,j-i+1}. \qquad (A.8)$$

The expected values that involve the vector $\epsilon$ are especial cases of the previous cases. The vector $\epsilon$ in the expected values $\mathbb{E}\{\mathbf{EA}\varepsilon\}$, $\mathbb{E}\{\mathbf{E}^\top\mathbf{A}\varepsilon\}$, and $\mathbb{E}\{\mathbf{EA}\epsilon^\top\}$ is

$$\epsilon = \begin{bmatrix} \varepsilon(n+1) & \varepsilon(n+2) & \cdots & \varepsilon(N) \end{bmatrix}^\top, \qquad (A.9)$$

as it is imposed by the input estimation method formulation. $\qquad\square$

## A.3. Calculation of Jacobian matrices in the affine input ML estimation method

The entries of the Jacobian matrix are the first order partial derivatives of the residual error $\mathbf{r}$ with respect to the optimization variables. The state-space representation of the weighing model allows to find the analytical expression of

the Jacobian. The partial derivative of the residual error $\mathbf{r}$ with respect to the optimization variable $a$ is

$$\mathbf{J}_a = \frac{\partial \mathbf{r}}{\partial a} = \frac{\partial \widehat{\mathbf{y}}}{\partial a} = \begin{bmatrix} 1 & 0 \end{bmatrix} \frac{\partial \mathbf{x}}{\partial a} = \begin{bmatrix} 1 & 0 \end{bmatrix} \mathbf{x}_a \tag{A.10}$$

where we use $\mathbf{x}_a = \partial \mathbf{x}/\partial a$ to simplify the notation. Now, from the derivative of the state equation, we have

$$\dot{\mathbf{x}}_a = \begin{bmatrix} 0 & 1 \\ \frac{-k_{\mathrm{s}}}{at+b+m} & \frac{-(a+k_{\mathrm{d}})}{at+b+m} \end{bmatrix} \mathbf{x}_a + \begin{bmatrix} 0 & 0 \\ \frac{k_{\mathrm{s}}t}{(at+b+m)^2} & \frac{k_{\mathrm{d}}t-b-m}{(at+b+m)^2} \end{bmatrix} \mathbf{x},$$

$$\text{with} \quad \mathbf{x}_a(0) = \begin{bmatrix} 0 \\ 0 \end{bmatrix}. \tag{A.11}$$

Then, the partial derivative of the residual error $\mathbf{r}$ with respect to the optimization variable $a$ results in an additional dynamic system.

By repeating the procedure, we obtain the partial derivatives with respect to $b$ as follows:

$$\dot{\mathbf{x}}_b = \begin{bmatrix} 0 & 1 \\ \frac{-k_{\mathrm{s}}}{at+b+m} & \frac{-(a+k_{\mathrm{d}})}{at+b+m} \end{bmatrix} \mathbf{x}_b + \begin{bmatrix} 0 & 0 \\ \frac{k_{\mathrm{s}}}{(at+b+m)^2} & \frac{a+k_{\mathrm{d}}}{(at+b+m)^2} \end{bmatrix} \mathbf{x},$$

$$\mathbf{J}_b = \begin{bmatrix} 1 & 0 \end{bmatrix} \mathbf{x}_b, \quad \text{with} \quad \mathbf{x}_b(0) = \begin{bmatrix} 0 \\ 0 \end{bmatrix}. \tag{A.12}$$

The partial derivatives of the residual error $\mathbf{r}$ with respect to the initial conditions yield

$$\dot{\mathbf{x}}_{\mathbf{x}_{\mathrm{ini},1}} = \begin{bmatrix} 0 & 1 \\ \frac{-k_{\mathrm{s}}}{at+b+m} & \frac{-(a+k_{\mathrm{d}})}{at+b+m} \end{bmatrix} \mathbf{x}_{\mathbf{x}_{\mathrm{ini},1}},$$

$$\mathbf{J}_{\mathbf{x}_{\mathrm{ini},1}} = \begin{bmatrix} 1 & 0 \end{bmatrix} \mathbf{x}_{\mathbf{x}_{\mathrm{ini},1}}, \quad \text{with} \quad \mathbf{x}_{\mathrm{ini},1}(0) = \begin{bmatrix} 1 \\ 0 \end{bmatrix} \tag{A.13}$$

and

$$\dot{\mathbf{x}}_{\mathbf{x}_{\mathrm{ini},2}} = \begin{bmatrix} 0 & 1 \\ \frac{-k_{\mathrm{s}}}{at+b+m} & \frac{-(a+k_{\mathrm{d}})}{at+b+m} \end{bmatrix} \mathbf{x}_{\mathbf{x}_{\mathrm{ini},2}},$$

$$\mathbf{J}_{\mathbf{x}_{\mathrm{ini},2}} = \begin{bmatrix} 1 & 0 \end{bmatrix} \mathbf{x}_{\mathbf{x}_{\mathrm{ini},2}}, \quad \text{with} \quad \mathbf{x}_{\mathrm{ini},2}(0) = \begin{bmatrix} 0 \\ 1 \end{bmatrix}. \tag{A.14}$$

The last two additional dynamic systems are identical, except by their initialization.

The Jacobian matrix is constructed using the responses of the additional dynamic systems

$$\mathbf{J} = \begin{bmatrix} \mathbf{J}_a & \mathbf{J}_b & \mathbf{J}_{\mathbf{x}_{\mathrm{ini},1}} & \mathbf{J}_{\mathbf{x}_{\mathrm{ini},2}} \end{bmatrix} \tag{A.15}$$

# List of Publications

## Journal publications

G. Quintana-Carapia, I. Markovsky, R. Pintelon, P. Z. Csurcsia and D. Verbeke, "Bias and covariance of the least squares estimate in a structured errors-invariables problem," *Computational Statistics  Data Analysis*, Vol. 144, No. 106893, 2020, ISSN 0167-9473, doi: 10.1016/j.csda.2019.106893.

G. Quintana-Carapia, I. Markovsky, R. Pintelon, P. Z. Csurcsia and D. Verbeke, "Experimental validation of a data-driven step input estimation method for dynamic measurements," *IEEE Transactions on Instrumentation and Measurement*, vol. 69, no. 7, pp. 4843-4851, July 2020, doi: 10.1109/TIM.2019.2951865.

G. Quintana-Carapia, I. Markovsky, "Input parameters estimation from timevarying measurements," *Measurement*, Vol. 153, No. 1, pp. 107418, 2020, ISSN 0263-2241, doi: 10.1016/j.measurement.2019.107418.

## Conference publications

G. Quintana-Carapia, I. Markovsky, "Data driven dynamic measurements", In: *9th International Workshop on the Analysis of Dynamic Measurements*", Berlin, Germany, 2016.

G. Quintana-Carapia, I. Markovsky, "Data driven dynamic measurements", In: *35th Benelux Meeting on Systems and Control*", Soesterberg, The Netherlands, 2016.

# Bibliography

M. Alaziz, Z. Jia, R. Howard, X. Lin, and Y. Zhang. MotionTree: A Tree-Based In-Bed Body Motion Classification System Using Load-Cells. In *2017 IEEE/ACM International Conference on Connected Health: Applications*, *Systems and Engineering Technologies (CHASE)*, pages 127–136, 2017. doi: 10.1109/CHASE.2017.71.

L. Angrisani and A. Napolitano. Modulation quality measurement in wimax systems through a fully digital signal processing approach. *IEEE Transactions on Instrumentation and Measurement*, 59(9):2286–2302, 2010. ISSN 0018-9456. doi: 10.1109/TIM.2009.2034577.

S.E. Azam, E. Chatzi, and C. Papadimitriou. A dual kalman filter approach for state estimation via output-only acceleration measurements. *Mechanical Systems and Signal Processing*, 60-61:866–886, 2015. ISSN 0888-3270. doi: 10.1016/j.ymssp.2015.02.001.

F. Ballo, M. Gobbi, G. Mastinu, and G. Previati. A six axis load cell for the analysis of the dynamic impact response of a hybrid III dummy. *Measurement*, 90: 309–317, 2016. ISSN 0263-2241. doi: 10.1016/j.measurement.2016.04.047.

A. Beck and Y. C. Eldar. Structured total maximum likelihood: An alternative to structured total least squares. *SIAM Journal on Matrix Analysis and Applications*, 31(5):2623–2649, 2010. doi: 10.1137/090756338.

BIPM, IEC, IFCC, ILAC, ISO, IUPAC, IUPAP, and OIML. *Evaluation of measurement data - Guide to the expression of uncertainty in measurement*. (Geneva: International Organization for Standardization) (Joint Committee for Guides in Metrology, JCGM 101:2008.), 2008.

G. Boschetti, R. Caracciolo, D. Richiedei, and A. Trevisani. Model-based dynamic compensation of load cell response in weighing machines affected by environ-

mental vibrations. *Mechanical Systems and Signal Processing*, 34(1–2):116–130, 2013. ISSN 0888-3270. doi: 10.1016/j.ymssp.2012.07.010.

J. Cai, X. Qu, W. Xu, and G. Ye. Robust recovery of complex exponential signals from random Gaussian projections via low rank Hankel matrix reconstruction. *Applied and Computational Harmonic Analysis*, 41(2):470–490, 2016. ISSN 1063-5203. doi: 10.1016/j.acha.2016.02.003.

O. Casas, R. Dalazen, and A. Balbinot. 3D load cell for measure force in a bicycle crank. *Measurement*, 93:189–201, 2016. ISSN 0263-2241. doi: 10.1016/j.measurement.2016.07.031.

M.G. Cox and B.R. Siebert. The use of a Monte Carlo method for evaluating uncertainty and expanded uncertainty. *Metrologia*, 43(4):S178, 2006. doi: 10.1088/0026-1394/43/4/s03.

B.A. de Castro, F.G. Baptista, and F. Ciampa. New signal processing approach for structural health monitoring in noisy environments based on impedance measurements. *Measurement*, 137:155–167, 2019. ISSN 0263-2241. doi: 10.1016/j.measurement.2019.01.054.

G. D'Emilia, A. Gaspari, and E. Natale. Evaluation of aspects affecting measurement of three-axis accelerometers. *Measurement*, 77:95–104, 2016. ISSN 0263-2241. doi: 10.1016/j.measurement.2015.08.031.

A. Dienstfrey and P.D. Hale. Analysis for dynamic metrology. *Measurement Science and Technology*, 25(3):1–12, 2014.

A. Diniz, M. de Almeida, J. Vianna, A. Oliveira, and A. Fabro. Methodology for estimating measurement uncertainty in the dynamic calibration of industrial temperature sensors. *Journal of the Brazilian Society of Mechanical Sciences and Engineering*, 39(3):1053–1060, 2017. ISSN 1678-5878.

S. Eichstädt, C. Elster, T.J. Esward, and J.P. Hessling. Deconvolution filters for the analysis of dynamic measurement processes: a tutorial. *Metrologia*, 47(5): 522–533, 2010. doi: 10.1088/0026-1394/47/5/003.

S. Eichstädt, A. Link, Harris P., and C. Elster. Deconvolution filters for the analysis of dynamic measurement processes: a tutorial. *Metrologia*, 49(3):401–410, 2012. doi: 10.1088/0026-1394/49/3/401.

S. Eichstädt, N. Makarava, and C. Elster. On the evaluation of uncertainties for state estimation with the Kalman filter. *Measurement Science and Technology*, 27 (12):125009, 2016.

C. Elster and A. Link. Uncertainty evaluation for dynamic measurements modelled by a linear time-invariant system. *Metrologia*, 45(4):464, 2008.

C. Elster, A. Link, and T. Bruns. Analysis of dynamic measurements and determination of time-dependent measurement uncertainty using a second-order model. *Measurements science and technology*, 18(12):3682–3687, 2007. ISSN 0957-0233. doi: 10.1088/0957-0233/18/12/002.

T.J. Esward. Investigating dynamic measurement applications through modelling and simulation, 2016. ISSN 01718096.

T.J. Esward, C. Elster, and Hessling J.P. Analysis of dynamic measurements: New challenges require new solutions. In *In Proceedings of XIX IMEKO World Congress*, 2009.

R. Feiz and M. Rezghi. A splitting method for total least squares color image restoration problem. *Journal of Visual Communication and Image Representation*, 46:48–57, 2017. ISSN 1047-3203. doi: 10.1016/j.jvcir.2017.03.001.

A. Ferrero and S. Salicone. Measurement uncertainty. *IEEE Instrumentation Measurement Magazine*, 9(3):44–51, 2006. ISSN 1094-6969. doi: 10.1109/MIM. 2006.1637979.

J. Fraden. *Handbook of Modern Sensors*. Springer, San Diego, CA, 5 edition, 2016. ISBN 978-3-319-19302-1.

G. Guo, S. Zhong, and L. Yao. Sensitivity effect of single load cell on total output of a combinatorial structure. In L. Yao, S. Zhong, H. Kikuta, J.-G. Juang, and M. Anpo, editors, *Advanced Mechanical Science and Technology for the Industrial Revolution 4.0*, pages 105–111. Springer, 2018. ISBN 978-981-10-4109-9.

P. da Silva Hack and C.S. ten Caten. Measurement Uncertainty: Literature Review and Research Trends. *IEEE Transactions on Instrumentation and Measurement*, 61 (8):2116–2124, 2012. ISSN 0018-9456. doi: 10.1109/TIM.2012.2193694.

P.D. Hale, A. Dienstfrey, J.C.M. Wang, D.F. Williams, A. Lewandowski, D.A. Keenan, and T.S. Clement. Traceable Waveform Calibration With a Covariance-Based Uncertainty Analysis. *IEEE Transactions on Instrumentation and Measurement*, 58(10):3554–3568, 2009. ISSN 0018-9456. doi: 10.1109/TIM.2009. 2018012.

J.M. Hammersley and D.C. Handscomb. *Monte Carlo Methods*. Methuen's monographs on applied probability and statistics. Methuen, 1975. ISBN 9780416523409.

W. Hernandez. Improving the Response of a Load Cell by Using Optimal Filtering. *Sensors*, 6(7):697–711, 2006. ISSN 1424-8220. doi: 10.3390/s6070697.

J.P. Hessling. A novel method of estimating dynamic measurement errors. *Measurement Science and Technology*, 17(10):2740–2750, 2006. doi: 10.1088/0957-0233/17/10/028.

J.P. Hessling. A novel method of dynamic correction in the time domain. *Measurement Science and Technology*, 19(7):1–10, 2008. doi: 10.1088/0957-0233/19/7/075101.

J.P. Hessling. Metrology for non-stationary dynamic measurements. In M. Sharma, editor, *Advances in Measurement Systems*, chapter 9, pages 221–256. InTech, 2010. ISBN 978-3-319-05353-0. doi: 10.5772/8730.

J.P. Hessling. Propagation of dynamic measurement uncertainty. *Measurement Science and Technology*, 22(10):105105, 2011. doi: 10.1088/0957-0233/22/10/105105.

J.P. Hessling. Deterministic Sampling for Quantification of Modeling Uncertainty of Signals. In F.P. García Márquez and N. Zaman, editors, *Digital Filters and Signal Processing*, chapter 3, pages 53–79. IntechOpen, Rijeka, 2013. doi: 10.5772/52193.

Q. Huang, Z. Teng, X. Tang, H. Lin, and H. Wen. Mass Measurement Method for the Electronic Balance Based on Continuous-Time Sigma-Delta Modulator. *IEEE Transactions on Instrumentation and Measurement*, 65(6):1300–1309, 2016. ISSN 0018-9456. doi: 10.1109/TIM.2015.2490358.

International Recommendation OIML R 51 1. *Automatic catchweighing instruments Part 1: Metrological and technical requirements - Tests*. International Organization for Legal Metrology, 2006.

M. Jafaripanah, Al-Hashimi B.M., and White N.M. Application of analog adaptive filters for dynamic sensor compensation. *IEEE Transactions on Instrumentation and Measurement*, 54(1):245–251, 2005. ISSN 0018-9456. doi: 10.1109/TIM.2004.839763.

T. Jia, H. Wang, X. Shen, Z. Jiang, and K. He. Target localization based on structured total least squares with hybrid TDOA-AOA measurements. *Signal Processing*, 143:211–221, 2018. ISSN 0165-1684. doi: 10.1016/j.sigpro.2017.09.011.

Y.Q. Jing, Q.H. Meng, P.F. Qi, M. Zeng, and Y.J. Liu. Signal processing inspired from the olfactory bulb for electronic noses. *Measurement Science and Technology*, 28(1):015105, 2016. doi: 10.1088/1361-6501/28/1/015105.

T. Kailath, H. Sayed, and B. Hassibi. *Linear Estimation*. Prentice Hall, NJ, 1 edition, 2000. ISBN 0-13-022464-2.

Z. Kesilmiş and T. Baran. A geometric approach to beam type load cell response for fast weighing. *MAPAN*, 31(2):153–158, 2016. ISSN 0974-9853. doi: 10. 1007/s12647-016-0168-2.

J. Kiviet and G. Phillips. Higher-order asymptotic expansions of the least-squares estimation bias in first-order dynamic regression models. *Computational Statistics & Data Analysis*, 56(11):3705–3729, 2012. ISSN 0167-9473. doi: 10.1016/j.csda.2010.07.013.

J. Kiviet and G. Phillips. Improved variance estimation of maximum likelihood estimators in stable first-order dynamic regression models. *Computational Statistics & Data Analysis*, 76:424–448, 2014. ISSN 0167-9473. doi: 10.1016/j. csda.2013.09.021.

S. Kueppers, H. Cetinkaya, and N. Pohl. A compact 120 ghz sige:c based 2Ã8 fmcw mimo radar sensor for robot navigation in low visibility environments. In *2017 European Radar Conference (EURAD)*, pages 122–125, 2017.

W. Lee, H. Yoon, C. Han, K. Joo, and K. Park. Physiological signal monitoring bed for infants based on load-cell sensors. *Sensors*, 16(3), 2016. ISSN 1424-8220. doi: 10.3390/s16030409.

P. Lemmerling and S. Van Huffel. Structured total least squares. In S. Van Huffel and P. Lemmerling, editors, *Total Least Squares and Errors-in-Variables Modeling: Analysis*, *Algorithms and Applications*, pages 79–91. Springer, 2002. ISBN 978-94-017-3552-0. doi: 10.1007/978-94-017-3552-0_8.

A. Link and C. Elster. Uncertainty evaluation for IIR (infinite impulse response) filtering using a state-space approach. *Measurement Science and Technology*, 20 (5):1–5, 2009. doi: 10.1088/0957-0233/20/5/055104.

A. Link, A. Täubner, W. Wabinski, T. Bruns, and C. Elster. Modelling accelerometers for transient signals using calibration measurements upon sinusoidal excitation. *Measurement*, 40(9–10):928–935, 2007. ISSN 0263-2241. doi: 10.1016/j.measurement.2006.10.011.

L. Ljung. *System Identification - Theory for the User*. Prentice-Hall, Englewood Cliffs, NJ, 1987. ISBN 0-13-881640.

I. Markovsky. An application of system identification in metrology. *Control Engineering Practice*, 43:85–93, 2015a. doi: 10.1016/j.conengprac.2015.07.001.

I. Markovsky. Comparison of adaptive and model-free methods for dynamic measurement. *IEEE Signal Proc. Letters*, 22:1094–1097, 2015b. doi: 10.1109/ LSP.2014.2388369.

I. Markovsky and S. Van Huffel. Overview of total least-squares methods. *Signal Processing*, 87(10):2283–2302, 2007. ISSN 0165-1684. doi: 10.1016/j.sigpro. 2007.04.004.

N. Mastronardi and D. O'Leary. Fast robust regression algorithms for problems with Toeplitz structure. *Computational Statistics & Data Analysis*, 52(2):1119–1131, 2007. ISSN 0167-9473. doi: 10.1016/j.csda.2007.05.008.

C. Matthews, F. Pennecchi, S. Eichstädt, A. Malengo, T.J. Esward, I. Smith, C. Elster, A. Knott, F. Arrhén, and A. Lakka. Mathematical modelling to support traceable dynamic calibration of pressure sensors. *Metrologia*, 51(3):326–338, 2014. doi: 10.1088/0026-1394/51/3/326.

D.Q. Mayne. Model predictive control: Recent developments and future promise. *Automatica*, 50(12):2967–2986, 2014. ISSN 0005-1098. doi: 10.1016/j. automatica.2014.10.128.

R. Middleton and G.C. Goodwin. *Digital control and estimation: a unified approach*. Prentice-Hall, Englewood Cliffs, NJ, 1990. ISBN 0â13â211798â3.

M. Munther, D.I. Moon, B. Kim, J.W. Han, K. Davami, and M. Meyyappan. Array of chemiresistors for single input multiple output (simo) variation-tolerant all printed gas sensor. *Sensors and Actuators B: Chemical*, 299:126971, 2019. ISSN 0925-4005. doi: 10.1016/j.snb.2019.126971.

M. Niedźwiecki and P. Pietrzak. High-Precision FIR-Model-Based Dynamic Weighing System. *IEEE Transactions on Instrumentation and Measurement*, 65(10): 2349–2359, 2016. ISSN 0018-9456. doi: 10.1109/TIM.2016.2575180.

M. Niedźwiecki, M. Meller, and P. Pietrzak. System identification based approach to dynamic weighing revisited. *Mechanical Systems and Signal Processing*, 80: 582–599, 2016. ISSN 0888-3270. doi: 10.1016/j.ymssp.2016.04.007.

J. Nocedal and S. Wright. *Numerical Optimization*. Springer Verlag, New York, 2 edition, 2006. ISBN 978-0-387-30303-1.

J. Ogorevc, J. Bojkovski, I. Pušnik, and J. Drnovšek. Dynamic measurements and uncertainty estimation of clinical thermometers using Monte Carlo method. *Measurement Science and Technology*, 27(9):1–14, 2016. doi: 10.1088/0957-0233/ 27/9/095001.

G. Olmi. Load Cell Training for the Students of Experimental Stress Analysis. *Experimental Techniques*, 40(3):1147–1161, 2016. ISSN 1747-1567. doi: 10.1007/ s40799-016-0115-8.

H. Palanthandalam-Madapusi, T. Van Pelt, and D. Bernstein. Parameter consistency and quadratically constrained errors-in-variables least-squares identification. *International Journal of Control*, 83(4):862–877, 2010. ISSN 1366–5820. doi: 10.1080/00207170903470666.

Y. Pan, G.Q. Luo, H. Jin, and W. Cao. Direction-of-Arrival Estimation With ULA: A Spatial Annihilating Filter Reconstruction Perspective. *IEEE Access*, 6:23172–23179, 2018. ISSN 2169-3536. doi: 10.1109/ACCESS.2018.2828799.

A. Papoulis and S. U. Pillai. *Probability, Random Variables, and Stochastic Processes*. McGraw Hill, New York, 4 edition, 2002. ISBN 0-07-112256-7.

P. Pietrzak, M. Meller, and M. Niedźwiecki. Dynamic mass measurement in checkweighers using a discrete time-variant low-pass filter. *Mechanical Systems and Signal Processing*, 48(1–2):67–76, 2014. ISSN 0888-3270. doi: 10.1016/j.ymssp.2014.02.013.

R. Pintelon and J. Schoukens. *System Identification: A Frequency Domain Approach*. IEEE Press, Piscataway, NJ, 2 edition, 2012. ISBN 978-0470640371.

R. Pintelon, Y. Rolain, M. V. Bossche, and J. Schoukens. Towards an ideal data acquisition channel. *IEEE Transactions on Instrumentation and Measurement*, 39 (1):116–120, 1990. ISSN 0018-9456. doi: 10.1109/19.50428.

J. Piskorowski and T. Barcinski. Dynamic compensation of load cell response: A time-varying approach. *Mechanical Systems and Signal Processing*, 22(7):1694–1704, 2008. ISSN 0888-3270. doi: 10.1016/j.ymssp.2008.01.001.

G. Quintana-Carapia and Markovsky. Input parameters estimation from time-varying measurements. *Measurement*, 153(1):107418, 2020. ISSN 0263-2241. doi: 10.1016/j.measurement.2019.107418.

G. Quintana-Carapia, I. Markovsky, R. Pintelon, P. Zoltán, and D. Verbeke. Bias and covariance of the least squares estimate of a structured errors-in-variables problem. *Computational Statistics and Data Analysis*, 144(106893):1–2, 2019a. ISSN 0167-9473. doi: 10.1016/j.csda.2019.106893.

G. Quintana-Carapia, I. Markovsky, R. Pintelon, P. Zoltán, and D. Verbeke. Experimental validation of a data-driven step input estimation method for dynamic measurements. *IEEE Transactions on Instrumentation and Measurement*, 1(1):1–1, 2019b. ISSN 1557-9662. doi: 10.1109/TIM.2019.2951865.

S. Rhode, K. Usevich, I. Markovsky, and F. Gauterin. A recursive restricted total least-squares algorithm. *IEEE Transactions on Signal Processing*, 62(21):5652–5662, 2014. ISSN 1053-587X. doi: 10.1109/TSP.2014.2350959.

M. Rossander, E. Dyachuk, S. Apelfröjd, K. Trolin, A. Goude, H. Bernhoff, and S. Eriksson. Evaluation of a Blade Force Measurement System for a Vertical Axis Wind Turbine Using Load Cells. *Energies*, 8(6):5973–5996, 2015. ISSN 1996-1073. doi: 10.3390/en8065973.

B. Saggin, S. Debei, and M. Zaccariotto. Dynamic error correction of a thermometer for atmospheric measurements. *Measurement*, 30(3):223–230, 2001. ISSN 0263-2241.

W.Q. Shu. Dynamic weighing under nonzero initial conditions. *IEEE Transactions on Instrumentation and Measurement*, 42(4):806–811, 1993. ISSN 0018-9456. doi: 10.1109/19.234489.

T. Söderström. Errors-in-variables methods in system identification. *Automatica*, 43(6):939–958, 2007. ISSN 0005-1098. doi: 10.1016/j.automatica.2006.11.025.

T. Söderström. *Errors-in-Variables Methods in System Identification*. Springer, 2018. ISBN 978-3-319-75001-9. doi: 10.1007/978-3-319-75001-9.

G. Stewart. Stochastic Perturbation Theory. *SIAM Review*, 32(4):579–610, 1990. doi: 10.1137/1032121.

R. Tasaki, T. Yamazaki, H. Ohnishi, M. Kobayashi, and S. Kurosu. Continuous weighing on a multi-stage conveyor belt with FIR filter. *Measurement*, 40(7–8):791–796, 2007. ISSN 0263-2241. doi: 10.1016/j.measurement.2006.05.010. Precision Measurement of Force, Mass, and Torque.

Tedea-Huntleigh. Aluminum Single-Point Load Cell 1004, 2015. `http://docs.vpgtransducers.com/?id=2831`.

K. Ushiki, K. Nishimori, N. Honma, and H. Makino. Intruder detection performance of simo and mimo sensors with same number of channel responses. *IEICE Transactions*, 96-B:2499–2505, 2013.

R. Vaccaro. A Second-Order Perturbation Expansion for the SVD. *SIAM J. Matrix Anal. Appl.*, 15(2):661–671, 1994. ISSN 0895-4798. doi: 10.1137/S0895479891224245.

S. Van Huffel and J. Vandewalle. *The total least squares problem: computational aspects and analysis*. SIAM, 1991. doi: 10.1137/1.9781611971002.

S. Van Huffel, C. Cheng, N. Mastronardi, C. Paige, and A. Kukush. Total Least Squares and Errors-in-variables Modeling. *Computational Statistics & Data Analysis*, 52(2):1076–1079, 2007. ISSN 0167-9473. doi: 10.1016/j.csda.2007.07.001.

N. Vlajic and A. Chijioke. Traceable dynamic calibration of force transducers by primary means. *Metrologia*, 53(4):S136, 2016.

L. Wang, Y. Yan, Y. Hu, and X. Qian. Rotational speed measurement through electrostatic sensing and correlation signal processing. *IEEE Transactions on Instrumentation and Measurement*, 63(5):1190–1199, 2014. ISSN 0018-9456. doi: 10.1109/TIM.2013.2292283.

D. Wiklund and M. Peluso. Quantifying and specifying the dynamic response of flowmeters. In *ISA2002 Technical Conference*, pages 463–476, 2002.

A. Yeredor and B. De Moor. On homogeneous least-squares problems and the inconsistency introduced by mis-constraining. *Computational Statistics & Data Analysis*, 47(3):455–465, 2004. doi: 10.1016/j.csda.2003.12.001.

N. Zahradka, I. Jeong, and P. Searson. Distinguishing positions and movements in bed from load cell signals. *Physiological Measurement*, 39(12):1–11, 2018. doi: 10.1088/1361-6579/aaeca8.